

---

Masters Theses

Student Theses and Dissertations

---

2011

## Optimal control of a helicopter unmanned aerial vehicle (UAV)

David John Nodland

Follow this and additional works at: [https://scholarsmine.mst.edu/masters\\_theses](https://scholarsmine.mst.edu/masters_theses)



Part of the [Electrical and Computer Engineering Commons](#)

Department:

---

### Recommended Citation

Nodland, David John, "Optimal control of a helicopter unmanned aerial vehicle (UAV)" (2011). *Masters Theses*. 5417.

[https://scholarsmine.mst.edu/masters\\_theses/5417](https://scholarsmine.mst.edu/masters_theses/5417)

This thesis is brought to you by Scholars' Mine, a service of the Missouri S&T Library and Learning Resources. This work is protected by U. S. Copyright Law. Unauthorized use including reproduction for redistribution requires the permission of the copyright holder. For more information, please contact [scholarsmine@mst.edu](mailto:scholarsmine@mst.edu).



OPTIMAL CONTROL OF A HELICOPTER UNMANNED AERIAL VEHICLE (UAV)

by

DAVID JOHN NODLAND

A THESIS

Presented to the Faculty of the Graduate School of the  
MISSOURI UNIVERSITY OF SCIENCE AND TECHNOLOGY

In Partial Fulfillment of the Requirements for the Degree

MASTER OF SCIENCE IN ELECTRICAL ENGINEERING

2011

Approved by

Jagannathan Sarangapani, Advisor  
Kelvin T. Erickson  
Maciej Zawodniok



### **PUBLICATION THESIS OPTION**

This thesis consists of the following two papers: paper 1, pages 10-57, D. Nodland, H. Zargarzadeh, and S. Jagannathan, “Neural Network-based Optimal Output Feedback Control for Trajectory Tracking of a Helicopter UAV,” to be submitted to *IEEE Transactions on Neural Networks*, and paper 2, pages 58-91, D. Nodland, A. Ghosh, H. Zargarzadeh, and S. Jagannathan, “Neuro-Optimal Control of an Unmanned Helicopter,” in *Journal of Defense Modeling and Simulation Special Issue: Intelligent Behaviors in Military Unmanned Systems*, 2012, to appear. Paper 2 has been augmented in this thesis with material on hardware implementation.

## ABSTRACT

This thesis addresses optimal control of a helicopter unmanned aerial vehicle (UAV). Helicopter UAVs may be widely used for both military and civilian operations. Because these helicopters are underactuated nonlinear mechanical systems, high-performance controller design for them presents a challenge. This thesis presents an optimal controller design via both state and output feedback for trajectory tracking of a helicopter UAV using a neural network (NN). The state and output-feedback control system utilizes the backstepping methodology, employing kinematic and dynamic controllers while the output feedback approach uses an observer in addition to these controllers. The online approximator-based dynamic controller learns the Hamilton-Jacobi-Bellman (HJB) equation in continuous time and calculates the corresponding optimal control input to minimize the HJB equation forward-in-time. Optimal tracking is accomplished with a single NN utilized for cost function approximation. The overall closed-loop system stability is demonstrated using Lyapunov analysis.

Simulation results are provided to demonstrate the effectiveness of the proposed control design for trajectory tracking. A description of the hardware for confirming the theoretical approach, and a discussion of material pertaining to the algorithms used and methods employed specific to the hardware implementation is also included. Additional attention is devoted to challenges in implementation as well as to opportunities for further research in this field. This thesis is presented in the form of two papers.

## **ACKNOWLEDGMENTS**

### **PERSONAL ACKNOWLEDGMENTS**

I would like to thank my advisor, Dr. Jagannathan Sarangapani, for his support and assistance over the course of my thesis research. I would also like to thank Dr. Kelvin Erickson and Dr. Maciej Zawodniok for their guidance, assistance, and willingness to serve on my advisory committee. The research work presented in the following pages was aided by funding from the Army Research Labs; I am grateful for this funding. In addition, I would like to thank Dr. Travis Dierks for his assistance at numerous points in my graduate studies, especially with some of the more difficult steps in the mathematical proofs, Dr. Arpita Ghosh for her assistance in preparing materials for publication early in the research, and Hassan Zargarzadeh for his assistance with software and with control systems theory. Finally, I am thankful to God for the opportunities I have had.

### **FUNDING ACKNOWLEDGMENT**

Research was sponsored by the Army Research Laboratory and was accomplished under Cooperative Agreement Number W911NF-10-2-0077. The views and conclusions contained in this document are those of the authors and should not be interpreted as representing the official policies, either expressed or implied, of the Army Research Laboratory or the U.S. Government. The U.S. Government is authorized to reproduce and distribute reprints for Government purposes notwithstanding any copyright notation herein.

## TABLE OF CONTENTS

	Page
PUBLICATION THESIS OPTION.....	iii
ABSTRACT.....	iv
ACKNOWLEDGEMENTS.....	v
LIST OF ILLUSTRATIONS.....	viii
<b>SECTION</b>	
1. INTRODUCTION.....	1
1.1. BACKGROUND .....	1
1.2. OBJECTIVE .....	5
1.3. ORGANIZATION .....	6
1.4. CONTRIBUTIONS .....	7
1.5. REFERENCES .....	8
<b>PAPER</b>	
1. NEURAL NETWORK-BASED OPTIMAL OUTPUT FEEDBACK CONTROL FOR TRAJECTORY TRACKING OF A HELICOPTER UAV.....	10
1.1. ABSTRACT.....	10
1.2. INTRODUCTION .....	10
1.3. HELICOPTER DYNAMIC MODEL.....	13
1.4. METHODOLOGY .....	17
1.4.1. Nonlinear Optimal Tracking of the Unmanned Helicopter.....	17
1.4.2. Kinematic Controller.....	19
1.4.3. Observer Design.....	19
1.4.4. Virtual Controller .....	22
1.4.5. Hamilton-Jacobi-Bellman Equation.....	24
1.4.6. Single Online Approximator (SOLA)-Based Optimal Control of Helicopter.....	27
1.4.7. Stability Analysis .....	30
1.5. SIMULATION RESULTS .....	32
1.6. CONCLUSION.....	37



1.7. REFERENCES .....	37
1.8. APPENDIX.....	39
PAPER	
2. NEURAL-NETWORK-BASED OPTIMAL CONTROL OF A HELICOPTER UNMANNED AERIAL VEHICLE (UAV) WITH HARDWARE IMPLEMENTATION.....	58
2.1. ABSTRACT.....	58
2.2. INTRODUCTION .....	58
2.3. DYNAMIC MODEL OF THE HELICOPTER.....	63
2.4. NONLINEAR OPTIMAL TRACKING OF THE HELICOPTER UAV .....	67
2.4.1. Kinematic Controller.....	68
2.4.2. Virtual Controller .....	68
2.4.3. Hamilton-Jacobi-Bellman Equation.....	70
2.4.4. Single Online Approximator (SOLA)-Based Optimal Control of Helicopter.....	73
2.4.5. Stability Analysis .....	75
2.5. SIMULATION RESULTS .....	80
2.6. HARDWARE RESULTS .....	87
2.7. CONCLUSION.....	89
2.8. REFERENCES .....	90
SECTION	
2. CONCLUSIONS AND FUTURE WORK .....	92
2.1 CONCLUSIONS.....	92
2.2 FUTURE WORK .....	93
VITA.....	94

## LIST OF ILLUSTRATIONS

	Page
Figure 1.1. Helicopter UAV Built from Modified Align Trex 500 Airframe.....	1
Figure 1.2. Helicopter UAV with Antenna for Threat Detection.....	3
Figure 1.3 Thesis Organization.....	7
<b>PAPER 1</b>	
Figure 1.1. Helicopter Dynamics.....	15
Figure 1.2. Output Feedback Control Scheme.....	18
Figure 1.3. 3-D Perspective of Position during Take-off and Circular Maneuver.....	34
Figure 1.4. Helicopter Position Vs. Time for Tracking.....	34
Figure 1.5. 3-D Perspective of Position and Orientation during Landing.....	35
Figure 1.6. 3-D Perspective of Position during Landing.....	35
Figure 1.7. Observer State Estimation Error.....	36
Figure 1.8. Observer Output Estimation Error.....	36
<b>PAPER 2</b>	
Figure 2.1. Control Scheme for Optimal Tracking of Helicopter.....	67
Figure 2.2. Helicopter Altitude during Take-off.....	81
Figure 2.3. Helicopter Altitude during Landing.....	82
Figure 2.4. 2D Helicopter Trajectory Tracking.....	82
Figure 2.5. 3D Perspective of Helicopter Trajectory Tracking.....	83
Figure 2.6. Absolute Error in Altitude during Take-off.....	83
Figure 2.7. Main Rotor Control Input during Take-off.....	84
Figure 2.8. Vertical Velocity during Take-off.....	84
Figure 2.9. Absolute Error in Vertical Velocity during Take-off.....	84
Figure 2.10. Acceleration during Take-off.....	85
Figure 2.11. Magnitude of U-vector.....	85
Figure 2.12. Instantaneous Cost during Take-off.....	85
Figure 2.13. Cumulative Cost during Take-off.....	86
Figure 2.14. 3D Landing While Changing Heading.....	86
Figure 2.15. 3D Trajectory Tracking.....	86

Figure 2.16. Take-off and Circular Hovering..... 87  
Figure 2.17. Processor & Sensor Boards..... 89

# 1. INTRODUCTION

## 1.1. BACKGROUND

Control of helicopter UAVs is a significant challenge facing a number of researchers and organizations today [1]-[8]. There are many applications for helicopter UAVs, ranging from search-and-rescue operations, interdiction efforts, and reconnaissance and surveillance to aerial transport and forest fire monitoring. Helicopter UAVs have the advantage of lower cost and weight and fewer safety concerns than conventional helicopters and are useful for many tasks that would be unsafe or inconvenient for a human pilot.



Figure 1.1. Helicopter UAV Built from Modified Align Trex 500 Airframe

One key role for helicopter UAVs is counter-explosive operations [17]. Key operational activities for helicopter UAVs include [17]: “Preventing an adversary from conducting activities that result in the emplacement of IEDs [Improvised Explosive Devices], thus thwarting an attack: this is likely to require use of the full spectrum of Joint capabilities to defeat or disrupt the adversary....” As well as “Detecting IED materiel and components, including stored HME [Home-made Explosives] and smuggled components, as well as emplaced devices themselves. This requires a combination of ISR [Intelligence, Surveillance, and Reconnaissance] capability, together with responsive processes and effective training, to ensure that potential IED activity detected is analyzed and the results disseminated to all those who need to be aware of it, in order that appropriate action can be taken as swiftly as possible.”

There are a number of specific ways that Helicopter UAVs can counter threats [17]. “In simple terms, A & S [Air & Space] Power is capable of defeating emplaced IEDs by detecting devices and by neutralizing and mitigating their effects, as follows: Detecting devices using dedicated airborne and Space-based ISR and airborne Non-Traditional ISR (NTISR), exploiting existing capabilities and capitalizing on technological enhancements, including those offered by CCD technology.” These devices can be neutralized or have their effects mitigated through “Airborne EW [Electronic Warfare] capabilities, including Electronic Attack (EA), by employing ECM [Electronic Counter-Measures] to disrupt or detonate RCIEDs [Radio-controlled IEDs], the initiation or disruption of IEDs using kinetic targeting via airborne (or potentially Space) platform-based weapon systems, including by direct fire, and by the physical avoidance of emplaced IEDs using Air Mobility, utilizing Fixed-Wing (FW) and Rotary-Wing (RW)

intra-theatre airlift, including the use of air dispatch capabilities.” Another helpful feature is that “A UAV, which minimizes risk to human life may be preferable because it can provide long endurance and is difficult to detect in the air” [17]. For applications such as counter-explosive operations, where low-speed and hovering capabilities are useful, a helicopter UAV may become the tool of choice. In addition, helicopter UAVs can deliver supplies to positions which cannot be safely supplied from the ground. For example [18], “Supplying small forward operating bases using trucks requires escorting forces, and exposes [military] convoys to the threat of mines. The standard solution is helicopter drop-off, but every force in theater is short of helicopters....” These are just some of the current defense applications of helicopter UAVs.



Figure 1.2. Helicopter UAV with Antenna for Threat Detection

The objective of controlling helicopter UAVs is to manipulate their position and orientation such that they can take-off, hover and fly along a desired trajectory between waypoints, and land autonomously. For control of a helicopter [1], it is necessary to produce moments and forces on the vehicle with two goals: first, to position the helicopter in equilibrium such that the desired trim state is achieved, and second, to control the helicopter's velocity, position and orientation such that it hovers as desired with minimum error.

Unfortunately, helicopter dynamics are complex and very nonlinear [13]. The dynamics of the helicopter UAV are not only nonlinear but also coupled with each other and under-actuated, which makes the UAV difficult to control. In addition, there is a significant amount of interaction among the control inputs as well in the physical dynamics of the system [13], particularly as a result of the swashplate mechanical linkages and the torques created by drag against the rotors.

A helicopter has six degrees of freedom (able to move in three dimensions and change orientation about three orthogonal axes), but can only apply four control inputs – thrust and roll, pitch, and yaw torques. Although a helicopter may have more than four hardware inputs, these inputs reduce to the four just mentioned, meaning that helicopters are underactuated systems.

Helicopter UAVs, with their low weight compared to larger helicopters, are also very quick and agile, and respond to control inputs rapidly. This combination of features results in a difficult controls problem. To address this problem, a number of approaches have been developed [1]-[8], [11]-[14]. In [1] and [2], a controller is developed for flight control and modeling is performed with experimental verification, but the control design

does not accommodate coupling in the dynamics. In [3], the controller accommodates the coupling in the dynamics but requires feedback linearization, with the observer estimating the feedback-linearized states rather than the actual states. Pseudo-control hedging has been employed [5] for nonlinear control of a helicopter UAV along with nonlinear backstepping-based control [6], but optimal control is not a part of these works.

Neural networks have been employed [7] with a cost function, along with a neural-network-based controller that can operate without full knowledge of the dynamics [8], but nonlinear optimal control for a range of flight trajectories is unavailable. Complete control systems have been designed and implemented in [9], [10], and [11], but without proof of optimality. Optimal control has been performed for a helicopter UAV, but the optimal controller is linear, rather than nonlinear [12]. A very interesting contribution to the area of nonlinear controllers for helicopter UAVs was provided in [13], but no attempt was made at optimality. Separately, an observer for output feedback was introduced in [14], with potential for application to helicopters. Nonlinear online optimal control has been shown in discrete time [15] and continuous time [16], but was provided for a general theoretical case. This thesis builds on previous work to provide a nonlinear online optimal control scheme for state feedback as well as for output feedback of helicopter UAVs.

## **1.2. OBJECTIVE**

The objective of this thesis is to develop and verify optimal control schemes for both state and output feedback control of unmanned, underactuated helicopters, forward-in-time, with the helicopter dynamics expressed in a form appropriate for backstepping



control. The control schemes apply to both hovering and trajectory tracking, and the controller tuning is independent of the trajectory. The control scheme is fully online and is demonstrated to be stable.

### **1.3. ORGANIZATION**

This thesis begins with this introductory section followed by the first paper, “Neural Network-based Optimal Output Feedback Control for Trajectory Tracking of a Helicopter UAV,” which develops the controls approach with output feedback. The second paper, “Neural-Network-Based Optimal Control of a Helicopter Unmanned Aerial Vehicle (UAV) with Hardware Implementation,” is introduced next and develops the controls approach with state feedback. The second paper is augmented by a section describing the hardware for experimental verification of the theoretical contributions. The advantage of state feedback is that it does not require an observer and the angular velocity (which makes up part of the states) may be directly measured for the hardware implementation with a 3-axis gyro. The disadvantage is that the translational velocity (which makes up the rest of the states) must be obtained indirectly from a Global Positioning System (GPS) unit and the ultrasonic range finder. The advantage of output feedback is that it can directly measure the position (part of the outputs) using GPS and an ultrasonic range finder. The disadvantage is that this approach requires that the orientation (which makes up the rest of the outputs) must be obtained by integrating the angular velocity (which introduces error), and an observer is needed. Because each approach has advantages and disadvantages, both approaches are developed.

After the second paper, a final section concludes the thesis discussing the work that has been completed and opportunities for future research. The block diagram below visually shows the organization of the body of the thesis:

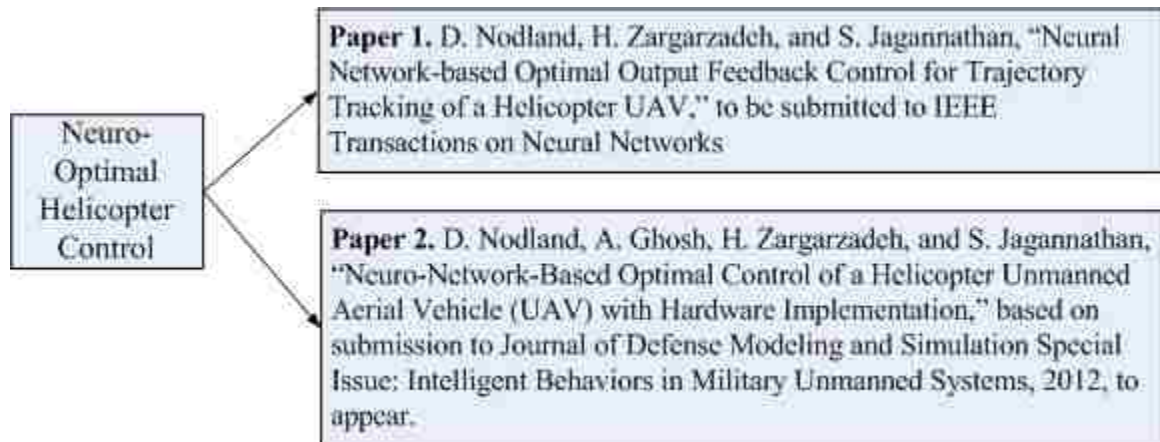


Figure 1.3 Thesis Organization

#### 1.4. CONTRIBUTIONS

The primary contribution of this thesis is the development of nonlinear online optimal control schemes for state feedback as well as for output feedback of helicopter UAVs. The optimal controller in this work has been previously developed for backstepping systems, but has not yet been applied to rotary-wing aircraft. This optimal controller previously required that  $f(0) = 0$ , but the virtual controller in this work obviates the need for that requirement. The optimal controller and the virtual controller together constitute a novel dynamic controller, which is able to track a variety of

trajectories with a single set of fixed gains. In other words, the controller tuning is independent of the desired trajectory.

Lyapunov-based closed-loop stability proofs are provided along with simulation results for theoretical verification, and show the proposed control scheme's convergence. Hardware implementation is also described to show how the theoretical contribution is implemented.

## 1.5. REFERENCES

- [1] T. J. Koo and S. Sastry, "Output Tracking Control Design of a Helicopter Model Based on Approximate Linearization," *Proceedings of the 37th IEEE Conference on Decision and Control*, pp. 3635-3640, 1998.
- [2] B. F. Mettler, M. B. Tischler and T. Kanade, "System Identification Modelling of a Small Scale Rotorcraft for Flight Control Design," *International Journal of Robotics Research*, Vol. 20, pp. 795-807, 2000.
- [3] N. Hovakimyan, N. Kim, A. J. Calise, J. V. R. Prasad, "Adaptive Output Feedback for High Bandwidth Control of an Unmanned Helicopter," *Proceedings of AIAA Guidance, Navigation, and Control Conference*, Montreal, Canada, pp. 1-11, 2001.
- [4] E. N. Johnson and S. K. Kannan, "Adaptive Trajectory Control for Autonomous Helicopters," *Journal of Guidance, Control and Dynamics*, Vol. 28, pp. 524-538, 2005.
- [5] I. Palunko, R. Fierro and C. Sultan, "Nonlinear Modeling and Output Feedback Control Design for a Small-scale Helicopter," *Proceedings of 17th Mediterranean Conference on Control and Automation*, Greece, 2009.
- [6] B. Ahmed, H. R. Pota and M. Garratt, "Flight Control of a Rotary Wing UAV Using Backstepping," *International Journal of Robust and Nonlinear Control*, Vol. 20, pp. 639-658, 2010.
- [7] R. Enns and J. Si, "Helicopter Trimming and Tracking Control Using Direct Neural Dynamic Programming," *IEEE Transactions on Neural Networks*, Vol. 14, pp. 929-939, 2003.

- [8] S. Lee, C. Ha and B. S. Kim, "Adaptive Nonlinear Control System Design for Helicopter Robust Command Augmentation," *Aerospace Science and Technology*, Vol. 9, pp. 241-251, 2005.
- [9] C. M. Ivler, M. B. Tischler and M. H. Mansur, et al., "Control System Development and Flight Test Experience with the MQ-8B Fire Scout Vertical Take-off Unmanned Aerial Vehicle (VTUAV)," *American Helicopter Society 63rd Annual Forum*, 2007.
- [10] A.Y. Ng, A. Coates, M. Diel, V. Ganapathi, et al., "Inverted Autonomous Helicopter Flight Via Reinforcement Learning," *Experimental Robotics IX*, edited by M. Ang, O. Khatib. Springer-Verlag, 2006.
- [11] V. Gavrilets, B. Mettler, and E. Feron, "Human-inspired Control Logic for Automated Maneuvering of a Miniature Helicopter," *AIAA Journal on Guidance, Control, and Dynamics*, Vol. 27, pp. 752-759, 2004.
- [12] P. Abbeel, A. Coates, M. Quigley, and A.Y. Ng, "An Application of Reinforcement Learning to Aerobatic Helicopter Flight," *Neural Information Processing Systems Conference*, Vancouver, 2006.
- [13] R. Mahoney and T. Hamel, "Robust Trajectory Tracking for a Scale Model Autonomous Helicopter," *International Journal of Robust and Nonlinear Control*, Vol. 14, pp. 1035-1059, 2004.
- [14] T. Dierks and S. Jagannathan, "Output Feedback Control of a Quadrotor UAV Using Neural Networks," *IEEE Transactions on Neural Networks*, Vol. 21, pp. 50-66, 2010.
- [15] T. Dierks and S. Jagannathan, "Optimal Control of Affine Nonlinear Discrete-time Systems," *Proceedings of the Mediterranean Conference on Control and Automation*, pp. 1390-1395, 2009.
- [16] T. Dierks and S. Jagannathan, "Optimal Control of Affine Nonlinear Continuous-time Systems," *Proceedings of American Control Conference*, pp. 1568-1573, Baltimore, 2010.
- [17] Naskrent, D., et al., "NATO Air and Space Power in Counter-IED Operations: a Primer," Joint Air Power Competence Center, 2010.
- [18] Unnamed Author. (2011, September 7). Defense Industry Daily [Online]. Available: <http://www.defenseindustrydaily.com/USMC-Looks-for-an-Unmanned-Cargo-Helicopter-06672/>

## PAPER

# 1. NEURAL NETWORK-BASED OPTIMAL OUTPUT FEEDBACK CONTROL FOR TRAJECTORY TRACKING OF A HELICOPTER UAV

## 1.1. ABSTRACT

Helicopter unmanned aerial vehicles (UAVs) may be widely used for both military and civilian operations. Because these helicopters are underactuated nonlinear mechanical systems, high-performance controller design for them presents a challenge. This paper presents an optimal controller design via output feedback for trajectory tracking of a helicopter UAV using a neural network (NN). The output-feedback control system utilizes the backstepping methodology, employing kinematic and dynamic controllers and an observer. The online approximator-based dynamic controller learns the infinite-horizon Hamilton-Jacobi-Bellman (HJB) equation in continuous time and calculates the corresponding optimal control input to minimize the HJB equation forward-in-time. Optimal tracking is accomplished with a single NN utilized for cost function approximation. The overall closed-loop system stability is demonstrated using Lyapunov analysis. Finally, simulation results are provided to demonstrate the effectiveness of the proposed control design for trajectory tracking.

## 1.2. INTRODUCTION

Unmanned helicopters are unmanned aerial vehicles (UAVs) which are capable of independent flight. Due to their versatility and maneuverability, unmanned helicopters are invaluable for both civilian and military applications where human intervention may

be restricted. For unmanned helicopter control [1], it is essential to produce moments and forces on the UAV to position the helicopter such that the desired regulated state is achieved, and to control the helicopter's velocity, position, and orientation such that it tracks a desired trajectory. The dynamics of the helicopter UAV are not only nonlinear, but are also coupled with each other and underactuated, which makes the control design challenging. Both inputs and dynamics are coupled on a helicopter, particularly as a result of the swashplate mechanical linkages and the torques created by drag against the rotors. A helicopter has six degrees of freedom (DOF) which must be controlled with only four control inputs in order to manipulate the thrust and the three rotational torques.

In order to develop the controllers for such unmanned helicopters, Koo and Sastry [1] have utilized an approximate linearization-based control [1] that transforms the system into linear form. Mettler et al. [2] have introduced a model for the helicopter independent of an accompanying control scheme [2]. Hovakimyan et al. [3] have implemented an output feedback control scheme with a neural network (NN)-based controller using feedback linearization [3]. Johnson and Kannan [4] have employed an inner and outer loop control using pseudo-control hedging [4], and Ahmed et al. [5] have introduced a backstepping-based controller for the helicopter [5]. Frazzoli [6] and Mahoney [7] have both generated control schemes for Lyapunov-based control of helicopter UAVs. However, none of these works [1]-[7] presents an optimal control scheme for an unmanned helicopter.

Optimal control of linear systems accompanied by quadratic cost functions can be achieved by solving the Riccati equation [8]. In contrast, the optimal control of nonlinear continuous or discrete-time systems is a much more challenging task that often requires

solving the nonlinear Hamilton-Jacobi-Bellman (HJB) equation, which does not have a closed-form solution.

Therefore, Enns and Si [9] have used neural network dynamic programming (NDP)-based optimal control of a helicopter UAV [9] using offline training. Lee et al. [10] introduced a robust command augmentation system using a NN, but inversion errors can lead to problems [10].

In the recent NDP literature, Dierks and Jagannathan [11] introduced an optimal regulation and tracking controller for nonlinear discrete-time systems in affine form. Here, the discrete-time Hamilton-Jacobi-Bellman equation is solved online and forward-in-time. An online approximator (OLA) is tuned to learn the HJB equation, with a second OLA utilized to minimize the cost function [11]. Dierks and Jagannathan [12] have extended this NDP scheme to continuous-time systems in affine form by using a single online approximator (SOLA) [12]. However, such NDP-based optimal control schemes are not available to nonlinear systems that require the backstepping approach.

Therefore, a SOLA-based scheme for the optimal tracking control of a helicopter's nonlinear continuous-time feedback system is considered in this paper via a backstepping approach. A kinematic controller generates the desired velocities. The dynamic controller learns the continuous-time HJB equation and then calculates the corresponding optimal control input to minimize the HJB equation forward-in-time by assuming known system dynamics. The proposed tracking controller includes a single NN for approximating the cost function with the NN weights tuned online. A NN observer is employed to obtain the states from the outputs. Lyapunov analysis is utilized

to demonstrate the stability of the closed-loop system. Simulation results are included for both hovering and following a desired maneuver.

The main contribution of this paper includes the development of an optimal controller for tracking a trajectory of an unmanned underactuated helicopter, forward in time, where the helicopter system is expressed in a form appropriate for backstepping control. The controller tuning is independent of the trajectory. A NN-based OLA is utilized to approximate the cost function and the overall stability is guaranteed. The optimal controller has been previously developed for backstepping systems, but has not yet been applied to rotary-wing aircraft. This optimal controller previously required that  $f(0) = 0$ , but the virtual controller in this work obviates the need for that requirement. In addition, this controller is extended for application to an output feedback system. The observer for this has been developed for a quadrotor [14], but the present application to a helicopter is novel, and is not accompanied by the virtual and kinematic controllers employed in [14]. The current work builds on [7], [12], and [14], from the fields of helicopter, optimal, and quadrotor control, respectively; however, this work both uses previous developments for a new application and adds to these three works with a closed-loop stability proof demonstrating the proposed control scheme's convergence with output feedback, rather than with state feedback.

### 1.3. HELICOPTER DYNAMIC MODEL

Consider the helicopter shown in Figure 2.1 with six degrees of freedom (DOF) defined in the inertial coordinate frame  $Q^a$ , where its position coordinates are given by  $\rho = [x \ y \ z] \in Q^a$  and its orientation described as yaw, pitch, and roll, respectively, is



given by Euler angles  $\Theta = [\phi \ \theta \ \psi] \in Q^a$ . The equations of motion are expressed in the body fixed frame  $Q^b$  which is associated with the helicopter's center of mass. The  ${}^b x$ -axis is defined parallel to the helicopter's direction of travel and the  ${}^b y$ -axis is defined perpendicular to the helicopter's direction of travel, while the  ${}^b z$ -axis is defined as projecting orthogonally downwards from the  $xy$ -plane of the helicopter. The dynamics of the helicopter is given by the Newton-Euler equation in the body fixed coordinate system and can be written as in [7] but in the form provided in [14] as

$$M \begin{bmatrix} \dot{v} \\ \dot{\omega} \end{bmatrix} = \bar{S}(\omega) + \begin{bmatrix} 0^{3 \times 1} \\ N_2 \end{bmatrix} + \begin{bmatrix} G(R) \\ 0^{3 \times 1} \end{bmatrix} + U + \tau_d \quad (1)$$

where the mass-inertia matrix  $M$  is defined as

$$M = \text{diag} \{ mI \ \mathcal{J} \} \in \mathbb{R}^{6 \times 6},$$

$m \in \mathbb{R}$  is a positive scalar denoting the mass of the helicopter,  $I \in \mathbb{R}^{3 \times 3}$  is the identity

matrix,  $\mathcal{J} \in \mathbb{R}^{3 \times 3}$  is the positive-definite inertia matrix,  $\bar{S}(\omega) = \begin{bmatrix} 0^{3 \times 1} & -\omega \times \mathcal{J} \omega \end{bmatrix}^T$ ,

$N_2 \in \mathbb{R}^{3 \times 1}$  represents the nonlinear aerodynamic effects,  $G(R) = m\bar{g}e_3 \in \mathbb{R}^{3 \times 1}$  represents

the gravity vector with  $\bar{g}$  the gravitational acceleration, and  $\tau_d = \begin{bmatrix} \tau_{d1}^T & \tau_{d2}^T \end{bmatrix}^T$  represents

unknown bounded disturbances such that  $\|\tau_d\| < \tau_M$  for all time  $t$ , with  $\tau_M$  a known

positive constant. Also,  $v = \begin{bmatrix} v_x & v_y & v_z \end{bmatrix} \in \mathbb{R}^{3 \times 1}$  and  $\omega = \begin{bmatrix} \omega_x & \omega_y & \omega_z \end{bmatrix} \in \mathbb{R}^{3 \times 1}$  represent

the translational velocity and angular velocity vectors, respectively. The kinematics of the helicopter are given by

$$\dot{\rho} = Rv \quad (2)$$

and

$$\dot{\Theta} = T^{-1}\omega \quad (3)$$

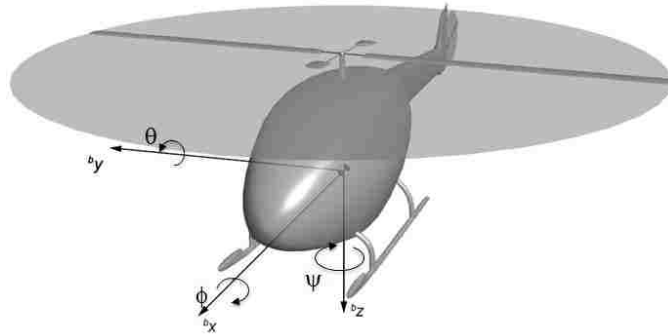


Figure 1.1. Helicopter Dynamics

The translational rotation matrix used to relate a vector in body fixed frame to the inertial coordinate frame is defined as [14]

$$R(\Theta) = \begin{bmatrix} c_\theta c_\phi & s_\psi s_\theta c_\phi - c_\psi s_\phi & c_\psi s_\theta c_\phi + s_\psi s_\phi \\ c_\theta s_\phi & s_\psi s_\theta s_\phi + c_\psi c_\phi & c_\psi s_\theta s_\phi - s_\psi c_\phi \\ -s_\theta & s_\psi c_\theta & c_\psi c_\theta \end{bmatrix} \quad (4)$$

with  $\|R\|_F < R_{\max}$  for a known constant  $R_{\max}$  and  $R^{-1} = R^T$ , where  $s_\bullet$  and  $c_\bullet$  denote the  $\sin(\bullet)$  and  $\cos(\bullet)$  functions, respectively. The transformation matrix from the angular velocity to the derivative of the orientation is

$$T(\Theta) = \frac{1}{c_\theta} \begin{bmatrix} 0 & s_\psi & c_\psi \\ 0 & c_\theta c_\psi & -c_\theta s_\psi \\ c_\theta & s_\theta s_\psi & s_\theta c_\psi \end{bmatrix} \quad (5)$$

and is bounded according to  $\|T\|_F < T_{\max}$  for a known constant  $T_{\max}$ , provided

$-\pi/2 < \psi < \pi/2$  and  $-\pi/2 < \theta < \pi/2$  such that the helicopter trajectory does not pass

through any singularities [1], with  $t_\bullet$  used to represent  $\tan(\bullet)$ . Throughout this work,  $\|\bullet\|$

denotes a Euclidean norm and  $\|\bullet\|_F$  denotes a Frobenius norm. Note also that  $(\times)$  denotes the vector cross product. The nonlinear aerodynamic effects taken into consideration for modeling of the helicopter are given by  $N_2 = Q_M e_3 - Q_T e_2$ , with  $Q_M$  and  $Q_T$  aerodynamic constants for which values are given in the simulation section, and originally found in [7]. Note that  $e_1$ ,  $e_2$ , and  $e_3$  are unit vectors directed along the x-, y-, and z-axes, respectively, in the inertial reference frame. The vector  $U \in \mathbb{R}^{6 \times 1}$  is given by

$$U = \begin{bmatrix} E_3^b & 0^{3 \times 3} \\ 0^{3 \times 1} & \text{diag}([p_{11} \ p_{22} \ p_{33}]) \end{bmatrix} \begin{bmatrix} u \\ w_1 \\ w_2 \\ w_3 \end{bmatrix} \quad (6)$$

where the control vector  $u_v = [u \ w_1 \ w_2 \ w_3]$ , with  $u$  providing the thrust in the z-direction,  $w_1$ ,  $w_2$  and  $w_3$  providing the rotational torques in the x-, y-, and z-directions, respectively,  $p_{ii}$  positive definite constants that make up a gain array, and  $E_3^b = [001]^T$ .

Defining the new augmented variables  $X = [\rho^T \ \Theta^T]^T \in \mathbb{R}^{6 \times 1}$  and  $V = [v^T \ \omega^T]^T \in \mathbb{R}^{6 \times 1}$ , (1) can be rewritten in a form suitable for backstepping as

$$\dot{X} = AV + \xi \quad (7)$$

$$\dot{V} = f(V) + M^{-1}U \quad (8)$$

where  $f(V) = M^{-1}(\bar{S}(\omega) + [0^{3 \times 1} \ \mathcal{N}_2]^T) + \bar{G}$  with  $\bar{G} = M^{-1}[G(R) \ 0^{3 \times 1}] \in \mathbb{R}^{6 \times 1}$ , and  $\xi \in \mathbb{R}^{6 \times 1}$

is the bounded sensor measurement noise such that  $\|\xi\| \leq \xi_M$  for a known constant  $\xi_M$ .

Equation (8) is in the body reference frame, while equation (7) is in the earth reference frame. Note that these last two equations take the form

$$\dot{x}_1 = f_1(x_1) + g_1(x_1)x_2 + \xi \quad (9)$$

$$\dot{x}_2 = f_2(x_2) + g_2(x_2)u \quad (10)$$

with  $f_1(x_1) = 0$ . This system is a candidate for backstepping control [13]. The dynamic controller operates in the body reference frame, with equation (7) necessary to bring these results back to the earth reference frame. Also,  $A = \text{diag}\left(\begin{bmatrix} R & T^{-1} \end{bmatrix}\right) \in \mathbb{R}^{6 \times 6}$ . Writing explicitly,  $f(V)$  yields

$$f(V) = \begin{bmatrix} 1/m & 0 & 0 & 0 & 0 & 0 \\ 0 & 1/m & 0 & 0 & 0 & 0 \\ 0 & 0 & 1/m & 0 & 0 & 0 \\ 0 & 0 & 0 & 1/\mathcal{J}_x & 0 & 0 \\ 0 & 0 & 0 & 0 & 1/\mathcal{J}_y & 0 \\ 0 & 0 & 0 & 0 & 0 & 1/\mathcal{J}_z \end{bmatrix} \left( \begin{bmatrix} 0 \\ 0 \\ 0 \\ -\omega_x \times \mathcal{J}_x \omega_x \\ -\omega_y \times \mathcal{J}_y \omega_y \\ -\omega_z \times \mathcal{J}_z \omega_z \end{bmatrix} + \begin{bmatrix} 0 \\ 0 \\ 0 \\ 0 \\ -Q_T \\ Q_M \end{bmatrix} + \begin{bmatrix} 0 \\ 0 \\ m\bar{g} \\ 0 \\ 0 \\ 0 \end{bmatrix} \right) \quad (11)$$

In this section, the dynamic model of the helicopter with six degrees of freedom has been presented. The control methodology is addressed next.

## 1.4. METHODOLOGY

**1.4.1. Nonlinear Optimal Tracking of the Unmanned Helicopter.** The overall control objective for the unmanned helicopter is to track a desired trajectory  $X_d(t)$  and a desired heading (yaw) while maintaining stable flight. Full knowledge of the helicopter states is required to achieve the control objective. Therefore, a NN observer is designed to estimate the states from the outputs. In Figure 2, the entire NN-based output feedback control scheme for optimal tracking of the desired trajectory by the helicopter is illustrated. Note that the dynamic controller is comprised of the items within the dashed boundary. This output feedback control scheme consists of a kinematic controller to

generate the desired velocity for the dynamic controller, a virtual controller to provide a feedforward term  $u_d$ , an optimal controller to generate the NN-based optimal feedback term  $\hat{u}_e^*$ , and an observer to estimate the states. Summing the control terms from the virtual and optimal (SOLA-based) controllers yields the NN-based control input for the helicopter dynamics  $\hat{u}_v$ , which is an estimate of the desired control input  $u_v$ . The details are provided next.

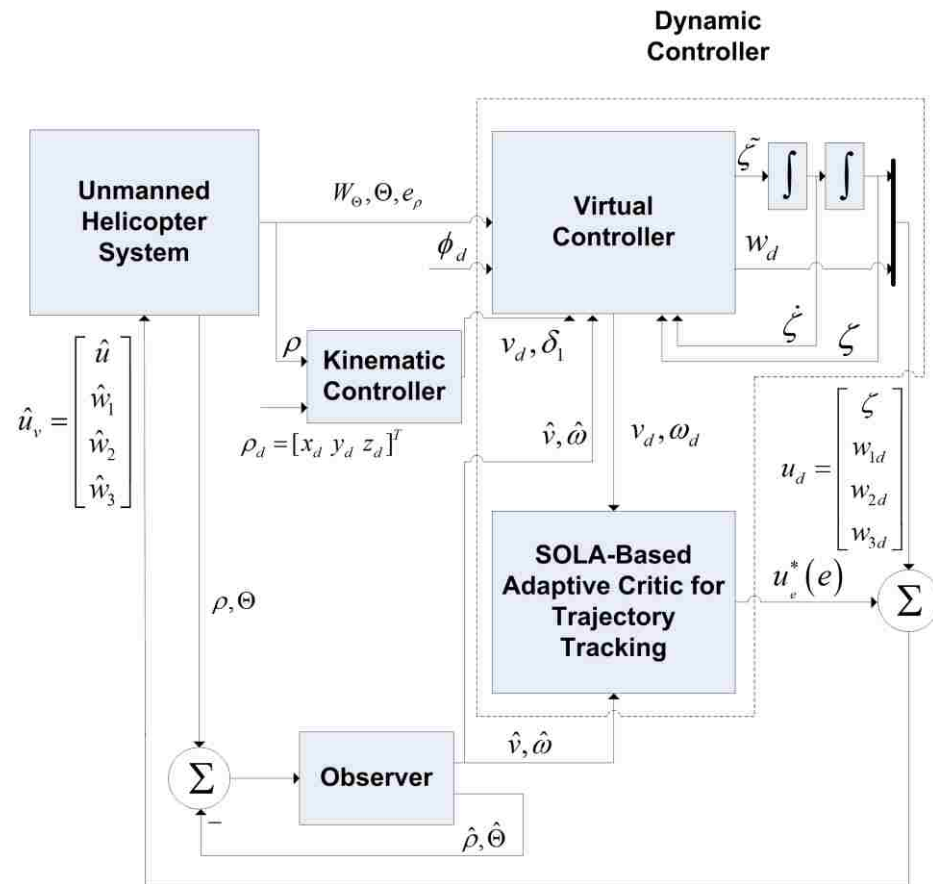


Figure 1.2. Output Feedback Control Scheme

**1.4.2. Kinematic Controller.** To design the kinematic controller for the unmanned helicopter, define the position tracking error as

$$\delta_1 = \rho_d - \rho \quad (12)$$

The observer's velocity estimate  $\hat{v}$  may be used to obtain the desired velocity,  $v_d$  as in [7]

$$v_d = \hat{v} - \frac{1}{m} \delta_1 \quad (13)$$

Note that the notation  $(\hat{\bullet})$  is used here to denote an estimate. In addition, it is important to note that there exist desired trajectories which may reach unstable operating regions as the orientation about the  $x$ - and  $y$ - axes approaches  $\pm\pi/2$ . It is possible to avoid these singularities by redefining Euler angles or with an alternative approach employing quaternions, but there are still physical constraints to be considered. In other words, if the main rotor blades move into a plane perpendicular to the ground, the helicopter becomes unstable. This is a consequence of the physical limitations of helicopters. Therefore, trajectories requiring that these orientations be maintained should not be assigned to the helicopter.

**1.4.3. Observer Design.** The following section extends the work in [14] by Dierks and Jagannathan to a helicopter system. An observer is used to estimate the system states based on the system model and outputs. The helicopter states to be estimated are given by  $V$  with the observer's estimate of these states given by  $\hat{V}$  with the state estimation error given by  $\tilde{V} = V - \hat{V}$ . The output is  $X$ , with the integrated observer's estimate of the output given by  $\hat{X}$ , and the error between the actual output and the integrated observer's estimate of the output given by  $\tilde{X}$ , with  $\tilde{X} = X - \hat{X}$ .

The observer is NN-based, and functions by estimating the output and comparing the estimate to the actual output. Referring back to (7) and (8), if  $A$  and  $\xi$  are known, then  $X$  may be easily obtained by integrating  $\dot{X}$ , and rearranging and solving yields  $V$ . But since  $X$  is known,  $A$  may be accurately obtained, meaning that  $\xi$  and the NN approximation error  $\varepsilon_o$  are the only sources of error in determining  $V$ .

To begin, a neural network basis vector  $x_o$  is selected such that

$\hat{x}_o = [1 \quad \hat{X} \quad \hat{V}^T \quad \tilde{X}^T]^T$ , with the NN estimate given by  $\hat{f}_{o1} = \hat{W}_o^T \sigma(V_o^T \hat{x}_o)$ . For this neural network estimate,  $\sigma(\bullet)$  represents the activation function and  $W_o$  and  $V_o$  are the weights, with  $\hat{W}_o$  an estimate of  $W_o$ , which has an upper bound  $\|W_o\|_F \leq W_{Mo}$ . Similarly to the estimates of the states and outputs and their errors, the observer weight error is defined such that  $\tilde{W}_o = W_o - \hat{W}_o$ . In addition, positive gains  $K_{o1}, K_{o2}, K_{o3}$  are selected such that  $K_{o1} > K_{o3}$ ,  $K_{o3} > 2N_o/\kappa_{o1}$ , and  $K_{o2} = K_{o3}(K_{o1} - K_{o3})$ , where  $N_o$  is the number of hidden layer neurons.

The NN estimate is then used to calculate the observer's estimate of the states as

$$\dot{\hat{Z}} = \hat{f}_{o1} + K_{o2}A^{-1}\tilde{X} \quad (14)$$

which is promptly used in addition to the output error to calculate the estimate of the output by using the dynamic equation

$$\dot{\hat{X}} = A\hat{Z} + K_{o1}\tilde{X} \quad (15)$$

At this point, the states may be estimated as

$$\hat{V} = \hat{Z} + K_{o3}A^{-1}\tilde{X} \quad (16)$$

The weight update law is then used to update the weights as below

$$\dot{\hat{W}}_o = F_o \sigma(V_o^T x_o) \tilde{X}^T - \kappa_{o1} F_o \hat{W}_o \quad (17)$$

with  $F_o = F_o^T > 0$  and  $\kappa_{o1} > 0$  tunable gains. The NN approximation error  $\varepsilon_o$  is bounded such that  $\|\varepsilon_o\| \leq \varepsilon_{Mo}$ , with  $\varepsilon_{Mo}$  a known constant. The observer NN weights are randomly initialized. The observer error dynamics are

$$\begin{aligned} \dot{\tilde{X}} &= A\tilde{V} - (K_{o1} - K_{o3})\tilde{X} + \xi \\ \dot{\tilde{Z}} &= (f_o + (A^T - K_{o3}\dot{A}^{-1})\tilde{X}) - \hat{f}_{o1} - K_{o2}A^{-1}\tilde{X} - (A^T - K_{o3}\dot{A}^{-1})\tilde{X} \end{aligned} \quad (18)$$

and the observer estimation error dynamics are

$$\dot{\tilde{V}} = -K_{o3}\tilde{V} + \tilde{f}_{o1} - A^{-1}(K_{o2} - K_{o3}(K_{o1} - K_{o3}))\tilde{X} - A^T\tilde{X} + \xi_1 \quad (19)$$

with  $\xi_1$  a vector of positive constants containing a number of error terms. In (18), note that  $\dot{A}^{-1}$  denotes the derivative of  $A^{-1}$  rather than the inverse of  $\dot{A}$ . These equations are useful for proving Theorem 1, which is now introduced.

*Theorem 1 (Boundedness of observer estimation errors).* Given the observer defined in (14), (15), and (16), with NN weight update law as given in (17), then there are positive gains  $K_{o1}, K_{o2}, K_{o3}$  for which  $K_{o1} > K_{o3}$ ,  $K_{o3} > 2N_o/\kappa_{o1}$ ,  $K_{o2} = K_{o3}(K_{o1} - K_{o3})$ , where  $N_o$  is the number of hidden layer neurons, such that the observer estimation error  $\tilde{X}$ , as well as  $\tilde{V}$  and  $\tilde{W}_o$  are UUB, with bounds

$$\|\tilde{X}\| > \sqrt{\frac{2\eta_o}{K_{o1} - K_{o3}}} \text{ or } \|\tilde{V}\| > \sqrt{\eta_o / \left( \frac{K_{o3}}{2} - \frac{N_o}{\kappa_{o1}} \right)} \text{ or } \|\tilde{W}_o\|_F > \sqrt{2\eta_o / \kappa_{o1}}. \text{ In addition, selecting}$$

the values of  $K_{o1}, K_{o2}, K_{o3}$  and  $\kappa_{o1}$  allows the bound on the errors to be made arbitrarily small. Proof is provided in the appendix.



**1.4.4. Virtual Controller.** The next step is to design the virtual controller, which is used to obtain the virtual control output or desired input  $u_d = [\zeta w_{1d} w_{2d} w_{3d}]^T$ . This process is performed by first defining a set of error terms. The first,  $\delta_1 = \rho_d - \rho$ , was introduced with the kinematic controller. The second error term to be minimized is  $\hat{\delta}_2 = m(\hat{v} - v_d)$ , with  $\hat{\delta}_2$  a velocity tracking error that incorporates the helicopter's mass. The third and fourth errors to be considered are  $\epsilon_3 = \phi_d - \phi$  and  $\epsilon_4 = \dot{\phi} - \dot{\phi}_d$ , with  $\phi_d$  the desired heading, which consider the error in the helicopter's heading and the rate at which this error is changing. A fifth error term considers the error in the thrust and may be expressed as

$$\hat{\delta}_3 = m\bar{g}e_3 - m\dot{v}_d + \hat{\delta}_2 + \frac{1}{m}\delta_1 - \zeta R(\Theta)e_3 \quad (20)$$

with all of the variables in (20) as previously defined. For convenience, a term

$$Y_d = \hat{\delta}_2 + \hat{\delta}_3 + \frac{d}{dt}(m\bar{g}e_3 - m\dot{v}_d + \hat{\delta}_2 + \frac{1}{m}\delta_1) \quad (21)$$

is introduced prior to the final error term necessary for this development, which allows this final error term to be written as

$$\hat{\delta}_4 = Y_d - (\dot{\zeta} R(\Theta)e_3 + \zeta R(\Theta)skew(\hat{\omega})e_3) \quad (22)$$

The choice of these particular error terms is analyzed in further detail in [7]. Selecting

$$\tilde{\zeta} R(\Theta)e_3 - \zeta R(\Theta)skew(e_3)\tilde{w}_d = \hat{\delta}_3 + \hat{\delta}_4 + \dot{Y}_d - 2\dot{\zeta} R(\Theta)skew(\hat{\omega})e_3 \quad (23)$$

to be solved for control of the main rotor thrust, pitch, and roll, and

$$\ddot{\phi} = \ddot{\phi}_d - \epsilon_3 - \epsilon_4 \quad (24)$$

to be solved for control of the yaw [7], a solution for both equations is

$$\begin{bmatrix} \tilde{w}_{1d} \\ \tilde{w}_{2d} \\ \tilde{\zeta} \end{bmatrix} = \begin{bmatrix} 0 & \zeta & 0 \\ -\zeta & 0 & 0 \\ 0 & 0 & 1 \end{bmatrix}^{-1} R(\Theta)^T (\dot{Y}_d - 2\dot{\zeta} R(\Theta) \text{skew}(\hat{\omega}) e_3 + \hat{\delta}_3 + \hat{\delta}_4) \quad (25)$$

from which  $\tilde{w}_{1d}$ ,  $\tilde{w}_{2d}$ , and  $\tilde{\zeta}$  may be obtained (with  $\tilde{\zeta}$  obtained recursively). This

solution was obtained by making use of the property  $\text{skew}(e_3)\tilde{w}_d = e_3 \times \tilde{w}_d = -\text{skew}(\tilde{w}_d)e_3$ ,

and rearranging and rewriting (23). Defining the relationship between the angular

velocity and the orientation as

$$\dot{\Theta} = \frac{1}{\cos(\theta)} \begin{pmatrix} 0 & s_\psi & c_\psi \\ 0 & c_\theta c_\psi & -c_\theta s_\psi \\ c_\theta & s_\theta s_\psi & s_\theta c_\psi \end{pmatrix} \hat{\omega} = T^{-1} \hat{\omega} \quad (26)$$

it is now possible to rearrange (8) in terms of  $\hat{\omega}$  and set  $\hat{\omega} = \tilde{w}_d$ , while considering only

the virtual control inputs. Doing this yields

$$\tilde{w}_d = -\mathcal{J}^{-1} \hat{\omega} \times \mathcal{J} \hat{\omega} + |Q_M| \mathcal{J}^{-1} e_3 - |Q_T| \mathcal{J}^{-1} e_2 + \mathcal{J}^{-1} P w_d$$
 Taking the derivative of (26),

rearranging, and considering only the yaw (first element in orientation vector) results in

$$\ddot{\phi} = -e_1^T T^{-1} \dot{T} T^{-1} \hat{\omega} + \frac{1}{c_\theta} (s_\psi \tilde{w}_{2d} + c_\psi \tilde{w}_{3d}) \quad (27)$$

Then, employing both (24) and (27) and rearranging allows  $\tilde{w}_{3d}$  to be obtained as

$$\tilde{w}_{3d} = \frac{c_\theta}{c_\psi} (\ddot{\phi}_d - \epsilon_4 - \epsilon_3 + e_1^T T^{-1} \dot{T} T^{-1} \hat{\omega} - \frac{s_\psi}{c_\theta} \tilde{w}_{2d}) \quad (28)$$

Now the real inputs are obtained. To do this, first restate a portion of the dynamics to

obtain  $w_d$  from (8) as  $w_d = P^{-1} (\mathcal{J} \tilde{w}_d + \hat{\omega} \times \mathcal{J} \hat{\omega} - Q_M e_3 + Q_T e_2)$  with  $P = \text{diag}([p_{11} \ p_{22} \ p_{33}]^T)$  a

set of gains, and then obtain  $\zeta$  by double-integrating from  $\ddot{\zeta} = \tilde{\zeta}$  by using the value that

has just been obtained for  $\tilde{\zeta}$ . Combining the preceding results allows one to obtain the feedforward portion of the control input as

$$u_d = [\zeta \ w_{1d} \ w_{2d} \ w_{3d}]^T \quad (29)$$

from the values that have just been obtained for  $\zeta$ ,  $w_{1d}$ ,  $w_{2d}$ , and  $w_{3d}$ . Proof that the inputs generated by these equations assures convergence is provided in the Appendix.

**1.4.5. Hamilton-Jacobi-Bellman Equation.** In this section, based on the information provided by the kinematic controller, the optimal control input  $u_e^*$  is designed to ensure that the unmanned helicopter system in (1) tracks a desired trajectory  $X_d(t)$  in an optimal manner. This work extends that of [12] to output feedback control. For optimal tracking, the desired dynamics are defined as

$$\dot{V}_d = f(V_d) + g u_v^* \quad (30)$$

where  $f(V_d) \in \mathbb{R}^{6 \times 1}$  is the internal dynamics of the helicopter system rewritten in terms of the desired state  $V_d \in \mathbb{R}^{6 \times 1}$ ,  $g$  is bounded satisfying  $g_{min} \leq \|g\|_F \leq g_{max}$ , and  $u_v^* \in \mathbb{R}^{6 \times 1}$  is the desired control input corresponding to the desired states. For reference,  $g$  is provided here explicitly as

$$g = M^{-1} \begin{bmatrix} E_3^b & 0^{3 \times 3} \\ 0^{3 \times 1} & diag([p_{11} \ p_{22} \ p_{33}]) \end{bmatrix} \quad (31)$$

For this system,  $e = 0$  is a unique equilibrium point on compact set  $\Upsilon \subset \mathbb{R}^{6 \times 1}$  with  $f(0) = 0$ . By adding the feedforward term as will be presented later in this paper, however, it is possible to neglect the  $f(0) = 0$  requirement. Under these conditions, the

optimal control input for the unmanned helicopter system given in (30) can be determined [8]. Next, the state tracking error is defined as

$$e = \hat{V} - V_d \quad (32)$$

Now, taking the derivative of (32), considering the estimated dynamics  $\dot{\hat{V}} = f(\hat{V}) + gu_v$ , and including (30), the tracking error dynamics in (32) can be written as

$$\dot{e} = f(\hat{V}) + gu_v - \dot{V}_d = f_e(e) + gu_e \quad (33)$$

where  $f_e(e) = f(\hat{V}) - f(V_d)$  and  $u_e = u_v - u_v^*$ . The dynamics  $f_e(e)$  and  $g$  are assumed to be known throughout this paper; however, this assumption may be relaxed if the uncertainties are estimated online using NNs. In order to control (33) in an optimal manner, the control policy  $u_e$  should be selected such that it minimizes the cost function given by

$$W_T(e(t)) = \int_t^\infty r(e(\tau), u_e(\tau)) d\tau \quad (34)$$

where  $r(e(\tau), u_e(\tau)) = Q(e) + u_e^T B u_e$  and  $Q(e) > 0$  is the penalty on the states, with  $B \in \mathbb{R}^{6 \times 6}$  a positive semi-definite matrix. After this, the Hamiltonian for the HJB tracking problem is defined as

$$H_T(e, u_e) = r(e, u_e) + W_{T_e}^T(e)(f_e(e) + gu_e) \quad (35)$$

where  $W_{T_e}(e)$  is the gradient of  $W_T(e)$  with respect to  $e$ . The basis function used for the neural network is

$$\Phi(e) = [\nabla e \quad \nabla e^2 \quad \nabla e^3 \quad \nabla \sin(e) \quad \nabla \sin(2e) \quad \nabla \tanh(e) \quad \nabla \tanh(2e)]^T, \text{ with system}$$

errors bounded such that  $\|\Phi(e)\| \leq \Phi_M$  and  $\|\nabla_e \Phi(e)\| \leq \Phi'_M$ , which is true for any real

helicopter as long as the observer error is bounded, and is true for any physically realizable trajectory. Now, applying stationarity condition  $\partial H(e, u_e) / \partial u_e = 0$ , the optimal control input is found to be

$$u_e^*(e) = -B^{-1}g^T W_{Te}^*(e) / 2 \quad (36)$$

with  $u_e^*(e) \in \mathbb{R}^4$ . Substituting the optimal control input from (36) into the Hamiltonian (35) generates the HJB equation for the tracking problem as

$$0 = Q_e(e) + W_{Te}^{*T}(e) f_e(e) - W_{Te}^{*T}(e) g B^{-1} g^T W_{Te}^*(e) / 4 \quad (37)$$

with  $W_T^*(0)$ . The control input must be selected such that the cost function in (34) is finite, and it is assumed that there is an admissible controller [12]. At this point, Lemma 2 is introduced.

*Lemma 2 (Boundedness of system state errors)* [12]. Given the unmanned helicopter system with cost function (34) and optimal control input (36), let  $J_1(e)$  be a continuously differentiable, radially unbounded Lyapunov candidate function such that  $\dot{J}_1(e) = J_{1e}^T(e) \dot{e} = J_{1e}^T(e) (f_e(e) + g u_e^*) < 0$  with  $J_{1e}(e)$  the partial derivative of  $J_1(e)$ . In addition, let  $\bar{Q}(e) \in \mathbb{R}^{6 \times 6}$  be a positive definite matrix satisfying  $\|\bar{Q}(e)\| = 0$  only if  $\|e\| = 0$  and  $\bar{Q}_{min} \leq \|\bar{Q}(e)\| \leq \bar{Q}_{max}$  for  $e_{min} \leq \|e\| \leq e_{max}$  for positive constants  $\bar{Q}_{min}$ ,  $\bar{Q}_{max}$ ,  $e_{min}$ , and  $e_{max}$ . Also, let  $\bar{Q}(e)$  satisfy  $\lim_{e \rightarrow \infty} \bar{Q}(e) = \infty$  as well as

$$W_e^{*T} \bar{Q}(e) J_{1e} = r(e, u_e^*) = Q(e) + u_e^{*T} B u_e^* \quad (38)$$

then the following relation is true

$$J_{1e}^T (f_e(e) + g u_e^*) = -J_{1e}^T \bar{Q}(e) J_{1e} \quad (39)$$

Proof for Lemma 2 is provided in the Appendix.

Next, it is apparent that an expression including the optimally augmented control input in (36) can be written as

$$u_v = u_d - B^{-1}g^T W_{Te}^*(e) / 2 \quad (40)$$

with the desired feedforward control input  $u_d$  obtained from the virtual controller in the previous section. Next, the SOLA is introduced.

**1.4.6. Single Online Approximator (SOLA)-Based Optimal Control of Helicopter.** Usually, in adaptive-critic based techniques, two OLAs [12] are used for optimal control, with one used to approximate the cost function while the other is used to generate the control action. In this paper, the adaptive critic for optimal control of a helicopter is realized online using a single OLA. For the SOLA to learn the cost function, the cost function is rewritten using the OLA representation as

$$W(e) = \Gamma^T \Phi(e) + \varepsilon \quad (41)$$

where  $\Gamma$  is the constant target OLA vector,  $\Phi(e)$  is a linearly independent basis vector that satisfies  $\Phi(e) = 0$ , and  $\varepsilon$  is the OLA reconstruction error. The basis vector used in this case is the same as in the previous section. The target OLA vector and reconstruction errors are assumed to be upper bounded according to  $\|\Gamma\| \leq \Gamma_M$  and  $\|\varepsilon\| \leq \varepsilon_M$ ,

respectively [15]. The gradient of the OLA cost function in (41) is written as

$$\partial W(e) / \partial e = W_e(e) = \nabla_e^T \Phi(e) \Gamma + \nabla_e \varepsilon \quad (42)$$

Using (42), the optimal control input in (36) and the HJB equation in (37) can be written as

$$\begin{aligned} u_e^* &= -B^{-1}g^T \nabla_e^T \Phi(e) \Gamma / 2 - B^{-1}g^T \nabla_e \varepsilon / 2 \\ H^*(e, \Gamma) &= Q(e) + \Gamma^T \nabla_e \Phi(e) f_e(e) - \Gamma^T \nabla_e \Phi(e) C \nabla_e^T \Phi(e) \Gamma / 4 + \varepsilon_{HJB} = 0 \end{aligned} \quad (43)$$

where  $C = gB^{-1}g^T > 0$  is bounded such that  $C_{min} \leq \|C\| \leq C_{max}$  for known constants  $C_{min}$  and  $C_{max}$  and

$$\begin{aligned}\varepsilon_{HJB} &= \nabla_e \varepsilon^T (f_e(e) - \frac{1}{2} C (\nabla_e^T \Phi(e) \Gamma + \nabla_e \varepsilon)) + \frac{1}{4} \nabla_e \varepsilon^T C \nabla_e \varepsilon \\ &= \nabla_e \varepsilon^T (f_e(e) + g u_e^*) + \frac{1}{4} \nabla_e \varepsilon^T C \nabla_e \varepsilon\end{aligned}\quad (44)$$

is the OLA reconstruction error. The OLA estimate of (41) is

$$\hat{W}(e) = \hat{\Gamma}^T \Phi(e) \quad (45)$$

with  $\hat{\Gamma}$  the OLA estimate of the target vector  $\Gamma$ . In the same way, the estimate for the optimal control input based on (43) in terms of  $\hat{\Gamma}$  can be expressed as

$$\hat{u}_e^* = -B^{-1} g^T \nabla_e^T \Phi(e) \hat{\Gamma} / 2 \quad (46)$$

The overall control input

$$\hat{u}_v = u_d + \hat{u}_e \quad (47)$$

is therefore now based on the NN estimate.

Lyapunov analysis performed in the appendix to this work shows that the estimated control inputs approach the optimal control inputs with a bounded error.

Employing (43) and (45), the approximate Hamiltonian may now be written as

$$\hat{H}^*(e, \hat{\Gamma}) = Q(e) + \hat{\Gamma}^T \nabla_e \Phi(e) f_e(e) - \hat{\Gamma}^T \nabla_e \Phi(e) C \nabla_e^T \Phi(e) \hat{\Gamma} / 4 \quad (48)$$

Considering the definition of the OLA approximation of the cost function (45) and the Hamiltonian function (48), it is clear that both converge to zero when  $\|e\| = 0$ .

Consequently, once the system state errors have converged to zero, the cost function approximation is no longer updated [15]. Recollecting the HJB equation in (35), the OLA estimate  $\hat{\Gamma}$  should be tuned to minimize  $\hat{H}^*(e, \hat{\Gamma})$ . However, merely tuning  $\hat{\Gamma}$  to

minimize  $\hat{H}^*(e, \hat{\Gamma})$  does not ensure the stability of the nonlinear helicopter system during the OLA learning process.

Therefore, the OLA tuning algorithm [12] is designed to minimize (48) while considering the system stability and is given below

$$\begin{aligned} \dot{\hat{\Gamma}} = & -\alpha_1 \frac{\hat{\beta}}{(\hat{\beta}^T \hat{\beta} + 1)^2} (Q(e) + \hat{\Gamma}^T \nabla_e \Phi(e) f_e(e) \\ & - \hat{\Gamma}^T \nabla_e \Phi(e) C \nabla_e^T \Phi(e) \hat{\Gamma} / 4) + \Sigma(e, \hat{u}_e^*) 0.5 \alpha_2 \nabla_e \Phi(e) C J_{1e}(e) \end{aligned} \quad (49)$$

where  $\hat{\beta} = \nabla_e \Phi(e) f_e(e) - \nabla_e \Phi(e) C \nabla_e^T \Phi(e) \hat{\Gamma} / 2$ ,  $\alpha_1 > 0$  and  $\alpha_2 > 0$  are design constants,

$J_{1e}(e)$  is defined in *Lemma 2*, and the operator  $\Sigma(e, \hat{u}_e^*)$  is given by

$$\Sigma(e, \hat{u}_e^*) = \begin{cases} 0 & \text{if } J_{1e}^T(e) \dot{e} = J_{1e}^T(e) \\ & (f_e(e) - g B^{-1} g^T \nabla_e^T \Phi(e) \hat{\Gamma} / 2) < 0 \\ 1 & \text{otherwise} \end{cases} \quad (50)$$

Note that the weight update law is different than that in [12] as it is based on the observer's estimate of the states, rather than on the actual states themselves. The first term in (49) is the portion of the tuning law which minimizes (48) and is derived using a normalized gradient descent scheme with the auxiliary HJB error defined as below

$$E_{HJB} = (\hat{H}^*(e, \hat{\Gamma}))^2 / 2 \quad (51)$$

The second term in the OLA tuning law in (49) ensures that the system states remain bounded while the SOLA scheme learns the optimal cost function.

The dynamics of the OLA parameter estimation error is considered as  $\tilde{\Gamma} = \Gamma - \hat{\Gamma}$ . Since this yields  $Q(e) = -\Gamma^T \nabla_e \Phi(e) f_e(e) + \Gamma^T \nabla_e \Phi(e) C \nabla_e^T \Phi(e) \Gamma / 4 - \varepsilon_{HJB}$  from (43), the approximate HJB equation in (48) can be expressed in terms of  $\tilde{\Gamma}$  as



$$\begin{aligned} \hat{H}(e, \hat{\Gamma}) &= -\tilde{\Gamma}^T \nabla_e \Phi(e) f_e(e) + \frac{1}{2} \tilde{\Gamma}^T \nabla_e \Phi(e) C \nabla_e^T \Phi(e) \Gamma \\ &\quad - \frac{1}{4} \tilde{\Gamma}^T \nabla_e \Phi(e) C \nabla_e^T \Phi(e) \tilde{\Gamma} - \varepsilon_{HJB} \end{aligned} \quad (52)$$

Then, since  $\dot{\tilde{\Gamma}} = \hat{\Gamma}$  and  $\hat{\beta} = \nabla_e \Phi(e)(\dot{e}^* + C \nabla_e \varepsilon / 2) + \nabla_e \Phi(e) C \nabla_e^T \Phi(e) \tilde{\Gamma} / 2$ , where

$\dot{e} = f_e(e) + g u_e$ , the error dynamics of (49) are

$$\begin{aligned} \dot{\tilde{\Gamma}} &= \frac{\alpha_1}{\rho_1^2} \left( \nabla_e \Phi(e) \left( \dot{e}_1^* + \frac{C \nabla_e \varepsilon}{2} \right) + \frac{\nabla_e \Phi(e) C \nabla_e^T \Phi(e) \tilde{\Gamma}}{2} \right) \\ &\quad \left( \tilde{\Gamma}^T \nabla_e \Phi(e) \left( \dot{e}_1^* + \frac{C \nabla_e \varepsilon}{2} \right) + \frac{\tilde{\Gamma}^T \nabla_e \Phi(e) C \nabla_e^T \Phi(e) \tilde{\Gamma}}{2} + \varepsilon_{HJB} \right) \\ &\quad - \Sigma(e, \hat{u}_e^*) \frac{\alpha_2}{2} \nabla_e \Phi(e) g B^{-1} g^T J_{1e}(e) \end{aligned} \quad (53)$$

where  $\rho_1 = (\hat{\beta}^T \hat{\beta} + 1)$ . Next, it is necessary to examine the stability of the SOLA-based adaptive scheme for optimal control along with the stability of the helicopter system.

**1.4.7. Stability Analysis.** The proofs to be introduced shortly are built on the basis of the work of [7] and [12]. It is found that the control input consists of a predetermined feedforward term and an optimal feedback term that is a function of the gradient of the optimal cost function. In order to implement the optimal control in (34), the SOLA based control law is used to learn the optimal feedback tracking control after necessary modifications, such that the OLA tuning algorithm is able to minimize the Hamiltonian while maintaining the stability of the helicopter system.

Lemma 2 has been introduced already and gives the boundedness of  $\|J_{1e}\|$  and therefore the system state errors, which is necessary for Theorem 3. First, however, a definition is needed.

*Definition:* An equilibrium point  $e_e$  is said to be uniformly ultimately bounded (UUB) if there exists a compact set  $S \subset \mathbb{R}^n$  such that for every  $e_0 \in S$  there exists a bound  $D$  and time  $T(D, e_0)$  such that  $\|e(t) - e_e\| \leq D$  for all  $t \geq t_0 + T$ .

This definition will be used for Theorem 3, which will be provided shortly. Theorem 3 reveals that the SOLA convergence to the HJB function is UUB for tracking of the states and will establish the optimality of the SOLA-based adaptive critic controller feedback term. Lemma 4 will then be provided because it provides a stability condition needed for the proof for Theorem 5. Theorem 5 establishes the feedforward term stability and the stability of the entire resulting system.

*Theorem 3 (Optimality and convergence of the SOLA-based adaptive critic controller feedback term and boundedness of tracking error resulting from optimal control input [12].* Given the nonlinear helicopter UAV system defined in (1), with target HJB equation (37), let the SOLA tuning law be given by (49). Let the control input be given by (46). Then the velocity tracking error and NN parameter estimation errors of the cost function term are UUB for all  $t \geq t_0 + T$ , and the tracking error feedback system is controlled in a near optimal manner. That is,  $\|u_e^* - \hat{u}_e^*\| \leq \varepsilon_u$  for a small positive constant  $\varepsilon_u$ .

Theorem 3 is proven in identically the same way as the first two steps of Theorem 5, with proof to follow shortly for Theorem 5. For the proof of Theorem 5, Lemma 4 is needed.

*Lemma 4 (Stability condition).* If an affine nonlinear system is asymptotically stable and the cost function given in [12] is smooth, then the closed-loop dynamics are asymptotically stable [12].

*Theorem 5 (Overall system stability).* Given the unmanned helicopter system with target HJB equation (37), let the tuning law for the SOLA be given by (49), and let the feedforward control input be as in (29). Then there exist constants  $b_{J_e}$  and  $b_{\tilde{\Gamma}}$  such that the OLA approximation error  $\tilde{\Gamma}$  and  $\|J_{1e}(e)\|$  are UUB for all  $t \geq t_0 + T$  with ultimate bounds given by  $\|J_{1e}(e)\| \leq b_{J_e}$  and  $\|\tilde{\Gamma}\| \leq b_{\tilde{\Gamma}}$ . Further, OLA reconstruction error  $\|W^* - \hat{W}\| \leq \varepsilon_{r1}$  and  $\|u_v^* - \hat{u}_v^*\| \leq \varepsilon_{r2}$  for small positive constants  $\varepsilon_{r1}$  and  $\varepsilon_{r2}$ . Note that a logical extension of Theorem 5 is that because  $\|u_v^* - \hat{u}_v^*\| \leq \varepsilon_{r2}$ , it is also the case that  $\|V_d - V\| \leq \varepsilon_{r3}$ , for a positive constant  $\varepsilon_{r3}$ . This is true because the system has known dynamics, with the optimal control input  $u_v^*$  generating the desired states  $V_d$ , and the neural-network-based estimate of the optimal control input  $\hat{u}_v^*$  generating the actual states  $V$ .

## 1.5. SIMULATION RESULTS

Simulation results for the unmanned helicopter are presented in this section. All simulations are performed in Simulink and demonstrate the performance of the proposed control scheme when the helicopter is hovering, landing, and tracking trajectories. The simulations take into account the aerodynamic features presented as part of the helicopter model earlier in this paper. The constants used for simulation are  $\bar{g} = 9.8m/s^2$ ,  $m = 9.6kg$ ,  $p = \text{diag}([1.1 \ 1.1 \ 1.1]^T)$ ,  $\mathcal{J} = \text{diag}([0.4 \ 0.56 \ 0.29]^T) kg \cdot m^2$ ,  $\alpha_1 = 100$ ,

$\alpha_2 = 1$ ,  $l_t = 1.2m$  ( $x$ -axis dimension from the helicopter's center of gravity to the tail rotor),  $l_m = 0.27m$ ,  $Q_M = 0.002$ , and  $Q_T = 0.0002$ . The optimal controller used seven hidden layer neurons for all simulations in this section, with gains

$B = \text{diag}([0.1 \ 0.1 \ 0.1 \ 0.1 \ 0.001]^T)$ . The NN basis function is as given previously. All NN weights are initialized to zero except for the observer's weights, which are randomly

initialized. The observer NN uses five hidden layer neurons, with gains  $K_{o1} = 22$ ,

$K_{o2} = 121$ , and  $K_{o3} = 11$ ,  $F_o = 10$  and  $\kappa_{o1} = 1$ , and a basis function as previously given.

Figure 2.3 demonstrates the helicopter's ability to follow a trajectory in two dimensions while hovering. Figure 2.4 shows the helicopter's ability to track a trajectory in three dimensions. For the two plots in Figure 2.5 and Figure 2.6, the heading is changed mid-maneuver from 1 radian to -1 radian. Figure 2.5 provides a 3-D view of the helicopter performing a landing maneuver, showing both the position and orientation as the helicopter lands. Figure 2.6 provides a 3-D view of the helicopter performing a landing maneuver, but in this case shows the actual versus desired trajectories throughout the maneuver. Figure 2.7 and Figure 2.8 show the observer performance for tracking the system states in Figure 2.7 as well as for tracking the system outputs in Figure 2.8.

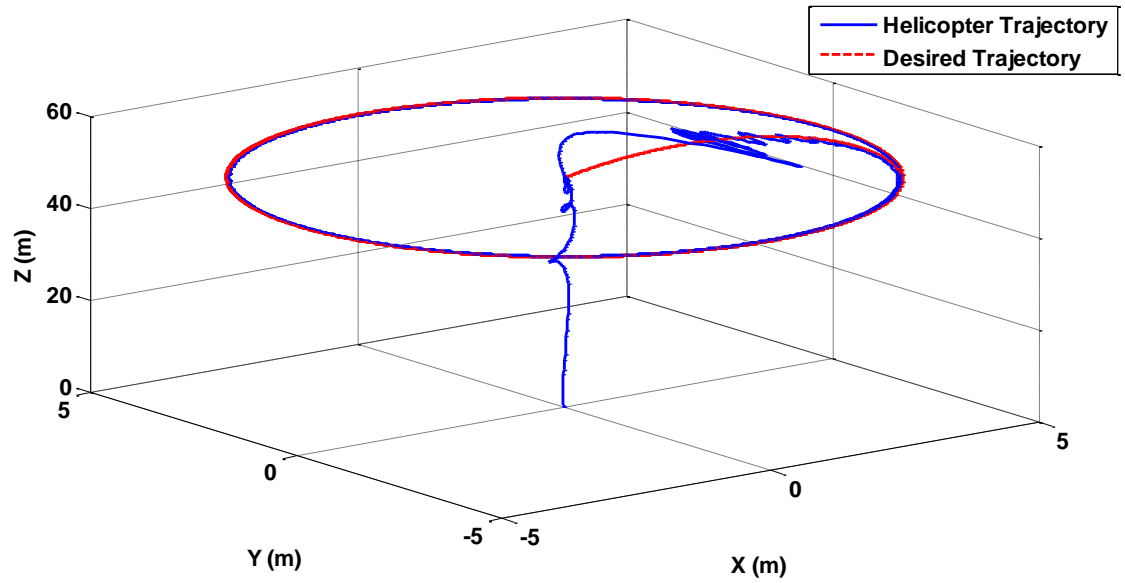


Figure 1.3. 3-D Perspective of Position during Take-off and Circular Maneuver

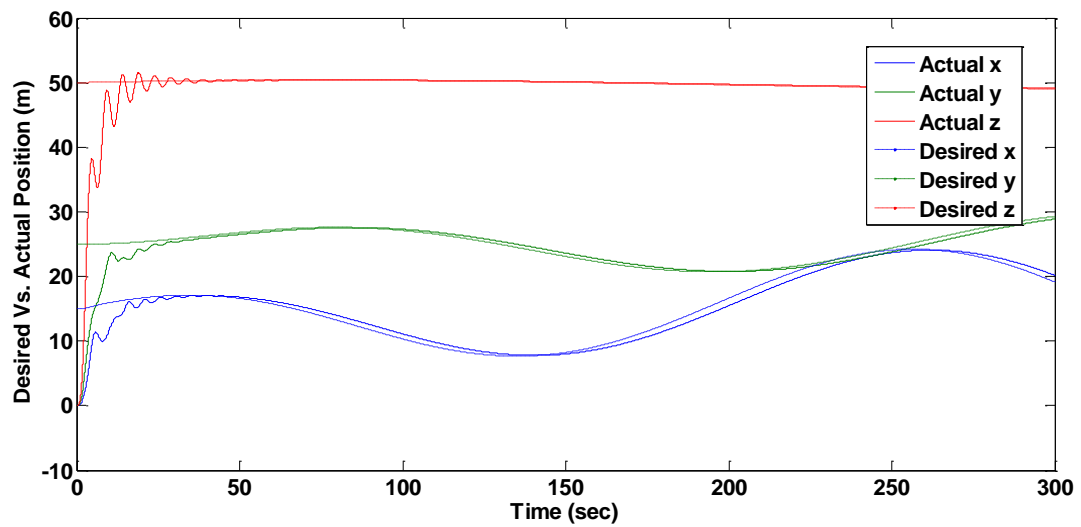


Figure 1.4. Helicopter Position Vs. Time for Tracking

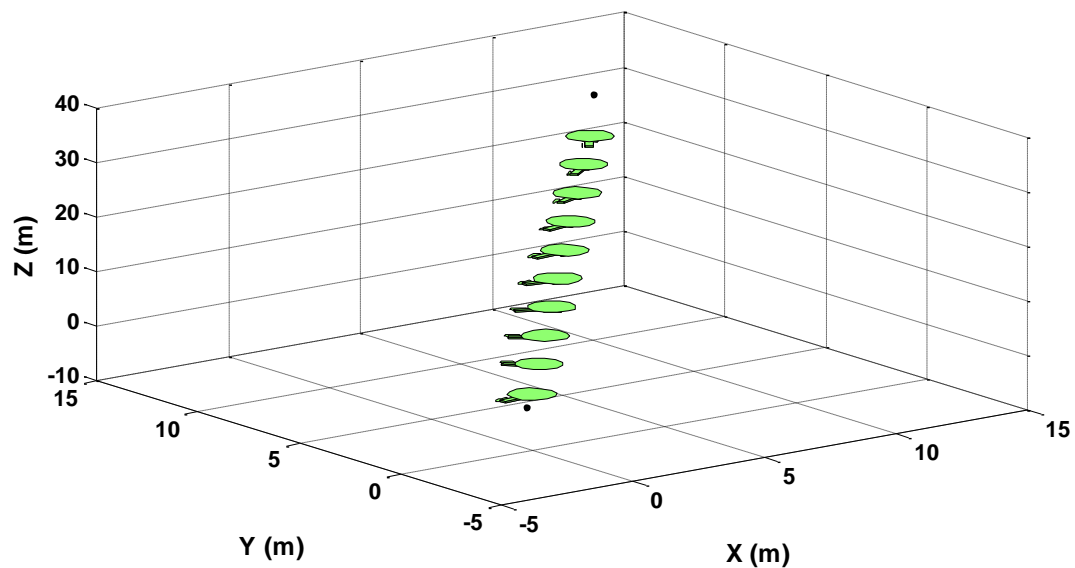


Figure 1.5. 3-D Perspective of Position and Orientation during Landing

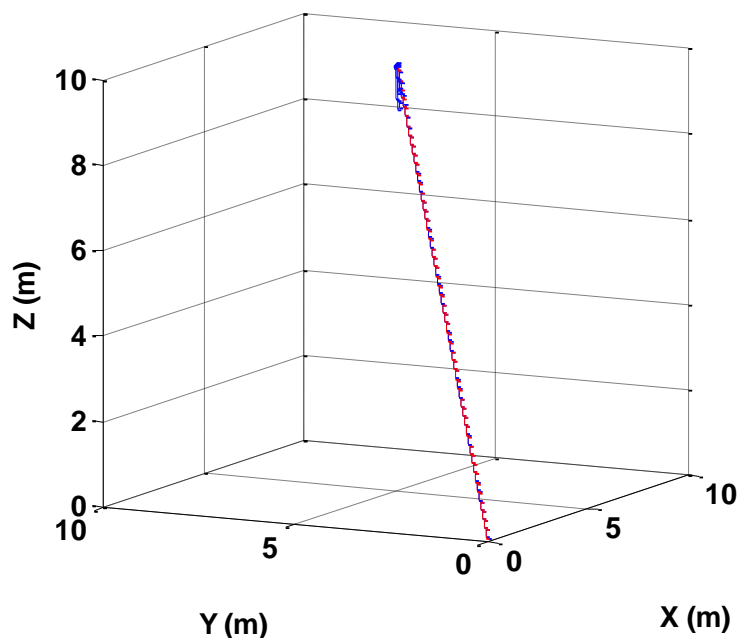


Figure 1.6. 3-D Perspective of Position during Landing

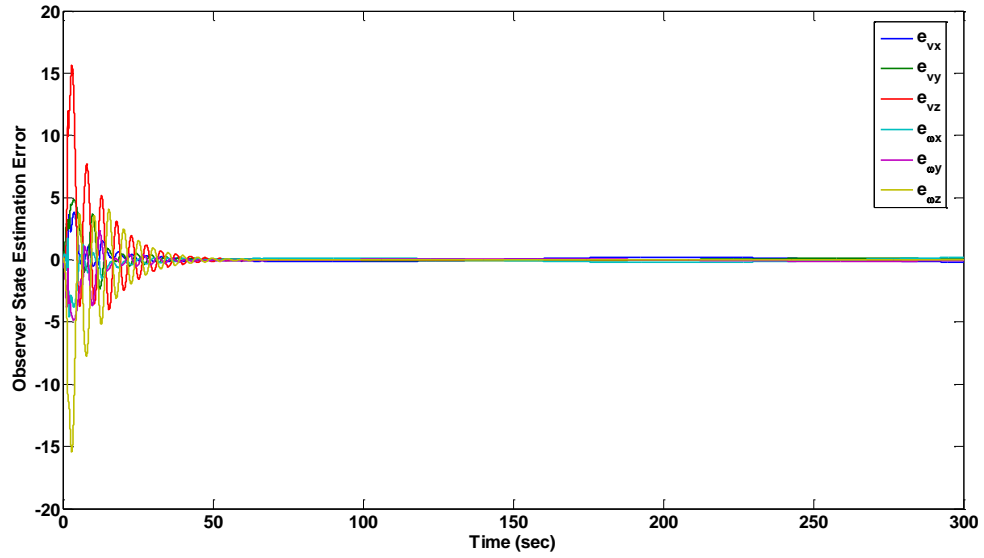


Figure 1.7. Observer State Estimation Error

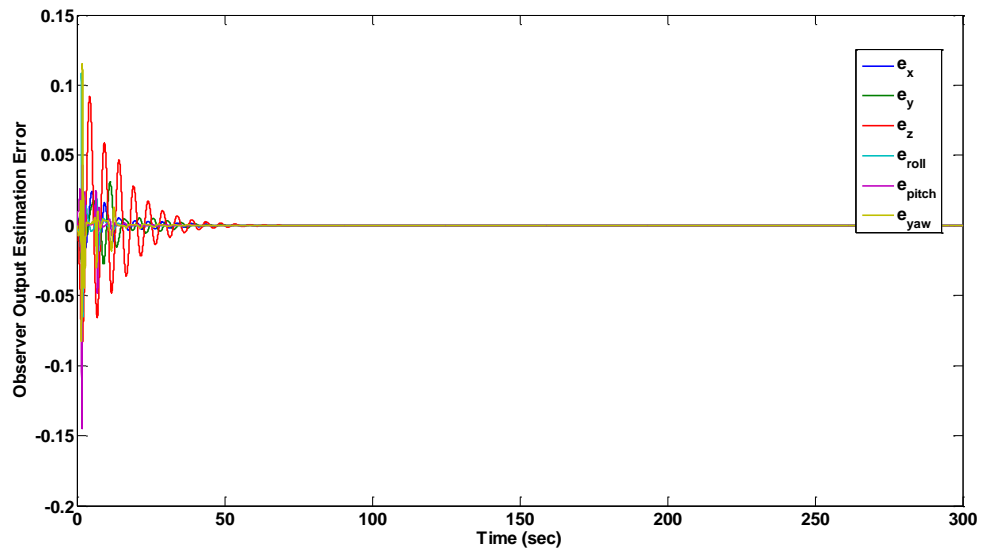


Figure 1.8. Observer Output Estimation Error

## 1.6. CONCLUSION

A NN-based optimal control law has been proposed which uses a single online approximator for optimal regulation and tracking control of an unmanned helicopter with known dynamics having a dynamic model in strict-feedback form. The SOLA-based adaptive approach is designed to learn the infinite horizon continuous-time HJB equation, and the corresponding optimal control input that minimizes the HJB equation is calculated forward-in-time. A feedforward controller has been introduced to compensate for the helicopter's weight and requirement for rotor thrust when in hover, and to permit trajectory tracking. Furthermore, it has been shown that the estimated control input approaches the target optimal control input with a small bounded error. A kinematic control structure has been used to obtain the desired velocity such that the desired position is achieved. A NN-based observer has been employed for obtaining the states from the outputs. The stability of the system has been analyzed, and simulation results confirm that the unmanned helicopter is capable of regulation and trajectory tracking.

## 1.7. REFERENCES

- [1] T. J. Koo and S. Sastry, "Output Tracking Control Design of a Helicopter Model Based on Approximate Linearization," *Proceedings of the 37th IEEE Conference on Decision and Control*, pp. 3635-3640, 1998.
- [2] B. F. Mettler, M. B. Tischler and T. Kanade, "System Identification Modelling of a Small-scale Rotorcraft for Flight Control Design," *International Journal of Robotics Research*, Vol. 20, pp. 795-807, 2000.
- [3] N. Hovakimyan, N. Kim, A. J. Calise, J. V. R. Prasad, "Adaptive Output Feedback for High-bandwidth Control of an Unmanned Helicopter," *Proceedings of AIAA Guidance, Navigation, and Control Conference*, Montreal, Canada, pp.1-11, 2001.



- [4] E. N. Johnson and S. K. Kannan, "Adaptive Trajectory Control for Autonomous Helicopters," *Journal of Guidance, Control and Dynamics*, Vol. 28, pp. 524-538, 2005.
- [5] B. Ahmed, H. R. Pota and M. Garratt, "Flight Control of a Rotary Wing UAV Using Backstepping," *International Journal of Robust and Nonlinear Control*, Vol. 20, pp. 639-658, 2010.
- [6] E. Frazzoli, M. A. Dahleh and E. Feron, "Trajectory Tracking Control Design for Autonomous Helicopters Using a Backstepping Algorithm," *Proceedings of American Control Conference*, pp. 4102-4107, 2000.
- [7] R. Mahoney and T. Hamel, "Robust Trajectory Tracking for a Scale Model Autonomous Helicopter," *International Journal of Robust and Nonlinear Control*, Vol. 14, pp. 1035-1059, 2004.
- [8] F. L. Lewis and V. L. Syrmos, "Optimal Control," 2nd ed. Wiley, Hoboken, NJ, 1995.
- [9] R. Enns and J. Si, "Helicopter Trimming and Tracking Control Using Direct Neural Dynamic Programming," *IEEE Transactions on Neural Networks*, Vol. 14, pp. 929-939, 2003.
- [10] S. Lee, C. Ha and B. S. Kim, "Adaptive Nonlinear Control System Design for Helicopter Robust Command Augmentation," *Aerospace Science and Technology*, Vol. 9, pp. 241-251, 2005.
- [11] T. Dierks and S. Jagannathan, "Optimal Control of Affine Nonlinear Discrete-time Systems. *Proceedings of the Mediterranean Conference on Control and Automation*, pp. 1390-1395, 2009.
- [12] T. Dierks and S. Jagannathan, "Optimal Control of Affine Nonlinear Continuous-time Systems. *Proceedings of American Control Conference*, pp. 1568-1573, 2010.
- [13] H.K. Khalil, "Nonlinear Systems," 3rd ed. Prentice-Hall, Upper Saddle River, NJ, 2002.
- [14] T. Dierks and S. Jagannathan, "Output Feedback Control of a Quadrotor UAV Using Neural Networks *IEEE Transactions on Neural Networks*, Vol. 21, pp. 50-66, 2010.
- [15] F. L. Lewis, S. Jagannathan, and A. Yesilderek, "Neural Network Control of Robot Manipulators and Nonlinear Systems," London, U.K., Taylor & Francis, 1999.

## 1.8. APPENDIX

Proof of Theorem 1: Begin with the Lyapunov candidate function

$$J_o = 0.5\tilde{X}^T \tilde{X} + 0.5\tilde{V}^T \tilde{V} + 0.5tr\{\tilde{W}_o^T F_o^{-1} \tilde{W}_o\} \quad (54)$$

Taking the derivative,

$$\dot{J}_o = 0.5\tilde{X}^T \dot{\tilde{X}} + 0.5\tilde{V}^T \dot{\tilde{V}} + 0.5tr\{\dot{\tilde{W}}_o^T F_o^{-1} \tilde{W}_o\} \quad (55)$$

Substituting the error dynamics from (18) and (19) along with the weight update law (17) into the derivative of the Lyapunov candidate function yields

$$\begin{aligned} \dot{J}_o = & \tilde{X}^T (A\tilde{V} - (K_{o1} - K_{o3})\tilde{X} + \xi) + \tilde{V}^T (-K_{o3}\tilde{V} + \tilde{f}_{o1} \\ & - A^{-1}K_{o2}\tilde{X} + A^{-1}K_{o3}(K_{o1} - K_{o3})\tilde{X} - A^T\tilde{X} + \xi_1) \\ & + tr\left\{\tilde{W}_o^T F_o^{-1} \left(-F_o\sigma(V_o^T x_o)\tilde{X}^T + \kappa_{o1}F_o\hat{W}_o\right)\right\} \end{aligned} \quad (56)$$

Defining  $\hat{\sigma}_o = \sigma(V_o^T \hat{x}_o)$  and expanding (56) results in

$$\begin{aligned} \dot{J}_o = & \tilde{X}^T A\tilde{V} - \tilde{X}^T (K_{o1} - K_{o3})\tilde{X} + \tilde{X}^T \xi - \tilde{V}^T K_{o3}\tilde{V} + \tilde{V}^T \tilde{f}_{o1} - \tilde{V}^T A^{-1}K_{o2}\tilde{X} \\ & + \tilde{V}^T A^{-1}K_{o3}(K_{o1} - K_{o3})\tilde{X} - \tilde{V}^T A^T\tilde{X} + \tilde{V}^T \xi_1 + tr\left\{\tilde{W}_o^T F_o^{-1} \left(-F_o\hat{\sigma}_o\tilde{X}^T + \kappa_{o1}F_o\hat{W}_o\right)\right\} \end{aligned} \quad (57)$$

Noting that  $K_{o2} = K_{o3}(K_{o1} - K_{o3})$  and cancelling out the two terms  $\tilde{X}^T A\tilde{V}$  and  $\tilde{V}^T A^T\tilde{X}$  as well as  $\tilde{V}^T A^{-1}K_{o2}\tilde{X}$  and  $\tilde{V}^T A^{-1}K_{o3}(K_{o1} - K_{o3})\tilde{X}$  reveals a simplified form of (57)

$$\begin{aligned} \dot{J}_o = & -\tilde{X}^T (K_{o1} - K_{o3})\tilde{X} + \tilde{X}^T \xi - \tilde{V}^T K_{o3}\tilde{V} + \tilde{V}^T \tilde{f}_{o1} \\ & + \tilde{V}^T \xi_1 + tr\left\{\tilde{W}_o^T F_o^{-1} \left(-F_o\hat{\sigma}_o\tilde{X}^T + \kappa_{o1}F_o\hat{W}_o\right)\right\} \end{aligned} \quad (58)$$

Using the fact that  $\tilde{f}_{o1} = \tilde{W}_o^T \sigma(V_o^T \hat{x}_o) = \tilde{W}_o^T \hat{\sigma}_o$  allows a term to be moved inside the trace function so that

$$\begin{aligned} \dot{J}_o = & -\tilde{X}^T (K_{o1} - K_{o3})\tilde{X} + \tilde{X}^T \xi - \tilde{V}^T K_{o3}\tilde{V} \\ & + \tilde{V}^T \xi_1 - tr\left\{\tilde{W}_o^T \left(\hat{\sigma}_o\tilde{X}^T - \hat{\sigma}_o\tilde{V}^T - \kappa_{o1}\tilde{W}_o\right)\right\} \end{aligned} \quad (59)$$

Next, bounds may be applied such that  $\|\hat{\sigma}_o\| \leq \sqrt{N_o}$ ,  $\|W_o\|_F \leq W_{Mo}$ , and

$\text{tr}\{\tilde{W}_o^T(W_o - \tilde{W}_o)\} \leq \|\tilde{W}_o\|_F W_{Mo} - \|\tilde{W}_o\|_F^2$ ,  $\|\xi\| \leq \xi_M$ , and  $\|\xi_1\| \leq \xi_{1M}$ . This allows (59) to be

upper-bounded such that

$$\begin{aligned} j_o \leq & -(K_{o1} - K_{o3})\|\tilde{X}\|^2 + \|\tilde{X}\|\xi_M - K_{o3}\|\tilde{V}\|^2 + \|\tilde{V}\|\xi_{1M} - \kappa_{o1}\|\tilde{W}_o\|_F^2 \\ & - \|\tilde{W}_o\|_F\|\tilde{X}\|\sqrt{N_o} + \|\tilde{W}_o\|_F\|\tilde{V}\|\sqrt{N_o} + \kappa_{o1}\|\tilde{W}_o\|_F W_{Mo} \end{aligned} \quad (60)$$

Rewriting the first two terms of (60)

$$-(K_{o1} - K_{o3})\|\tilde{X}\|^2 + \|\tilde{X}\|\xi_M = -\frac{(K_{o1} - K_{o3})}{2}\|\tilde{X}\|^2 - \frac{(K_{o1} - K_{o3})}{2}\left(\|\tilde{X}\|^2 - \frac{2\|\tilde{X}\|\xi_M}{K_{o1} - K_{o3}}\right) \quad (61)$$

Completing the square with respect to  $\|\tilde{X}\|$  results in

$$\begin{aligned} -(K_{o1} - K_{o3})\|\tilde{X}\|^2 + \|\tilde{X}\|\xi_M = & -\frac{(K_{o1} - K_{o3})}{2}\|\tilde{X}\|^2 - \\ & \frac{(K_{o1} - K_{o3})}{2}\left(\|\tilde{X}\| - \frac{\xi_M}{K_{o1} - K_{o3}}\right)^2 + \frac{\xi_M^2}{2(K_{o1} - K_{o3})} \end{aligned} \quad (62)$$

Repeating the process with the third and fourth terms of (60)

$$-K_{o3}\|\tilde{V}\|^2 + \|\tilde{V}\|\xi_{1M} = -\frac{K_{o3}}{2}\|\tilde{V}\|^2 - \frac{K_{o3}}{2}\left(\|\tilde{V}\|^2 - \frac{2\|\tilde{V}\|\xi_{1M}}{K_{o3}}\right) \quad (63)$$

Completing the square with respect to  $\|\tilde{V}\|$  results in

$$-\frac{K_{o3}}{2}\|\tilde{V}\|^2 - \frac{K_{o3}}{2}\left(\|\tilde{V}\| - \frac{\xi_{1M}}{K_{o3}}\right)^2 + \frac{\xi_{1M}^2}{2K_{o3}} \quad (64)$$

Then, rewriting the last four terms of (60)

$$\begin{aligned}
& -\kappa_{o1} \|\tilde{W}_o\|_F^2 - \|\tilde{W}_o\|_F \|\tilde{X}\| \sqrt{N_o} + \|\tilde{W}_o\|_F \|\tilde{V}\| \sqrt{N_o} + \kappa_{o1} \|\tilde{W}_o\|_F W_{Mo} \\
& = -\frac{\kappa_{o1}}{2} \|\tilde{W}_o\|_F^2 - \|\tilde{W}_o\|_F \|\tilde{X}\| \sqrt{N_o} - \frac{\kappa_{o1}}{4} \left( \|\tilde{W}_o\|_F^2 - \frac{4 \|\tilde{W}_o\|_F \|\tilde{V}\| \sqrt{N_o}}{\kappa_{o1}} \right) \\
& - \frac{\kappa_{o1}}{4} \left( \|\tilde{W}_o\|_F^2 - 4W_{Mo} \|\tilde{W}_o\|_F \right)
\end{aligned} \tag{65}$$

Completing the squares with respect to  $\|\tilde{W}_o\|_F$  allows the four terms in (65) to be

rewritten as

$$\begin{aligned}
& -\frac{\kappa_{o1}}{2} \|\tilde{W}_o\|_F^2 - \|\tilde{W}_o\|_F \|\tilde{X}\| \sqrt{N_o} - \frac{\kappa_{o1}}{4} \left( \|\tilde{W}_o\|_F - \frac{2 \|\tilde{V}\| \sqrt{N_o}}{\kappa_{o1}} \right)^2 \\
& + \frac{\|\tilde{V}\|^2 N_o}{\kappa_{o1}} - \frac{\kappa_{o1}}{4} \left( \|\tilde{W}_o\|_F - 2W_{Mo} \right)^2 + \kappa_{o1} W_{Mo}^2
\end{aligned} \tag{66}$$

Combining the above results in equations (62), (64), and (66) yields

$$\begin{aligned}
j_o \leq & -\frac{(K_{o1} - K_{o3})}{2} \|\tilde{X}\|^2 - \frac{(K_{o1} - K_{o3})}{2} \left( \|\tilde{X}\| - \frac{\xi_M}{K_{o1} - K_{o3}} \right)^2 + \frac{\xi_M^2}{2(K_{o1} - K_{o3})} - \frac{K_{o3}}{2} \|\tilde{V}\|^2 \\
& - \frac{K_{o3}}{2} \left( \|\tilde{V}\| - \frac{\xi_{1M}}{K_{o3}} \right)^2 + \frac{\xi_{1M}^2}{2K_{o3}} - \frac{\kappa_{o1}}{2} \|\tilde{W}_o\|_F^2 - \|\tilde{W}_o\|_F \|\tilde{X}\| \sqrt{N_o} - \frac{\kappa_{o1}}{4} \left( \|\tilde{W}_o\|_F - \frac{2 \|\tilde{V}\| \sqrt{N_o}}{\kappa_{o1}} \right)^2 \\
& + \frac{\|\tilde{V}\|^2 N_o}{\kappa_{o1}} - \frac{\kappa_{o1}}{4} \left( \|\tilde{W}_o\|_F - 2W_{Mo} \right)^2 + \kappa_{o1} W_{Mo}^2
\end{aligned} \tag{67}$$

A new positive-definite term  $\eta_o$  will be defined, such that

$\eta_o = \left( \xi_{1M}^2 / 2K_{o3} \right) + \kappa_{o1} W_{Mo}^2 + \left( \xi_M^2 / (2(K_{o1} - K_{o3})) \right)$ . This allows (67) to be rewritten as

$$\begin{aligned}
j_o \leq & -\frac{(K_{o1} - K_{o3})}{2} \|\tilde{X}\|^2 - \frac{(K_{o1} - K_{o3})}{2} \left( \|\tilde{X}\| - \frac{\xi_M}{K_{o1} - K_{o3}} \right)^2 - \frac{K_{o3}}{2} \|\tilde{V}\|^2 \\
& - \frac{K_{o3}}{2} \left( \|\tilde{V}\| - \frac{\xi_{1M}}{K_{o3}} \right)^2 - \frac{\kappa_{o1}}{2} \|\tilde{W}_o\|_F^2 - \|\tilde{W}_o\|_F \|\tilde{X}\| \sqrt{N_o} - \frac{\kappa_{o1}}{4} \left( \|\tilde{W}_o\|_F - \frac{2\|\tilde{V}\| \sqrt{N_o}}{\kappa_{o1}} \right)^2 \\
& + \frac{\|\tilde{V}\|^2 N_o}{\kappa_{o1}} - \frac{\kappa_{o1}}{4} \left( \|\tilde{W}_o\|_F - 2W_{Mo} \right)^2 + \eta_o
\end{aligned} \tag{68}$$

The terms

$$-\frac{(K_{o1} - K_{o3})}{2} \left( \|\tilde{X}\| - \frac{\xi_M}{K_{o1} - K_{o3}} \right)^2, \quad -\frac{K_{o3}}{2} \left( \|\tilde{V}\| - \frac{\xi_{1M}}{K_{o3}} \right)^2, \quad -\frac{\kappa_{o1}}{4} \left( \|\tilde{W}_o\|_F - \frac{2\|\tilde{V}\| \sqrt{N_o}}{\kappa_{o1}} \right)^2, \text{ and}$$

$$-\frac{\kappa_{o1}}{4} \left( \|\tilde{W}_o\|_F - 2W_{Mo} \right)^2 \text{ will be negative given proper selection of the gains, with the}$$

selection criteria as previously given. In addition, the term  $-\|\tilde{W}_o\|_F \|\tilde{X}\| \sqrt{N_o}$  will be negative, regardless of the observer tuning. Because these terms cannot cause instability, they may be omitted from the remainder of the analysis. This allows (68) to be simplified and expressed as

$$j_o \leq -\frac{(K_{o1} - K_{o3})}{2} \|\tilde{X}\|^2 - \frac{K_{o3}}{2} \|\tilde{V}\|^2 - \frac{\kappa_{o1}}{2} \|\tilde{W}_o\|_F^2 + \frac{\|\tilde{V}\|^2 N_o}{\kappa_{o1}} + \eta_o \tag{69}$$

Factoring terms and rearranging (69) results in

$$j_o \leq -\frac{(K_{o1} - K_{o3})}{2} \|\tilde{X}\|^2 - \left( \frac{K_{o3}}{2} - \frac{N_o}{\kappa_{o1}} \right) \|\tilde{V}\|^2 - \frac{\kappa_{o1}}{2} \|\tilde{W}_o\|_F^2 + \eta_o \tag{70}$$

Given  $K_{o1} > K_{o3}$  and  $K_{o3} > 2N_o / \kappa_{o1}$  and

$$\|\tilde{X}\| > \sqrt{\frac{2\eta_o}{K_{o1} - K_{o3}}} \tag{71}$$

or

$$\|\tilde{V}\| > \sqrt{\frac{\eta_o}{\left(\frac{K_{o3}}{2} - \frac{N_o}{\kappa_{o1}}\right)}} \quad (72)$$

or  $\|\tilde{W}_o\|_F > \sqrt{2\eta_o/\kappa_{o1}}$ , (70) will be negative definite, resulting in the conclusion that the observer estimation error  $\tilde{X}$ , as well as  $\tilde{V}$  and  $\tilde{W}_o$  are UUB. In addition, selecting the values of  $K_{o1}$ ,  $K_{o2}$ ,  $K_{o3}$  and  $\kappa_{o1}$  allows the bound on the errors to be made arbitrarily small.  $\square$

Proof of Lemma 2: Applying the optimal control input to an affine nonlinear system, the cost function becomes

$$\dot{W}^*(e) = W_e^{*T}(e)\dot{e} = W_e^{*T}(e)(f_e(e) + gu_e^*) = -Q_e(e) - u_e^{*T}Bu_e^* \quad (73)$$

Since

$$W_e^{*T}\bar{Q}_e(e)J_{1e} = r(e, u_e^*) = Q_e(e) + u_e^{*T}Bu_e^* \quad (74)$$

one may obtain

$$\begin{aligned} (f_e(e) + gu_e^*) &= -(W_e^*W_e^{*T})^{-1}W_e^*(Q_e(e) + u_e^{*T}Bu_e^*) = \\ &= -(W_e^*W_e^{*T})^{-1}W_e^*W_e^{*T}\bar{Q}_e(e)J_{1e} = -\bar{Q}_e(e)J_{1e} \end{aligned} \quad (75)$$

from which one then has

$$J_{1e}^T(f_e(e) + gu_e^*) = -J_{1e}^T\bar{Q}_e(e)J_{1e} \quad (76)$$

concluding the proof for Lemma 2.  $\square$

Theorem 3 is proved in the same manner as the first two steps of Theorem 5, which will be proved shortly. The proof of Lemma 4 is provided in [12].

Proof of Theorem 5: First, begin with the positive definite Lyapunov function candidate

$$\begin{aligned}
J = & \alpha_2 J_1(e) + \tilde{\Gamma}^T \tilde{\Gamma} / 2 + \delta_1^T \delta_1 / 2 + \hat{\delta}_2^T \hat{\delta}_2 / 2 + \hat{\delta}_3^T \hat{\delta}_3 / 2 + \epsilon_3^T \epsilon_3 / 2 \\
& + \hat{\delta}_4^T \hat{\delta}_4 / 2 + \epsilon_4^T \epsilon_4 / 2 + \tilde{X}^T \tilde{X} / 2 + \tilde{V}^T \tilde{V} / 2 + 0.5 \text{tr} \{ \tilde{W}_o^T F_o^{-1} \tilde{W}_o \}
\end{aligned} \tag{77}$$

The proof may then be divided into steps, with the first part of the Lyapunov function candidate considered first.

**Step 1:** consider the optimal control Lyapunov function candidate

$$J_{HJB} = \alpha_2 J_1(e) + \tilde{\Gamma}^T \tilde{\Gamma} / 2 \tag{78}$$

Differentiating, one obtains

$$\dot{J}_{HJB} = \alpha_2 J_{1e}^T(e) \dot{e} + \tilde{\Gamma}^T \dot{\tilde{\Gamma}} \tag{79}$$

With  $J_1(e)$  and  $J_{1e}(e)$  as previously given. If  $\|e\| = 0$ ,  $J_{HJB}(e) = \tilde{\Gamma}^T \tilde{\Gamma} / 2$ ,  $\dot{J}_{HJB}(e) = 0$ ,

and  $\|\tilde{\Gamma}\|$  remains a bounded constant. For online learning, however, it is the case that

$\|e\| > 0$ . For convenience, define  $\dot{e}_1^* = f_e(e) + g u_e^*$ . Then, using the affine nonlinear

system, the optimal control input, and the tuning law's error dynamics along with the

derivative of the Lyapunov candidate function  $J_{HJB}$ , one arrives at

$$\begin{aligned}
\dot{J}_{HJB} = & \alpha_2 J_{1e}^T(e) (f_e(e) - 0.5 g B^{-1} g^T \nabla_e^T \Phi(e) \hat{\Gamma}) - (\alpha_1 / \rho^2) (\tilde{\Gamma}^T \nabla_e \Phi(e) (\dot{e}_1^* + 0.5 C \nabla_e \mathcal{E}))^2 \\
& - (\alpha_1 / 8 \rho^2) (\tilde{\Gamma}^T \nabla_e \Phi(e) C \nabla_e^T \Phi(e) \tilde{\Gamma})^2 - (\alpha_1 / \rho^2) \tilde{\Gamma}^T \nabla_e \Phi(e) (\dot{e}_1^* + 0.5 C \nabla_e \mathcal{E}) \varepsilon_{HJB} \\
& - \frac{3\alpha_1}{4\rho^2} \tilde{\Gamma}^T \nabla_e \Phi(e) (\dot{e}_1^* + \frac{C \nabla_e \mathcal{E}}{2}) \tilde{\Gamma}^T \nabla_e \Phi(e) C \nabla_e^T \Phi(e) \tilde{\Gamma} \\
& - (\alpha_1 / 2 \rho^2) \tilde{\Gamma}^T \nabla_e \Phi(e) C \nabla_e^T \Phi(e) \tilde{\Gamma} \varepsilon_{HJB} - \Sigma(e, \hat{u}_e) 0.5 \alpha_2 \tilde{\Gamma}^T \nabla_e \Phi(e) g B^{-1} g^T J_{1e}^T(e)
\end{aligned} \tag{80}$$

For convenience, all terms excluding the first and last in (80) will be considered first:

$$\begin{aligned}
\dot{J}_2 = & -(\alpha_1 / \rho^2) \tilde{\Gamma}^T (\nabla_e \Phi(e) (\dot{e}_1^* + 0.5 C \nabla_e \mathcal{E}) + 0.25 \tilde{\Gamma}^T \nabla_e \Phi(e) C \nabla_e^T \Phi(e) \tilde{\Gamma} + \varepsilon_{HJB}) \\
& + 0.5 \nabla_e \Phi(e) C \nabla_e^T \Phi(e) (\tilde{\Gamma}^T \nabla_e \Phi(e) (\dot{e}_1^* + 0.5 C \nabla_e \mathcal{E}))
\end{aligned} \tag{81}$$

Multiplying through the  $\tilde{\Gamma}^T$  term in (81) yields

$$\begin{aligned} \dot{J}_2 = & -(\alpha_1/\rho^2)(\tilde{\Gamma}^T \nabla_e \Phi(e)(\dot{e}_1^* + 0.5C\nabla_e \varepsilon) + 0.5\tilde{\Gamma}^T \nabla_e \Phi(e)C\nabla_e^T \Phi(e)) \\ & (\tilde{\Gamma}^T \nabla_e \Phi(e)(\dot{e}_1^* + 0.5C\nabla_e \varepsilon) + 0.25\tilde{\Gamma}^T \nabla_e \Phi(e)C\nabla_e^T \Phi(e)\tilde{\Gamma} + \varepsilon_{HJB}) \end{aligned} \quad (82)$$

Expanding (82) results in

$$\begin{aligned} \dot{J}_2 = & -(\alpha_1/\rho^2)(\tilde{\Gamma}^T \nabla_e \Phi(e)(\dot{e}_1^* + 0.5C\nabla_e \varepsilon))^2 - (\alpha_1/8\rho^2)(\tilde{\Gamma}^T \nabla_e \Phi(e)C\nabla_e^T \Phi(e)\tilde{\Gamma})^2 \\ & - (3\alpha_1/4\rho^2)(\tilde{\Gamma}^T \nabla_e \Phi(e)(\dot{e}_1^* + 0.5C\nabla_e \varepsilon))(\tilde{\Gamma}^T \nabla_e \Phi(e)C\nabla_e^T \Phi(e)\tilde{\Gamma}) \\ & - (\alpha_1/\rho^2)(\tilde{\Gamma}^T \nabla_e \Phi(e)(\dot{e}_1^* + 0.5C\nabla_e \varepsilon))\varepsilon_{HJB} - (\alpha_1/2\rho^2)(\tilde{\Gamma}^T \nabla_e \Phi(e)C\nabla_e^T \Phi(e)\tilde{\Gamma})\varepsilon_{HJB} \end{aligned} \quad (83)$$

Completing the squares with respect to  $\tilde{\Gamma}^T \nabla_e \Phi(e)(\dot{e}_1^* + 0.5C\nabla_e \varepsilon)$  and

$\tilde{\Gamma}^T \nabla_e \Phi(e)C\nabla_e^T \Phi(e)\tilde{\Gamma}$  allows (83) to be rewritten as

$$\begin{aligned} \dot{J}_2 = & -(\alpha_1/2\rho^2)(\tilde{\Gamma}^T \nabla_e \Phi(e)(\dot{e}_1^* + 0.5C\nabla_e \varepsilon))^2 - (\alpha_1/16\rho^2)(\tilde{\Gamma}^T \nabla_e \Phi(e)C\nabla_e^T \Phi(e)\tilde{\Gamma})^2 \\ & + (\alpha_1/\rho^2)\varepsilon_{HJB}^2 - (3\alpha_1/4\rho^2)(\tilde{\Gamma}^T \nabla_e \Phi(e)(\dot{e}_1^* + 0.5C\nabla_e \varepsilon))(\tilde{\Gamma}^T \nabla_e \Phi(e)C\nabla_e^T \Phi(e)\tilde{\Gamma}) \\ & + (\alpha_1/2\rho^2)\varepsilon_{HJB}^2 - (\alpha_1/2\rho^2)(\tilde{\Gamma}^T \nabla_e \Phi(e)(\dot{e}_1^* + 0.5C\nabla_e \varepsilon) + \varepsilon_{HJB})^2 \\ & - (\alpha_1/16\rho^2)(\tilde{\Gamma}^T \nabla_e \Phi(e)C\nabla_e^T \Phi(e)\tilde{\Gamma} + 4\varepsilon_{HJB})^2 \end{aligned} \quad (84)$$

Now, because the terms  $-(\alpha_1/2\rho^2)(\tilde{\Gamma}^T \nabla_e \Phi(e)(\dot{e}_1^* + 0.5C\nabla_e \varepsilon) + \varepsilon_{HJB})^2$  and

$-(\alpha_1/16\rho^2)(\tilde{\Gamma}^T \nabla_e \Phi(e)C\nabla_e^T \Phi(e)\tilde{\Gamma} + 4\varepsilon_{HJB})^2$  are negative definite, they will not cause

instability and will therefore be neglected from the remainder of the analysis. Rewriting

(84) without these two terms yields

$$\begin{aligned} \dot{J}_2 \leq & -(\alpha_1/2\rho^2)(\tilde{\Gamma}^T \nabla_e \Phi(e)(\dot{e}_1^* + 0.5C\nabla_e \varepsilon))^2 - (\alpha_1/16\rho^2)(\tilde{\Gamma}^T \nabla_e \Phi(e)C\nabla_e^T \Phi(e)\tilde{\Gamma})^2 \\ & - (3\alpha_1/4\rho^2)(\tilde{\Gamma}^T \nabla_e \Phi(e)(\dot{e}_1^* + 0.5C\nabla_e \varepsilon))(\tilde{\Gamma}^T \nabla_e \Phi(e)C\nabla_e^T \Phi(e)\tilde{\Gamma}) + (\alpha_1/2\rho^2)\varepsilon_{HJB}^2 \\ & + (\alpha_1/\rho^2)\varepsilon_{HJB}^2 \end{aligned} \quad (85)$$

Completing the square with respect to  $\tilde{\Gamma}^T \nabla_e \Phi(e)C\nabla_e^T \Phi(e)\tilde{\Gamma}$  in (85) results in



$$\begin{aligned}
\dot{J}_2 \leq & -(\alpha_1/2\rho^2)(\tilde{\Gamma}^T \nabla_e \Phi(e)(\dot{e}_1^* + 0.5C\nabla_e \varepsilon))^2 - (\alpha_1/32\rho^2)(\tilde{\Gamma}^T \nabla_e \Phi(e)C\nabla_e^T \Phi(e)\tilde{\Gamma})^2 \\
& - (\alpha_1/8\rho^2)(0.5\tilde{\Gamma}^T \nabla_e \Phi(e)C\nabla_e^T \Phi(e)\tilde{\Gamma} + 6\tilde{\Gamma}^T \nabla_e \Phi(e)(\dot{e}_1^* + 0.5C\nabla_e \varepsilon))^2 \\
& + (9\alpha_1/2\rho^2)(\tilde{\Gamma}^T \nabla_e \Phi(e)(\dot{e}_1^* + 0.5C\nabla_e \varepsilon))^2 + (3\alpha_1/2\rho^2)\varepsilon_{HJB}^2
\end{aligned} \tag{86}$$

Because the fourth term in (86) is negative semi-definite, it will not cause instability and will therefore be neglected from the remainder of the analysis. In addition, the first and fifth terms in (86) will be summed before rewriting (86) as

$$\begin{aligned}
\dot{J}_2 \leq & -(\alpha_1/32\rho^2)(\tilde{\Gamma}^T \nabla_e \Phi(e)C\nabla_e^T \Phi(e)\tilde{\Gamma})^2 \\
& + (4\alpha_1/\rho^2)(\tilde{\Gamma}^T \nabla_e \Phi(e)(\dot{e}_1^* + 0.5C\nabla_e \varepsilon))^2 (3\alpha_1/2\rho^2)\varepsilon_{HJB}^2
\end{aligned} \tag{87}$$

Taking bounds on (87) results in

$$\begin{aligned}
\dot{J}_2 \leq & (3\alpha_1/2\rho^2)\varepsilon_{HJB}^2 - (\alpha_1/32\rho^2)\|\tilde{\Gamma}^T \nabla_e \Phi(e)\|^4 C_{\min}^2 \\
& + (4\alpha_1/\rho^2)\|\tilde{\Gamma}^T \nabla_e \Phi(e)\|^2 \|\dot{e}_1^* + 0.5C\nabla_e \varepsilon\|^2
\end{aligned} \tag{88}$$

Completing the square with respect to  $\|\tilde{\Gamma}^T \nabla_e \Phi(e)\|^2$  in (88) results in

$$\begin{aligned}
\dot{J}_2 \leq & (3\alpha_1/2\rho^2)\varepsilon_{HJB}^2 - (\alpha_1/64\rho^2)\|\tilde{\Gamma}^T \nabla_e \Phi(e)\|^4 C_{\min}^2 \\
& - \frac{\alpha_1 C_{\min}^2}{\rho^2} \left( \frac{\|\tilde{\Gamma}^T \nabla_e \Phi(e)\|^2}{8} - \frac{16}{C_{\min}^2} \|\dot{e}_1^* + 0.5C\nabla_e \varepsilon\|^2 \right)^2 + (256\alpha_1/\rho^2 C_{\min}^2) \|\dot{e}_1^* + 0.5C\nabla_e \varepsilon\|^4
\end{aligned} \tag{89}$$

Because the fourth term in (89) is negative semi-definite, it will not cause instability and will therefore be neglected from the remainder of the analysis. Rewriting (89)

$$\begin{aligned}
\dot{J}_2 \leq & (3\alpha_1/2\rho^2)\varepsilon_{HJB}^2 - (\alpha_1/64\rho^2)\|\tilde{\Gamma}^T \nabla_e \Phi(e)\|^4 C_{\min}^2 \\
& + (256\alpha_1/\rho^2 C_{\min}^2) \|\dot{e}_1^* + 0.5C\nabla_e \varepsilon\|^4
\end{aligned} \tag{90}$$

Applying the Pythagorean Theorem, noting that  $\varepsilon_M'$  is an upper bound such that

$\|\nabla_e \mathcal{E}\| \leq \varepsilon'_M$ , and employing the relationship  $|\varepsilon_{HJB}| \leq \varepsilon'_M \delta(e) + \varepsilon_M'^2 C_{\max}$  with

$\delta(e) = \sqrt[4]{K^* \|J_{1e}(e)\|}$ , with  $K^*$  a constant, allows (90) to be rewritten as

$$\begin{aligned} \dot{J}_2 &\leq (3\alpha_1/2\rho^2) \left( \|\varepsilon'_M \delta(e)\|^2 + \|\varepsilon_M'^2 C_{\max}\|^2 \right) \\ &\quad - (\alpha_1/64\rho^2) \|\tilde{\Gamma}^T \nabla_e \Phi(e)\|^4 C_{\min}^2 \\ &\quad + (256\alpha_1/\rho^2 C_{\min}^2) \left( 2\|\dot{e}_1^*\|^2 + 2\|0.5C\nabla_e \mathcal{E}\|^2 \right)^2 \end{aligned} \quad (91)$$

By virtue of the fact that  $\|x+y\|^2 = \|x\|^2 + \|y\|^2$ . Now using the fact that

$(\|x\|^4 + \|y\|^4)/2 \geq \|x\|^2 \|y\|^2$  allows (91) to be rewritten as

$$\begin{aligned} \dot{J}_2 &\leq (3\alpha_1/2\rho^2) (\varepsilon_M'^4 + \delta^4(e) + \varepsilon_M'^4 C_{\max}^2) - (\alpha_1/64\rho^2) \|\tilde{\Gamma}^T \nabla_e \Phi(e)\|^4 C_{\min}^2 \\ &\quad + (256\alpha_1/\rho^2 C_{\min}^2) \left( 2\|\dot{e}_1^*\|^2 + 2\|0.5C\nabla_e \mathcal{E}\|^2 \right)^2 \end{aligned} \quad (92)$$

The last term in (92) may be rewritten as a result of the property that

$$\begin{aligned} (2\|x\|^2 + 2\|y\|^2)^2 &= 4(\|x\|^4 + \|y\|^4 + 2\|x\|^2 \|y\|^2) \\ &\leq 4(\|x\|^4 + \|y\|^4 + \|x\|^4 + \|y\|^4) = 8(\|x\|^4 + \|y\|^4) \end{aligned} \quad (93)$$

as

$$\begin{aligned} \dot{J}_2 &\leq (3\alpha_1/2\rho^2) (\varepsilon_M'^4 + \delta^4(e) + \varepsilon_M'^4 C_{\max}^2) - (\alpha_1/64\rho^2) \|\tilde{\Gamma}^T \nabla_e \Phi(e)\|^4 C_{\min}^2 \\ &\quad + (2048\alpha_1/\rho^2 C_{\min}^2) \left( \|\dot{e}_1^*\|^4 + \|0.5C\nabla_e \mathcal{E}\|^4 \right) \end{aligned} \quad (94)$$

Making use of the fact that  $\delta(e) = \|\dot{e}_1^*\|$  and with  $\|\nabla_e \mathcal{E}\| \leq \varepsilon'_M$  an upper bound on the OLA

reconstruction error, (94) may be written as

$$\dot{J}_2 \leq \alpha_1 \eta(\varepsilon) / \rho^2 - \alpha_1 \beta_1 \|\tilde{\Gamma}\|^4 / \rho^2 + \alpha_1 \beta_2 \delta^4(e) / \rho^2 \quad (95)$$

With  $\beta_1 = \Phi_{\min}^4 C_{\min}^2 / 64$ ,  $\beta_2 = (2048/C_{\min}^2) + 3/2$ , and

$\eta(\varepsilon) = 128\varepsilon_M^4 C_{\max}^4 / C_{\min}^2 + (3/2)(\varepsilon_M^4 + \varepsilon_M^4 C_{\max}^2)$ . Now, looking back at (80), it is necessary

to consider the case  $J_{1e}(e)\dot{e} < 0$  and  $\Sigma(e, \hat{u}_e) = 0$ :

$$\dot{J}_{HJB} \leq -\alpha_2 \|J_{1e}(e)\dot{e}\| + \frac{\alpha_1 \eta(\varepsilon)}{\rho^2} - \frac{\alpha_1 \beta_1}{\rho^2} \|\tilde{\Gamma}\|^4 + \frac{\alpha_1 \beta_2}{\rho^2} \delta^4(e) \quad (96)$$

This result may be rewritten taking a bound on  $\dot{e}$  as

$$\begin{aligned} \dot{J}_{HJB} &\leq -\alpha_2 \|J_{1e}(e)\| \dot{e}_{\min} + (\alpha_1 \eta(\varepsilon) / \rho^2) \\ &\quad - (\alpha_1 \beta_1 / \rho^2) \|\tilde{\Gamma}\|^4 + (\alpha_1 \beta_2 / \rho^2) K^* \|J_{1e}(e)\| \end{aligned} \quad (97)$$

Combining terms results in

$$\begin{aligned} \dot{J}_{HJB} &\leq -\|J_{1e}(e)\| (\alpha_2 \dot{e}_{\min} - (\alpha_1 \beta_2 / \rho^2) K^*) \\ &\quad + (\alpha_1 \eta(\varepsilon) / \rho^2) - (\alpha_1 \beta_1 / \rho^2) \|\tilde{\Gamma}\|^4 \end{aligned} \quad (98)$$

This is negative definite provided that  $\alpha_2 / \alpha_1 > \beta_2 K^* / \dot{e}_{\min}$  and

$\|J_{1e}(e)\| > \alpha_1 \eta(\varepsilon) / (\alpha_2 \rho^2 \dot{e}_{\min} - \alpha_1 \beta_2 K^*) \equiv b_{J_{e0}}$ , or  $\|\tilde{\Gamma}\| > \sqrt[4]{\eta(\varepsilon) / \beta_1} \equiv b_{\Gamma 0}$ . Therefore,

$\|J_{1e}(e)\|$ ,  $\|\tilde{\Gamma}\|$ , and  $\|e\|$  are UUB.

Next, it is necessary to consider the case  $J_{1e}(e)\dot{e} > 0$  and  $\Sigma(e, \hat{u}_e) = 1$ :

$$\begin{aligned} \dot{J}_{HJB} &\leq \alpha_2 J_{1e}^T(e) (f_e(e) - 0.5C\nabla_e^T \Phi(e)\hat{\Gamma}) \\ &\quad + (\alpha_1 \eta(\varepsilon) / \rho^2) - (\alpha_1 \beta_1 / \rho^2) \|\tilde{\Gamma}\|^4 + (\alpha_1 \beta_2 / \rho^2) \delta^4(e) \\ &\quad - 0.5\alpha_2 \tilde{\Gamma}^T \nabla_e \Phi(e) C J_{1e}^T(e) \end{aligned} \quad (99)$$

The term  $0.5\alpha_2 J_{1e}^T(e) C (\nabla_e^T \Phi(e)\hat{\Gamma} + \nabla_e \varepsilon)$  will be added and subtracted from (99) to obtain

$$\begin{aligned}
\dot{J}_{HJB} &\leq \alpha_2 J_{1e}^T(e) (f_e(e) - 0.5 C \nabla_e^T \Phi(e) \hat{\Gamma}) + (\alpha_1 \eta(\varepsilon) / \rho^2) - 0.5 \alpha_2 \tilde{\Gamma}^T \nabla_e \Phi(e) C J_{1e}^T(e) \\
&\quad - (\alpha_1 \beta_1 / \rho^2) \|\tilde{\Gamma}\|^4 + 0.5 \alpha_2 J_{1e}^T(e) C (\nabla_e^T \Phi(e) \Gamma + \nabla_e \varepsilon) \\
&\quad - 0.5 \alpha_2 J_{1e}^T(e) C (\nabla_e^T \Phi(e) \Gamma + \nabla_e \varepsilon) + (\alpha_1 \beta_2 / \rho^2) \delta^4(e)
\end{aligned} \tag{100}$$

Which may be expanded and rewritten from (100) as

$$\begin{aligned}
\dot{J}_{HJB} &\leq \alpha_2 J_{1e}^T(e) (f_e(e) + g u_e^*) + (\alpha_1 \eta(\varepsilon) / \rho^2) - \frac{\alpha_1 \beta_1}{\rho^2} \|\tilde{\Gamma}\|^4 \\
&\quad + \frac{\alpha_1 \beta_2}{\rho^2} K^* \|J_{1e}(e)\| + 0.5 \alpha_2 J_{1e}^T(e) C \nabla_e \varepsilon
\end{aligned} \tag{101}$$

Now, using the relationship for  $\bar{Q}(e)$  given in (39), taking the bounds on  $\bar{Q}(e)$ ,  $C$ , and

$\nabla_e \varepsilon$  and the norm on  $J_{1e}^T(e)$  allows (101) to be rewritten as

$$\begin{aligned}
\dot{J}_{HJB} &\leq \alpha_2 \bar{Q}_{\min} \|J_{1e}^T(e)\|^2 + (\alpha_1 \eta(\varepsilon) / \rho^2) - (\alpha_1 \beta_1 / \rho^2) \|\tilde{\Gamma}\|^4 \\
&\quad + (\alpha_1 \beta_2 / \rho^2) K^* \|J_{1e}(e)\| + 0.5 \alpha_2 \|J_{1e}^T(e)\| C_{\max} \varepsilon_M'
\end{aligned} \tag{102}$$

This last equation may be rewritten as below

$$\begin{aligned}
\dot{J}_{HJB} &\leq \frac{\alpha_1 \eta(\varepsilon)}{\rho^2} - \frac{\alpha_2 \bar{Q}_{\min}}{2} \left( \|J_{1e}(e)\| - \left( \frac{C_{\max} \varepsilon_M'}{2 \bar{Q}_{\min}} + \frac{\alpha_1 \beta_2 K^*}{\rho^2 \bar{Q}_{\min} \alpha_2} \right) \right)^2 \\
&\quad + \frac{\alpha_2 \bar{Q}_{\min}}{2} \left( \frac{C_{\max} \varepsilon_M'}{2 \bar{Q}_{\min}} + \frac{\alpha_1 \beta_2 K^*}{\rho^2 \bar{Q}_{\min} \alpha_2} \right)^2 - \frac{\alpha_1 \beta_1}{\rho^2} \|\tilde{\Gamma}\|^4 - \alpha_2 \frac{\bar{Q}_{\min}}{2} \|J_{1e}(e)\|^2
\end{aligned} \tag{103}$$

Lemma 4 yields

$$\begin{aligned}
\dot{J}_{HJB} &\leq -0.5 \alpha_2 \bar{Q}_{\min} \|J_{1e}(e)\|^2 - \alpha_1 \|\tilde{\Gamma}\|^4 \beta_1 / \rho^2 \\
&\quad + \alpha_1 \eta(\varepsilon) / \rho^2 + \alpha_2 C_{\max}^2 \varepsilon_M'^2 / (4 \bar{Q}_{\min}) + \alpha_1^2 \beta_2^2 K^{*2} / (\alpha_2 \rho^4 \bar{Q}_{\min})
\end{aligned} \tag{104}$$

with  $0 < \bar{Q}_{\min} \leq \|Q(e)\|$ . This is negative definite provided that

$$\|J_{1e}(e)\| > \sqrt{C_{\max}^2 \varepsilon_M'^2 / 2 \bar{Q}_{\min}^2} \equiv b_{J_{1e}} \quad \text{and} \quad \|\tilde{\Gamma}\| > \sqrt[4]{(\eta(\varepsilon) / \beta_1) + (\alpha_1 \beta_2^2 K^{*2} / \beta_1 \alpha_2 \bar{Q}_{\min})} \equiv b_{\Gamma}.$$

Therefore,  $\|J_{1e}(e)\|$ ,  $\|\tilde{\Gamma}\|$ , and  $\|e\|$  are UUB. In addition, defining the bounds

$$\Phi_{\min} \leq \|\Phi(e)\| \leq \Phi_{\max} \quad \text{and} \quad \|\nabla_e \Phi\| \leq \Phi'_{\max}, \quad \|W^* - \hat{W}\| \leq \|\tilde{\Gamma}\| \|\Phi(e)\| + \varepsilon_M \leq b_{\Gamma} \Phi_{\max} + \varepsilon_M \equiv \varepsilon_{r1}$$

and  $\|u_e^* - \hat{u}_e\| \leq (1/2) \lambda_{\max}(B^{-1}) g_M b_{\Gamma} \Phi'_{\max} + \lambda_{\max}(B^{-1}) g_M \varepsilon_M \equiv \varepsilon_{r2}$ , with  $\lambda_{\max}(B^{-1})$  denoting

the maximum eigenvalues of  $B^{-1}$ . The second part of the Lyapunov candidate function will be considered next.

**Step 2:** consider the feedforward control Lyapunov function candidate

$$J_{\text{feedforward}} = S_1 + S_2 + S_3 + S_4 \quad (105)$$

with  $S_1 = 0.5 \delta_1^T \delta_1$ ,  $S_2 = 0.5 \hat{\delta}_2^T \hat{\delta}_2$ ,  $S_3 = 0.5 \hat{\delta}_3^T \hat{\delta}_3 + 0.5 \epsilon_3^T \epsilon_3$ , and  $S_4 = 0.5 \hat{\delta}_4^T \hat{\delta}_4 + 0.5 \epsilon_4^T \epsilon_4$ . It

has been shown that this selection of Lyapunov candidate will guarantee stability in [7].

Applying elements integral to (29) gives the derivative of the Lyapunov function

$$\dot{J}_{\text{feedforward}} = \dot{S}_1 + \dot{S}_2 + \dot{S}_3 + \dot{S}_4 = -(1/m) \delta_1^T \dot{\delta}_1 - \hat{\delta}_2^T \dot{\hat{\delta}}_2 - \hat{\delta}_3^T \dot{\hat{\delta}}_3 - \hat{\delta}_4^T \dot{\hat{\delta}}_4 - \epsilon_3^T \dot{\epsilon}_3 - \epsilon_4^T \dot{\epsilon}_4 \quad (106)$$

so  $\dot{J}_{\text{feedforward}} < 0$ . To quickly review the elements in this stability analysis,  $\delta_1$  is used for

the error in the tracking along with  $\epsilon_3$ ,  $\hat{\delta}_2$  regulates the translational velocity,  $\hat{\delta}_3$  and  $\hat{\delta}_4$

take roll and pitch angles into consideration, and  $\epsilon_3$  and  $\epsilon_4$  are used for the error in the

orientation (yaw) and corresponding rotational velocity.

**Step 3:** consider the stability of the entire system. Combining

$$\begin{aligned} \dot{J}_{HJB} + \dot{J}_{\text{feedforward}} + \dot{J}_o = & -\frac{\alpha_2 \bar{Q}_{e,\min} \|J_{1e}(e)\|^2}{2} - \frac{\alpha_1 \|\tilde{\Gamma}\|^4 \beta_1}{\rho^2} + \frac{\alpha_1 \eta(\varepsilon)}{\rho^2} + \frac{\alpha_2 C_{\max}^2 \varepsilon_M'^2}{(4\bar{Q}_{e,\min})} \\ & + \frac{\alpha_1^2 \beta_2^2 K^{*2}}{(\alpha_2 \rho^4 \bar{Q}_{e,\min})} - (1/m) \delta_1^T \dot{\delta}_1 - \hat{\delta}_2^T \dot{\hat{\delta}}_2 - \hat{\delta}_3^T \dot{\hat{\delta}}_3 - \hat{\delta}_4^T \dot{\hat{\delta}}_4 - \epsilon_3^T \dot{\epsilon}_3 - \epsilon_4^T \dot{\epsilon}_4 \\ & + 0.5 \tilde{X}^T \dot{\tilde{X}} + 0.5 \tilde{V}^T \dot{\tilde{V}} + 0.5 \text{tr} \left\{ \tilde{W}_o^T F_o^{-1} \dot{\tilde{W}}_o \right\} \end{aligned} \quad (107)$$

Lemma 2 and Lemma 4 will then ensure  $\dot{J}_{HJB} < 0$  given that

$$\|J_{1e}(e)\| > \sqrt{C_{max}^2 \varepsilon_M'^2 / (2\bar{Q}_{e,min}^2)} \equiv b_{Je1}, \quad (108)$$

and

$$\|\tilde{\Gamma}\| > \sqrt[4]{\eta(\varepsilon) / \beta_1 + \alpha_1 \beta_2^2 K^{*2} / (\beta_1 \alpha_2 \bar{Q}_{e,min})} \equiv b_{\Gamma1} \quad (109)$$

if  $\Sigma(e, \hat{u}_e) = 1$ , or

$$\alpha_2 / \alpha_1 > \beta_2 K^* / \dot{e}_{min} \quad (110)$$

and

$$\|J_{1e}(e)\| > \alpha_1 \eta(\varepsilon) / (\alpha_2 \rho^2 \dot{e}_{min} - \alpha_1 \beta_2 K^*) \equiv b_{Je0} \quad (111)$$

or

$$\|\tilde{\Gamma}\| > \sqrt[4]{\eta(\varepsilon) / \beta_1} \equiv b_{\Gamma0} \quad (112)$$

if  $\Sigma(e, \hat{u}_e) = 0$ . In addition, it is also necessary that

$$\|\tilde{X}\| > \sqrt{2\eta_o / (K_{o1} - K_{o3})} \quad (113)$$

or

$$\|\tilde{V}\| > \sqrt{\eta_o / (0.5K_{o3} - (N_o / \kappa_{o1}))} \quad (114)$$

or

$$\|\tilde{W}_o\|_F > \sqrt{2\eta_o / \kappa_{o1}} \quad (115)$$

which allows the conclusion that  $\|W^*(e) - \hat{W}(e)\| \leq \|\tilde{\Gamma}\| \|\Phi(e)\| + \varepsilon_M \leq b_{\Gamma} \Phi_M + \varepsilon_M \equiv \varepsilon_{r1}$

and

$$\|u_e^*(e) - \hat{u}_e(e)\| \leq (\lambda_{max}(B^{-1}) g_M b_{\Gamma} \Phi_M' / 2) + (\lambda_{max}(B^{-1}) g_M \varepsilon_M' / 2) \equiv \varepsilon_{r2} \quad (116)$$

Then  $\dot{J}_{HJB} + \dot{J}_{feedforward} + \dot{J}_o < 0$  provided that the conditions in (108) - (115) hold. In other words, the overall system is UUB with the bounds from (108) and (109), completing the proof.  $\square$

The dynamics presented at the beginning of the paper provide

$$\bar{S}(\omega) = \begin{bmatrix} 0^{3 \times 1} & -\omega \times \mathcal{J}\omega \end{bmatrix}^T. \text{ Actually, however, this is a simplification of the real}$$

dynamics, which include an additional coupling term such that

$$\bar{S}(\omega) = [R(\Theta)Kw_d \quad -\omega \times \mathcal{J}\omega]^T, \text{ with}$$

$$K = \frac{1}{l_M} \begin{bmatrix} 0 & 1 & 0 \\ -1 & 0 & 1/l_t \\ 0 & 0 & 0 \end{bmatrix} \quad (117)$$

This coupling term is relatively small, but the robustness against neglecting the term has been demonstrated using a nonlinear controller and is available for the interested reader in [7] for the case of state feedback. The case for output feedback will be given below, following the approach given in [7]. Initially,  $\alpha_1 = (\hat{\delta}_1, \hat{\delta}_2, \hat{\delta}_3, \hat{\delta}_4, \epsilon_3, \epsilon_4) \in \mathbb{R}^{14}$  is defined as a vector that includes a set of errors that have previously been introduced. The error dynamics for the complete system model may then be given as

$$\dot{\alpha} = \begin{bmatrix} -\frac{1}{m}I_{3 \times 3} & \frac{1}{m}I_{3 \times 3} & 0_{3 \times 3} & 0_{3 \times 3} & 0_{1 \times 1} & 0_{1 \times 1} \\ -\frac{1}{m}I_{3 \times 3} & -I_{3 \times 3} & I_{3 \times 3} & 0_{3 \times 3} & 0_{1 \times 1} & 0_{1 \times 1} \\ 0_{3 \times 3} & -I_{3 \times 3} & -I_{3 \times 3} & I_{3 \times 3} & 0_{1 \times 1} & 0_{1 \times 1} \\ 0_{3 \times 3} & 0_{3 \times 3} & -I_{3 \times 3} & -I_{3 \times 3} & 0_{1 \times 1} & 0_{1 \times 1} \\ 0_{1 \times 1} & 0_{1 \times 1} & 0_{1 \times 1} & 0_{1 \times 1} & -1_{1 \times 1} & 1_{1 \times 1} \\ 0_{1 \times 1} & 0_{1 \times 1} & 0_{1 \times 1} & 0_{1 \times 1} & -1_{1 \times 1} & -1_{1 \times 1} \end{bmatrix} \alpha + \begin{bmatrix} 0_{3 \times 1} \\ R(\Theta)Kw_d \\ \frac{m+1}{m}R(\Theta)Kw_d \\ \frac{2m^2 + 2m + 1}{m^2}R(\Theta)Kw_d \\ 0_{3 \times 1} \\ 0_{3 \times 1} \end{bmatrix} \quad (118)$$

The norms of the errors may then be taken and described as

$\gamma = (|\delta_1|, |\hat{\delta}_2|, |\hat{\delta}_3|, |\hat{\delta}_4|, |\epsilon_3|, |\epsilon_4|) \in \mathbb{R}^6$ . Then, rewriting the feedforward Lyapunov candidate

terms,  $J_{feedforward} = 0.5|\gamma|^2$ . Taking the derivative,  $\dot{J}_{feedforward} = -\gamma^T \Lambda \gamma$ , with

$\Lambda = \text{diag}(1/m, 1, 1, 1, 1, 1) \in \mathbb{R}^{6 \times 6}$ . Bounding the magnitude of the small body forces results

in

$$\begin{aligned} \dot{J}_{feedforward} &\leq -\gamma^T \Lambda \gamma + |\hat{\delta}_2| |R(\Theta) K w_d| + \frac{m+1}{m} |\hat{\delta}_3| |R(\Theta) K w_d| \\ &+ \left( (2m^2 + m + 1)/m \right) |\hat{\delta}_4| |R(\Theta) K w_d| = -\gamma^T \Lambda \gamma + \sigma |w_d| \pi_0^T \gamma \end{aligned} \quad (119)$$

with  $\pi_0 = (0, 1, (m+1)/m, (2m^2 + m + 1)/m^2, 0, 0)$  and  $\sigma = (1/l_M l_T) \sqrt{2l_T^2 - 2l_T + 1} = \|K\|$ ,

where  $\|K\|$  corresponds to the offset between the main rotor shaft and the helicopter's center of gravity. This yields the result that the small body forces cannot exceed a given

bound, with a requirement for stability that  $\gamma^T \Lambda \gamma \geq \sigma |w_d| \pi_0^T \gamma$ . Next, it is necessary to

determine the bound resulting in tracking with UUB stability. Since  $P > I_{3 \times 3}$ ,  $\|P\|^{-1} < 1$ .

Next, defining  $c_0 = \|I_{3 \times 3}\|$  and  $|w_0| = |Q_M| + |Q_T|$ , the equation

$$P w_d = \tilde{J} \tilde{w}_d - \hat{\omega} \times \tilde{J} \hat{\omega} - |Q_M| e_3 + |Q_T| e_2, \text{ may be rewritten as } |w_d| \leq c_0 \hat{\omega}^2 + c_0 |\tilde{w}_d| + |w_0|.$$

Now,  $\|W_\Theta^{-1}\| \leq 1/\cos \theta \leq \sqrt{2}$  and  $\|\dot{W}_\Theta\| \leq \sqrt{2} |\dot{\Theta}|$  since

$$\dot{\Theta} = \frac{1}{c_\theta} \begin{pmatrix} 0 & s_\psi & c_\psi \\ 0 & c_\theta c_\psi & -c_\theta s_\psi \\ c_\theta & s_\theta s_\psi & s_\theta c_\psi \end{pmatrix} \hat{\omega} = W_\Theta^{-1} \hat{\omega} \quad (120)$$

Then, referencing  $\tilde{w}_{3d} = (\ddot{\phi} - \epsilon_4 - \epsilon_3 + e_1^T W_\Theta^{-1} \dot{W}_\Theta W_\Theta^{-1} \hat{\omega} - (s_\psi/c_\theta) \tilde{w}_{2d})(c_\theta/c_\psi)$  and

recognizing natural bounds such that  $-\pi/2 < \phi < \pi/2$  and  $-\pi/2 < \theta < \pi/2$ ,



$|\tilde{w}_d^3| \leq \langle \tau_1, \chi \rangle + \langle \pi_1, \gamma \rangle + 4\hat{\omega}^2 + \sqrt{2}|\tilde{w}_d^2|$  with  $\chi$  the trajectory such that

$$\chi = (|\ddot{\rho}_d|, |\rho_d^{(3)}|, |\rho_d^{(4)}|, |\dot{\Theta}_d|, |\ddot{\Theta}_d|) \in \mathbb{R}^5, \text{ with } \tau_1 = (0, 0, 0, 0, \sqrt{2})^T \text{ and}$$

$\pi_1 = (0, 0, 0, 0, \sqrt{2}, \sqrt{2})^T$ . Using the notation  $\tilde{w}_d^{(1,2)} = (\tilde{w}_d^1, \tilde{w}_d^2)$  and employing (25) yields

$$\zeta \tilde{w}_d^{(1,2)} = \text{skew}(e_3)R(\Theta)^T \dot{Y}_d + 2\zeta(\text{diag}(1, 1, 0))\hat{\omega} + \text{skew}(e_3)\hat{\delta}_3 + \text{skew}(e_3)\hat{\delta}_4 \quad (121)$$

which is upper-bounded such that  $|\zeta||\tilde{w}_d^{(1,2)}| \leq |\dot{Y}_d| + 2|\zeta|\hat{\omega} + \langle \pi_2, \gamma \rangle$ , with

$\pi_2 = (0, 0, 1, 1, 0, 0)^T$ . This results in

$$\begin{aligned} |\tilde{w}_d| &\leq |\tilde{w}_d^{(1,2)}| + |\tilde{w}_d^3| \leq |\tilde{w}_d^{(1,2)}| + \langle \tau_1, \chi \rangle + \langle \pi_1, \gamma \rangle + 4\hat{\omega}^2 + \sqrt{2}|\tilde{w}_d^2| \\ &\leq \left( (1 + \sqrt{2})/|\zeta| \right) |\zeta||\tilde{w}_d^{(1,2)}| + \langle \tau_1, \chi \rangle + \langle \pi_1, \gamma \rangle + 4\hat{\omega}^2 \end{aligned} \quad (122)$$

Then, bounding  $\dot{Y}_d$  results in  $|\dot{Y}_d| \leq \langle \tau_2, \chi \rangle + \langle \pi_3, \gamma \rangle + \sigma c_2 |w_d|$  with  $\tau_2 = (0, 0, m, 0, 0)^T$ ,

$$c_2 = (2m^2 + 2m + 1)/m, \text{ and } \pi_3 = \left( \frac{2m+1}{m^3}, \frac{2m^3+m+1}{m^3}, \frac{2(m+1)}{m}, \frac{2m+1}{m}, 0, 0 \right)^T. \text{ It is also}$$

possible to bound  $\hat{\omega}^3$  such that  $|\hat{\omega}^3| \leq \hat{\omega}^2 + \langle \tau_3, \chi \rangle + \langle \pi_4, \gamma \rangle$ , with  $\tau_3 = (0, 0, 0, \sqrt{2}, 0)^T$  and

$\pi_4 = \pi_1$ . With these steps,  $|\hat{\omega}| \leq 2|\hat{\omega}^{(1,2)}| + \langle \tau_3, \chi \rangle + \langle \pi_4, \gamma \rangle$  and

$$|\zeta| \leq \langle \tau_4, \chi \rangle + \langle \pi_5, \gamma \rangle \sigma c_3 |w_d|, \text{ with } \tau_4 = (0, m, 0, 0, 0), c_3 = (m+1)/m^2, \hat{\omega}^{(1,2)} = (\hat{\omega}^1, \hat{\omega}^2),$$

and  $\pi_5 = ((m+1)/m^2, 1/m, (2m+1)/m, 1, 0, 0)$ . If the preceding results are combined, one

may arrive at  $|\hat{\omega}| \leq (\langle q_1(\zeta), \chi \rangle + \langle p_1(\zeta), \gamma \rangle + \sigma c_4 |w_d|)/|\zeta|$  for a bound on the angular

velocity, with  $q_1(\zeta) = 2\tau_4 + |\zeta|\tau_3$ ,  $p_1(\zeta) = 2\pi_5 + |\zeta|\pi_4$ , and  $c_4 = 2c_3$ . The control input

torques may also then be bounded such that

$$|w_d| \leq \frac{1}{|\zeta|} \left( \langle q_2(\zeta), \chi \rangle + \langle p_2(\zeta), \gamma \rangle + \sigma c_5 |w_d| + 2|\dot{\zeta}| |\hat{\omega}| \right) + d_1 |\zeta| \hat{\omega}^2 + |\zeta| |w_0| \quad (123)$$

with  $q_2(\zeta) = (1 + \sqrt{2})\tau_2 + |\zeta|\tau_1$ ,  $p_2(\zeta) = (1 + \sqrt{2})\pi_3 + |\zeta|\pi_1 + \pi_2$ ,  $d_1 = 4 + c_0$ , and  $c_5 = c_2$ .

The control input governing the main rotor thrust may then be bounded such that

$$mg - \langle \tau_5, \chi \rangle - \langle \pi_6, \gamma \rangle \leq |\zeta| \leq mg + \langle \tau_5, \chi \rangle + \langle \pi_6, \gamma \rangle \quad \text{with } \tau_5 = (m, 0, 0, 0, 0)^T \text{ and}$$

$$\pi_6 = (1/m, 1, 1, 0, 0, 0)^T. \text{ Setting bounds } k_0, k_1, \text{ and } k_2 \text{ such that } |J_{\text{feedforward}}(0)| \leq k_0^2 \text{ (which}$$

is true since  $J_{\text{feedforward}}(0) = 0$ ),  $|\hat{\omega}(0)| \leq k_1$ , and  $|w_0| = (|Q_M| + |Q_T|) \leq k_2$ , with constants

$$p_3^0 = \left| mg\pi_1 + \pi_2 + (1 + \sqrt{2})\pi_3 + mgd_1k_1\pi_4 + 2k_1(1 + d_1)\pi_5 \right|, \quad p_3^1 = |\pi_1 + d_1k_1\pi_4|,$$

$$q_3^0 = \left| mg\tau_1 + (1 + \sqrt{2})\tau_2 + mgd_1k_1\tau_3 + 2k_1(1 + d_1)\tau_4 \right|, \quad q_3^1 = |\tau_1 + d_1k_1\tau_3|, \text{ and}$$

$c_6 = c_5 + 2k_1c_3 + d_1k_1c_4$ , and defining two bounds for the trajectory,  $B_1$  and  $B_2$  such that

$$B_1(\Delta) = \frac{k_0 \left[ (mg - \Delta) \left( 1 - (\sigma k_2 / k_0) |\pi_0| \right) + \Delta \sigma p_3^1 |\pi_0| - \sigma (c_6 + p_3^0 |\pi_0|) \right]}{\sigma (p_3^0 - \Delta p_3^1) (q_3^0 - \Delta q_3^1)} \quad (124)$$

and  $B_2(\Delta) = (\Delta - |\pi_6|k_0) / |\tau_5|$  with

$$\Delta_* = \left( \begin{array}{c} \arg \sup \\ \Delta \geq mg - (k_0(c_4 + 2|\pi_0||\pi_5|)) / (k_1|\pi_0|) \end{array} \left[ \min \{ B_1(\Delta), B_2(\Delta) \} \right] \right) \quad (125)$$

and

$$B_* = \sup_{\Delta \geq mg - (k_0(c_4 + 2|\pi_0||\pi_5|)) / (k_1|\pi_0|)} \left[ \min \{ B_1(\Delta), B_2(\Delta) \} \right] \quad (126)$$

then if  $|\chi| \leq B_*$ , the closed-loop system is locally UUB. Expressing part of this result

mathematically,  $|J_{\text{feedforward}}(t)| \leq k_0^2$ ,  $\hat{\omega}(t) < k_1 + k_0|\pi_0||\pi_4|(mg + \Delta_*) + |\pi_0||q_1(\zeta)|B_*$ , and

$\zeta > mg - \Delta_*$ . This locally UUB result may be obtained by guaranteeing that trajectory bounds  $B_1$  and  $B_2$  are positive, control input  $\zeta$  is lower bounded, and the angular

velocity  $\hat{\omega}(t)$  is upper bounded. To do this it is first necessary to define

$$q_3(\zeta) = q_2(\zeta) + 2k_1\tau_4 + d_1k_1q_1(\zeta) \text{ and } p_3(\zeta) = p_2(\zeta) + 2k_1\pi_5 + d_1k_1p_1(\zeta), \text{ while}$$

recognizing that  $mg - \Delta_* \leq |\zeta| \leq mg + \Delta_*$ . These results may then be bounded such that

$$p_3^0 - \Delta_* p_3^1 \leq p_3(\zeta) \leq p_3^0 + \Delta_* p_3^1 \text{ and } q_3^0 - \Delta_* q_3^1 \leq q_3(\zeta) \leq q_3^0 + \Delta_* q_3^1, \text{ with the condition that}$$

$\Delta_* \geq mg - (k_0(c_4 + 2|\pi_0||\pi_5|) / k_1|\pi_0|)$ . Then, since  $B_1$  and  $B_2$  are bounded, the following

three conditions may be specified:

$$\begin{aligned} |\hat{\omega}(0)| < K_{\hat{\omega}+\hat{\omega}} &= (1 / (mg - \Delta_*)|\pi_0|)(k_0(c_4 + 2|\pi_0||\pi_5|) \\ &+ k_0|\pi_4|(mg + \Delta_*) + |\pi_0||\tau_5|B_*) \end{aligned} \quad (127)$$

$$\sigma < \frac{(mg - \Delta_*)}{(c_6 + |\pi_0||p_3(\zeta)| + (1/k_0)(|p_3(\zeta)||q_3(\zeta)|B_* + (mg - \Delta_*)k_2|\pi_0|))} \quad (128)$$

and

$$|\pi_6|k_0 + |\tau_5|B_* < \Delta_* \quad (129)$$

All three of the bounds for the locally UUB result are valid at time  $t=0$ . If the first of the bounds for the locally UUB result is not valid for all time, and with the assumption that

$$|\zeta(t_1)| = \Delta_*, |J_{\text{feedforward}}(t)| \leq k_0^2 \text{ as well as } \hat{\omega}(t) \leq K_{\hat{\omega}} \text{ for } t \in [0, t_1], \text{ then } |\zeta(t_1)| > mg - \Delta_*,$$

and the bound on  $|\zeta|$  is not the first bound to be broken. If the second of the bounds is not

valid for all time, and with the assumption that  $|\zeta(t_1)| = \Delta_*$ ,  $|J_{\text{feedforward}}(t)| \leq k_0^2$  as well as

$$\hat{\omega}(t) \leq K_{\hat{\omega}} \text{ for } t \in [0, t_1], \text{ then } |\dot{\zeta}||\hat{\omega}| \leq K_{\dot{\zeta}}|\dot{\zeta}| \text{ and } \hat{\omega}^2 \leq K_{\hat{\omega}}|\hat{\omega}|. \text{ Using the previous results}$$

for a bound on the rotational torque inputs allows one to arrive at

$|w_d| \leq (\langle q_3(\zeta), \chi \rangle + \langle p_3(\zeta), \gamma \rangle + (mg - \Delta_*)|w_0|) / (mg - \Delta_* - \sigma c_6)$  From the second condition on the trajectory bounds,

$$\sigma < (mg - \Delta_*) / (c_6 + |\pi_0| |p_3(\zeta)| + a_0) \quad (130)$$

with  $a_0 \geq 0$ , it follows that  $mg - \Delta_* - \sigma c_6 > 0$ , and inserting this result into the initial requirement on the Lyapunov candidate function to ensure stability in the presence of small-body forces,

$$\gamma^T \Lambda \gamma \geq \left( \sigma / (mg - \Delta_* - \sigma c_6) \right) (\gamma^T p_3(\zeta) \pi_0^T \gamma + \gamma^T \pi_0 q_3(\zeta)^T \chi + (mg - \Delta_*) |w_0| \pi_0^T \gamma) \quad (131)$$

Noting that  $|J_{feedforward}(t)| \leq k_0^2$ ,  $|\chi| \leq B_*$ , and  $|w_0| \leq k_2$ , the resulting constraint on  $\sigma$  is equivalent to the second condition on the trajectory bounds, and the bound

$|J_{feedforward}(t)| \leq k_0^2$  is also not the first bound to be broken. From the third condition on the trajectory bounds, with the assumption that  $|\zeta(t)| > mg - \Delta_*$ ,  $|J_{feedforward}(t)| \leq k_0^2$  as well as  $\hat{\omega}(t_1) \leq K_{\hat{\omega}}$  for  $t \in [0, t_1]$ , and since

$$|\hat{\omega}| \leq (\langle q_1(\zeta), \chi \rangle + \langle p_1(\zeta), \gamma \rangle + \sigma c_4 |w_d|) / (mg - \Delta_*) \quad (132)$$

substituting the bound for  $|w_d|$  yields

$$|\hat{\omega}| \leq (1 / (mg - \Delta_*)) \left( \langle q_1(\zeta), \chi \rangle + \langle p_1(\zeta), \gamma \rangle + \frac{\sigma c_4}{(mg - \Delta_* - \sigma c_6)} (\langle q_3(\zeta), \chi \rangle + \langle p_3(\zeta), \gamma \rangle + (mg - \Delta_*) |w_0|) \right) \quad (133)$$

so the bound  $\hat{\omega}(t_1) \leq K_{\hat{\omega}}$  is not the first to be broken either. Because none of the bounds required for the locally UUB result may be broken before any other, it follows that all three bounds hold for all time and the closed-loop system is locally UUB.

## **2. NEURAL-NETWORK-BASED OPTIMAL CONTROL OF A HELICOPTER UNMANNED AERIAL VEHICLE (UAV) WITH HARDWARE IMPLEMENTATION**

### **2.1. ABSTRACT**

Helicopter UAVs can be extensively used for military missions as well as in civil operations, ranging from multi-role combat support and search and rescue, to border surveillance and forest fire monitoring. Helicopter UAVs are underactuated nonlinear mechanical systems with correspondingly challenging controller designs. This paper presents an optimal controller design for tracking of an underactuated helicopter using an adaptive critic neural network (NN) framework. The online approximator-based controller learns the infinite-horizon continuous-time Hamilton-Jacobi-Bellman (HJB) equation and then calculates the corresponding optimal control input that minimizes the HJB equation forward-in-time without using value and policy iterations. In the proposed technique, optimal tracking is accomplished by a single neural network (NN), which is tuned online using a novel weight update law. Stability analysis is performed and simulation results demonstrate the proposed control design.

### **2.2. INTRODUCTION**

Helicopter UAVs can play a key role in numerous military applications, including counter-explosive operations [1]. Key operational activities for helicopter UAVs include [1]: “Preventing an adversary from conducting activities that result in the emplacement of IEDs [Improvised Explosive Devices], thus thwarting an attack: this is likely to require use of the full spectrum of Joint capabilities to defeat or disrupt the adversary....” As well as “Detecting IED materiel and components, including stored HME [Home-made

Explosives] and smuggled components, as well as emplaced devices themselves. This requires a combination of ISR [Intelligence, Surveillance, and Reconnaissance] capability, together with responsive processes and effective training, to ensure that potential IED activity detected is analyzed and the results disseminated to all those who need to be aware of it, in order that appropriate action can be taken as swiftly as possible.”

There are a number of specific ways that Helicopter UAVs can counter threats [1]. “In simple terms, A & S [Air & Space] Power is capable of defeating emplaced IEDs by detecting devices and by neutralizing and mitigating their effects, as follows: Detecting devices using dedicated airborne and Space-based ISR and airborne Non-Traditional ISR (NTISR), exploiting existing capabilities and capitalizing on technological enhancements, including those offered by CCD technology.” These devices can be neutralized or have their effects mitigated through “Airborne EW [Electronic Warfare] capabilities, including Electronic Attack (EA), by employing ECM [Electronic Counter-Measures] to disrupt or detonate RCIEDs [Radio-controlled IEDs], the initiation or disruption of IEDs using kinetic targeting via airborne (or potentially Space) platform-based weapon systems, including by direct fire, and by the physical avoidance of emplaced IEDs using Air Mobility, utilizing Fixed-Wing (FW) and Rotary-Wing (RW) intra-theatre airlift, including the use of air dispatch capabilities.” Another helpful feature is that “A UAV, which minimizes risk to human life may be preferable because it can provide long endurance and is difficult to detect in the air” [1]. For applications such as counter-explosive operations, where low-speed and hovering capabilities are useful, a helicopter UAV may become the tool of choice. In addition, helicopter UAVs can deliver

supplies to positions which cannot be safely supplied from the ground. For example [2], “Supplying small forward operating bases using trucks requires escorting forces, and exposes [military] convoys to the threat of mines. The standard solution is helicopter drop-off, but every force in theater is short of helicopters....” These are just some of the current defense applications of helicopter UAVs.

Helicopter UAVs have many capabilities such as vertical take-off, hovering and trajectory tracking, and landing. For control of a helicopter [3], it is necessary to produce moments and forces on the vehicle with two goals: first, to position the helicopter in equilibrium such that the desired trim state is achieved, and second, to control the helicopter's velocity, position and orientation such that it hovers as desired with minimum error. The dynamics of the helicopter UAV are not only nonlinear but also coupled with each other and under actuated, which makes the UAV difficult to control. Both inputs and dynamics are coupled on a helicopter particularly as a result of the swashplate mechanical linkages and the torques created by drag against the rotors. The helicopter has six degrees of freedom (DOF) which must be controlled with only four control inputs – a single thrust and three torques inputs.

To solve the problem of controlling a rotary-wing UAV, several techniques have been proposed [3]-[9] employing model-based control. It has been shown [3] that the multivariable nonlinear helicopter model cannot be converted into a controllable linear system via exact state space linearization. In addition, for certain output functions, exact input-output linearization results in unstable zero dynamics [10]. Based on Newton-Euler equations, a dynamic model has been derived [3] considering the helicopter as a rigid body with input forces and torques applied to the center of mass. Previous researchers

have considered adaptive output feedback control of uncertain nonlinear systems with unknown dynamics and dimensions, and a controller for autonomous helicopter flight. Here the control problem [5] is separated into inner loop attitude control and outer loop trajectory control. A drawback of these controllers [4]-[6] is that the coupling between rolling (pitching) moments and lateral (longitudinal) accelerations is neglected. A backstepping-based controller has been presented in [7] for autonomously landing a helicopter. This controller also holds good for full flight control. The nonlinear controller computes the desired thrusts and flapping angles to get the commanded position and then computes the control inputs which achieve the desired thrust and flapping angles.

Controllers which are properly designed for offline adaptation are often robust to small variations in the system, but fail to adapt to larger changes in the system. Further, an offline scheme alone does not allow a neural network (NN) to learn any new dynamics it encounters during a new maneuver. The NN approaches [4] have been proposed to learn the dynamics of the unmanned helicopter online, but the observer used in this case estimates only the states of the feedback-linearized system and not the actual states of the helicopter dynamics. A nonlinear controller for a quadrotor unmanned aerial vehicle has been proposed in [9] by employing output feedback and NNs. This scheme addresses the problem of rotary-wing UAV control, but does not attempt optimal control. A single online approximator (SOLA)-based scheme has been introduced [11] to solve the optimal tracking control problem for affine nonlinear continuous-time systems with known dynamics. The SOLA-based adaptive approach has been designed to learn the infinite horizon continuous-time HJB equation, and the corresponding optimal control input that minimizes the HJB equation has been calculated forward-in-time.



However, optimal controller design for tracking an underactuated helicopter using NN has not yet been attempted, to the best of the authors' knowledge. Following a previous approach [11], in this paper the SOLA-based scheme for optimal tracking of a nonlinear continuous-time strict feedback system with known dynamics is considered. The online approximator-based dynamic controller learns the continuous-time Hamilton-Jacobi-Bellman (HJB) equation and then calculates the corresponding optimal control input that minimizes the HJB equation forward-in-time. This SOLA-based optimal control scheme is then extended for optimal tracking of a helicopter UAV with known dynamics. The proposed controller consists of a NN-based optimal controller and a virtual controller to supplement the optimal controller. The virtual controller generates a feedforward term needed by the optimal controller. The NN is tuned online using a novel weight update law.

The main contribution of this paper includes the development of an optimal controller for tracking the trajectory of an underactuated helicopter UAV, forward in time, where the helicopter system is expressed in a form appropriate for backstepping control. The controller tuning is independent of the trajectory in contrast with [9]. A NN-based OLA is utilized to approximate the cost function and the overall stability is guaranteed. The optimal controller has been previously developed for backstepping systems, but has not yet been applied to rotary-wing aircraft. This optimal controller previously required that  $f(0) = 0$ , but the virtual controller in this work obviates the need for that requirement. The current work builds on [11] and [7] from the fields of optimal and helicopter control; however, this work both uses previous developments for a new application and adds to these works with a closed-loop stability proof demonstrating the

proposed control scheme's convergence with state feedback. The closed-loop proof is not direct but involved, and is included near the end of the paper.

The paper begins by presenting the nonlinear model of the helicopter in the next section. Section 3 addresses the kinematic controller, the virtual controller, the continuous-time nonlinear optimal HJB tracking problem, and the solution of the HJB equation forward-in-time, making use of a single online approximator-based optimal controller. Section 2.4 concludes with stability analysis of the closed-loop system. The final sections include simulation results and concluding remarks.

### 2.3. DYNAMIC MODEL OF THE HELICOPTER

Consider a helicopter with six degrees of freedom (DOF) defined in the inertial coordinate frame  $\mathcal{Q}^a$ , where its position coordinates are given by  $\rho = [x, y, z]^T \in \mathcal{Q}^a$  and its orientation described as roll, pitch and yaw respectively, are given by  $\Theta = [\phi, \theta, \psi]^T \in \mathcal{Q}^a$ . The equations of motion can be expressed in the body fixed frame  $\mathcal{Q}^b$  which has as its origin the center of mass of the helicopter. The  ${}^b x$ -axis is defined parallel to the helicopter's direction of travel and the  ${}^b y$ -axis is defined perpendicular to the helicopter's direction of travel, while the  ${}^b z$ -axis is defined as projecting orthogonally downwards from the xy-plane of the helicopter. In addition, the following variables are used for the presentation of the dynamics:

$m \in \mathbb{R}$  is the helicopter's mass,

$F \in \mathbb{R}^{3 \times 1}$  is the body force applied to the helicopter's center of mass,

$\tau \in \mathbb{R}^{3 \times 1}$  is the body torque applied about the helicopter's center of mass,

$v = [v_x, v_y, v_z]^T \in \mathbb{R}^{3 \times 1}$  is the translational velocity vector,

$\omega = [\omega_x, \omega_y, \omega_z]^T \in \mathbb{R}^{3 \times 1}$  is the angular velocity vector,

$I \in \mathbb{R}^{3 \times 3}$  is the identity matrix,

$\mathcal{J} \in \mathbb{R}^{3 \times 3}$  is the positive-definite inertia matrix.

The kinematics of the helicopter are given as in equation (1) in Dierks [9] and equation (21) in Mahoney [7] as  $\dot{\rho} = Rv$  and  $\dot{\Theta} = T^{-1}\omega$ , along with the translational rotation matrix inverse  $T^{-1}$  used to relate a vector in body fixed frame to the inertial coordinate frame

$$T^{-1}(\Theta) = \frac{1}{c_\theta} \begin{bmatrix} 0 & s_\psi & c_\psi \\ 0 & c_\theta c_\psi & -c_\theta s_\psi \\ c_\theta & s_\theta s_\psi & s_\theta c_\psi \end{bmatrix} \quad (1)$$

and the rotational transformation matrix  $R$  used to relate a vector in body fixed frame to the inertial coordinate frame

$$R(\Theta) = \begin{bmatrix} c_\theta c_\psi & s_\phi s_\theta c_\psi - c_\phi s_\psi & c_\phi s_\theta c_\psi + s_\theta s_\psi \\ c_\theta s_\psi & s_\phi s_\theta s_\psi + c_\phi c_\psi & c_\phi s_\theta s_\psi - s_\phi c_\psi \\ -s_\theta & s_\phi c_\theta & c_\phi c_\theta \end{bmatrix} \quad (2)$$

The transformation matrix is bounded according to  $\|T\|_F < T_{max}$  for a known constant

$T_{max}$  provided  $-\pi/2 < \phi < \pi/2$  and  $-\pi/2 < \theta < \pi/2$  such that the helicopter trajectory

does not pass through any singularities [3]; also,  $\|R\|_F = R_{max}$  for a known constant  $R_{max}$

and  $R^{-1} = R^T$ . Throughout this work,  $\|\bullet\|$  denotes a Euclidean norm,  $\|\bullet\|_F$  denotes a

Frobenius norm, and  $s_\bullet$ ,  $c_\bullet$ , and  $t_\bullet$  denote the  $\sin(\bullet)$ ,  $\cos(\bullet)$ , and  $\tan(\bullet)$  functions,

respectively.

Let the mass-inertia matrix be  $M = \text{diag}\{mI, \mathcal{J}\}$  and the skew-symmetric matrix be  $\bar{S}(\omega) = [0^{3 \times 1}, -\omega \times \mathcal{J} \omega]^T$ . The dynamics of the helicopter are given by the Newton-Euler equation in the body fixed frame and can be written as [3], [9]

$$M \begin{bmatrix} \dot{v} \\ \dot{\omega} \end{bmatrix} = \bar{S}(\omega) \begin{bmatrix} v \\ \omega \end{bmatrix} + \begin{bmatrix} G(R) \\ 0^{3 \times 1} \end{bmatrix} + \begin{bmatrix} 0^{3 \times 1} \\ \mathcal{N} \end{bmatrix} + U + \tau_d \quad (3)$$

where  $\mathcal{N} = Q_M e_3 - Q_T e_2$ , with  $Q_M$  and  $Q_T$  aerodynamic constants for which values are given in the simulation section, and originally found in [7],  $G(R) \in \mathbb{R}^{3 \times 1}$  represents the gravity vector and is defined as  $G(R) = m\bar{g}e_3$ ,  $e_1, e_2$ , and  $e_3$ , are unit vectors directed along the  $x$ -,  $y$ -, and  $z$ -axes, respectively, in the inertial reference frame,  $\bar{g}$  denotes gravity, and

$$U = \begin{bmatrix} E_3^b & 0^{3 \times 3} \\ 0^{3 \times 1} & \text{diag}([p_{11} \ p_{22} \ p_{33}]) \end{bmatrix} \begin{bmatrix} u \\ w_1 \\ w_2 \\ w_3 \end{bmatrix} = \begin{bmatrix} E_3^b & 0^{3 \times 3} \\ 0^{3 \times 1} & \text{diag}([p_{11} \ p_{22} \ p_{33}]) \end{bmatrix} u_v \quad (4)$$

is the control input vector [7], with  $u_v$  the control vector composed of  $u$  which provides the thrust in the  $z$ -direction, and  $w_1, w_2$  and  $w_3$  which provide the rotational torques in the  $x$ -,  $y$ - and  $z$ - directions respectively. In addition,  $E_3^b$  is a unit vector in the positive  $z$ -direction, and  $[p_{11} \ p_{22} \ p_{33}]$  is a gain array. Because the matrix containing this gain array and  $E_3^b$  is in the set  $\mathbb{R}^{6 \times 4}$  and the input vector  $u_v \in \mathbb{R}^{4 \times 1}$  is a four-element vector,  $U$  becomes a six element column vector, making the input vector  $U$  the correct size for (3). Also,  $\tau_d = [\tau_{d1}^T, \tau_{d2}^T]^T$  represents unknown bounded disturbances such that  $\|\tau_d\| < \tau_M$  for all time  $t$ , with  $\tau_M$  a known positive constant. The system dynamics are

state-strict, which means that backstepping control can be applied. Defining

$X = [\rho^T \Theta^T]^T \in \mathbb{R}^{6 \times 1}$  and  $V = [v^T \omega^T]^T \in \mathbb{R}^{6 \times 1}$ , one can write

$$\dot{X} = AV + \xi \quad (5)$$

$$\dot{V} = f(V) + M^{-1}U \quad (6)$$

where  $f(V) = M^{-1} \left( \bar{S}(\omega) + \begin{bmatrix} 0^{3 \times 3} & \mathcal{N} \end{bmatrix}^T \right) + \bar{G}$  with  $\bar{G} = M^{-1} \begin{bmatrix} G(R) & 0^{3 \times 1} \end{bmatrix}^T \in \mathbb{R}^{6 \times 1}$ ,

with  $\xi \in \mathbb{R}^{6 \times 1}$  the bounded sensor measurement noise such that  $\|\xi\| \leq \xi_M$  for a known

constant  $\xi_M$ , and  $A = \begin{bmatrix} R & 0^{3 \times 3} \\ 0^{3 \times 3} & -R^x \end{bmatrix}$ , where  $R^x$  denotes a skew-symmetric representation

of the rotation matrix. Writing  $f(V)$  explicitly yields

$$f(V) = \begin{bmatrix} 1/m & 0 & 0 & 0 & 0 & 0 \\ 0 & 1/m & 0 & 0 & 0 & 0 \\ 0 & 0 & 1/m & 0 & 0 & 0 \\ 0 & 0 & 0 & 1/\mathcal{J}_x & 0 & 0 \\ 0 & 0 & 0 & 0 & 1/\mathcal{J}_y & 0 \\ 0 & 0 & 0 & 0 & 0 & 1/\mathcal{J}_z \end{bmatrix} \left( \begin{bmatrix} 0 \\ 0 \\ 0 \\ -\omega_x \times \mathcal{J}_x \omega_x \\ -\omega_y \times \mathcal{J}_y \omega_y \\ -\omega_z \times \mathcal{J}_z \omega_z \end{bmatrix} + \begin{bmatrix} 0 \\ 0 \\ 0 \\ 0 \\ -Q_T \\ Q_M \end{bmatrix} + \begin{bmatrix} 0 \\ 0 \\ m\bar{g} \\ 0 \\ 0 \\ 0 \end{bmatrix} \right) \quad (7)$$

Writing (6) explicitly yields

$$\dot{V} = f(V) + \begin{bmatrix} mI & 0^{3 \times 3} \\ 0^{3 \times 3} & \mathcal{J} \end{bmatrix}^{-1} \begin{bmatrix} E_3^b & 0^{3 \times 3} \\ 0^{3 \times 1} & \text{diag}([p_{11} \ p_{22} \ p_{33}]) \end{bmatrix} u_v \quad (8)$$

In this section, the dynamic model of the helicopter with six degrees-of-freedom (DOF) and four inputs has been presented. The inputs are functions of main rotor thrust  $T_{MR}$ , tail rotor thrust  $T_{TR}$ , the longitudinal tilt  $\alpha$ , and the lateral tilt  $\beta$  of the main rotor path plane with respect to the shaft. The remaining two control inputs in  $U$  are a function of these four actual control inputs.

## 2.4. NONLINEAR OPTIMAL TRACKING OF THE HELICOPTER UAV

In this section, the optimal control framework for selection of  $u_v$  is provided. Due to the NN approximating the cost function, an approximate optimal-based input  $\hat{u}_v$  will be generated. The first part of this section introduces the kinematic controller, which generates the desired velocity for the dynamic controller. After the kinematic controller, the virtual controller is introduced in Subsection 0 to provide a feedforward term  $u_d$  for the dynamic controller. Subsection 0 addresses the Hamilton-Jacobi-Bellman equation, providing the foundation for a NN-based optimal controller, which is discussed in Subsection 0 and provides the optimal control term  $\hat{u}_e^*$  used for the combined NN-based input to the helicopter dynamics,  $\hat{u}_v$ .

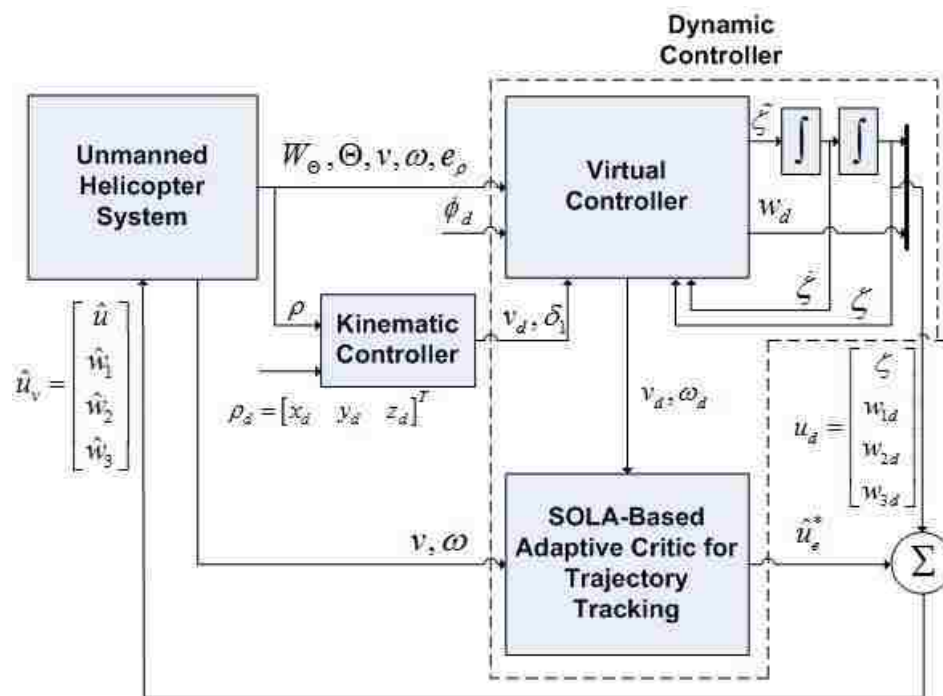


Figure 2.1. Control Scheme for Optimal Tracking of Helicopter

**2.4.1 Kinematic Controller.** The kinematic controller generates the desired velocity for the dynamic controller. To design the kinematic controller for the unmanned helicopter, the tracking error for the position must first be defined. The position tracking error is given by

$$\delta_1 = \rho_d - \rho \quad (9)$$

Also, it is essential to define  $v = \dot{\rho}$ , which then yields the desired velocity,  $v_d$  as in [7] as

$$v_d = v - \frac{1}{m} \delta_1 \quad (10)$$

In addition, it is important to note that there exist desired trajectories which may reach unstable operating regions as the orientation about the  $x$ - and  $y$ - axes approaches  $\pm \pi/2$ . This is a consequence of the physical limitations of helicopters. Therefore, trajectories requiring that these orientations be maintained should not be assigned to the helicopter.

**2.4.2. Virtual Controller.** The next step is to design the virtual controller, which is used to obtain the virtual control output or desired input  $u_d = [\zeta \ w_{1d} \ w_{2d} \ w_{3d}]^T$ . This process is performed by first defining a set of error terms. The first,  $\delta_1 = \rho_d - \rho$ , was introduced with the kinematic controller. The second error term to be minimized is  $\delta_2 = m(v - v_d)$ , with  $\delta_2$  a velocity tracking error that incorporates the helicopter's mass. The third and fourth errors to be considered are  $\epsilon_3 = \phi_d - \phi$  and  $\epsilon_4 = \dot{\phi} - \dot{\phi}_d$ , which consider the error in the helicopter's heading and the rate at which this error is changing. A fifth error term considers the error in the thrust and may be expressed as

$$\delta_3 = m\bar{g}e_3 - m\dot{v}_d + \delta_2 + \frac{1}{m} \delta_1 - \zeta R(\Theta)e_3 \quad (11)$$

with all of the variables in (11) as previously defined. For convenience, a term

$$Y_d = \delta_2 + \delta_3 + \frac{d}{dt}(m\bar{g}e_3 - m\dot{v}_d + \delta_2 + \frac{1}{m}\delta_1)$$

is introduced prior to the final error term necessary for this development, which allows this final error term to be written as

$$\delta_4 = Y_d - (\dot{\zeta}R(\Theta)e_3 + \zeta R(\Theta)skew(\omega)e_3)$$

The choice of these particular error terms is analyzed in further detail in [7].

Selecting

$$\tilde{\zeta}R(\Theta)e_3 - \zeta R(\Theta)skew(e_3)\tilde{w}_d = \dot{Y}_d - 2\dot{\zeta}R(\Theta)skew(\omega)e_3 + \delta_3 + \delta_4 \quad (12)$$

to be solved for control of the main rotor thrust, pitch, and roll, and

$$\ddot{\phi} = \ddot{\tilde{\phi}} - \epsilon_3 - \epsilon_4 \quad (13)$$

to be solved for control of the yaw [7], a solution for both equations is given by

$$\begin{bmatrix} \tilde{w}_{1d} \\ \tilde{w}_{2d} \\ \tilde{\zeta} \end{bmatrix} = \begin{bmatrix} 0 & \zeta & 0 \\ -\zeta & 0 & 0 \\ 0 & 0 & 1 \end{bmatrix}^{-1} R(\Theta)^T (\dot{Y}_d - 2\dot{\zeta}R(\Theta)skew(\omega)e_3 + \delta_3 + \delta_4) \quad (14)$$

From which  $\tilde{w}_{1d}$ ,  $\tilde{w}_{2d}$ , and  $\tilde{\zeta}$  are obtained (with  $\tilde{\zeta}$  obtained recursively). This solution was obtained by making use of the property  $skew(e_3)\tilde{w}_d = e_3 \times \tilde{w}_d = -skew(\tilde{w}_d)e_3$ , and rearranging and rewriting (12). Defining the relationship between the angular velocity and the orientation (from Section 2.3) as

$$\dot{\Theta} = \frac{1}{\cos(\theta)} \begin{pmatrix} 0 & s_\psi & c_\psi \\ 0 & c_\theta c_\psi & -c_\theta s_\psi \\ c_\theta & s_\theta s_\psi & s_\theta c_\psi \end{pmatrix} \omega = T^{-1}\omega \quad (15)$$

it is now possible to rearrange (6) in terms of  $\dot{\omega}$  and set  $\dot{\omega} = \tilde{w}_d$ , while considering only the virtual control inputs. Doing this yields



$$\tilde{w}_d = -\mathcal{J}^{-1}\omega \times \mathcal{J}\omega + |Q_M|\mathcal{J}^{-1}e_3 - |Q_T|\mathcal{J}^{-1}e_2 + \mathcal{J}^{-1}Pw_d \quad (16)$$

Taking the derivative of (15), rearranging, and considering only the yaw (first element in orientation vector) results in

$$\ddot{\phi} = -e_1^T T^{-1} \dot{T} T^{-1} \omega + \frac{1}{c_\theta} (s_\psi \tilde{w}_{2d} + c_\psi \tilde{w}_{3d}) \quad (17)$$

Then, employing both (13) and (17) and rearranging allows  $\tilde{w}_{3d}$  to be obtained as

$$\tilde{w}_{3d} = \frac{c_\theta}{c_\psi} (\ddot{\phi} - \epsilon_4 - \epsilon_3 + e_1^T T^{-1} \dot{T} T^{-1} \omega - \frac{s_\psi}{c_\theta} \tilde{w}_{2d})$$

Now the real inputs are obtained. To do this, first restate a portion of the dynamics to obtain  $w_d$  from (6) as

$$w_d = P^{-1} (\mathcal{J}\tilde{w}_d + \omega \times \mathcal{J}\omega - Q_M e_3 + Q_T e_2) \text{ with } P = \text{diag}([p_{11} \ p_{22} \ p_{33}]^T) \text{ a set of gains, and}$$

then obtain  $\zeta$  by double-integrating from

$$\ddot{\zeta} = \tilde{\zeta} \quad (18)$$

by using the value that has just been obtained for  $\tilde{\zeta}$ . Combining the preceding results allows one to arrive at the feedforward portion of the control input as

$$u_d = [\zeta \ w_{1d} \ w_{2d} \ w_{3d}]^T \quad (19)$$

from the values that have just been obtained for  $\zeta$ ,  $w_{1d}$ ,  $w_{2d}$ , and  $w_{3d}$ . Proof that the inputs generated by these equations assures convergence is provided in detail in [7].

**2.4.3. Hamilton-Jacobi-Bellman Equation.** In this section, the optimal control input is designed based on the dynamics of the helicopter given in (5) and (6) with the intention of minimizing the control input errors. The ideal dynamics (3) are of the form

$$\dot{V}_d = f(V_d) + gu_v^* \quad (20)$$

where  $V_d \in \mathbb{R}^{6 \times 1}$ ,  $f(V_d) \in \mathbb{R}^{6 \times 1}$ ,  $g \in \mathbb{R}^{6 \times 6}$  is bounded such that  $g_{min} \preceq g \preceq g_{max}$  and  $u_v^* \in \mathbb{R}^{6 \times 1}$  is the desired control input. For reference,  $g$  is provided here explicitly as

$$g = M^{-1} \begin{bmatrix} E_3^b & 0^{3 \times 3} \\ 0^{3 \times 1} & diag([p_{11} p_{22} p_{33}]) \end{bmatrix} \quad (21)$$

It has been assumed that the system is observable and controllable, with  $V = 0$  a unique equilibrium point on compact set  $Y \in \mathbb{R}^{6 \times 1}$  with  $f(0) = 0$  [11]. The addition of a term from the virtual controller to be introduced later in this paper makes it possible to neglect the  $f(0) = 0$  requirement. With these assumptions, the optimal control input for the unmanned helicopter system given in (20) can be determined [8]. It is important to note that the dynamics  $f(V)$  and  $g$  are assumed to be known. However, this assumption may be relaxed if some of the unknown parameters are estimated by using NNs. The tracking error  $e = V - V_d$  may be combined with the actual system dynamics  $\dot{V} = f(V) + gu_v$  to obtain the tracking error dynamics  $\dot{e} = f(V) + gu_v - \dot{V}_d = f_e(e) + gu_e$ , with  $f_e(e) = f(V) - f(V_d)$  and  $u_e = u_v - u_v^*$  is the feedback portion of the control input and  $u_v$  is the actual control input.

The infinite horizon HJB cost function for (20) is now given below in terms of the tracking error as

$$W(e(t)) = \int_t^\infty r(e(\tau), u_e(\tau)) d\tau \quad (22)$$

with  $r(e(t), u_e(t)) = Q(e) + u_e^T B u_e$ ,  $Q(e) > 0$  the positive definite penalty on the states and  $B \in \mathbb{R}^{6 \times 6}$  denoting a positive semi-definite matrix. The control input must be selected

such that the cost function in (22) is finite, or  $u_e$  must be admissible [11]. Next, the Hamiltonian for the cost function in (22) with control input  $u_e$  is defined as

$$H(e, u_e) = r(e, u_e) + W_e^T(e)(f(e) + gu_e) \quad (23)$$

with  $W_e(e)$  the gradient of  $W(e)$  with respect to  $e$ . The optimal control input  $u_e^*$  which minimizes the cost function in (22) also minimizes the Hamiltonian in (23). Thus the optimal control input can be obtained by solving the stationary condition

$\partial H(e, u_e) / \partial u_e = 0$  and is found to be

$$u_e^*(e) = -B^{-1}g^T W_e^*(e) / 2 \quad (24)$$

Substituting the optimal control input from (24) into the Hamiltonian (23) while retaining  $H(e, u_e^*, W_e^*(e)) = 0$  gives the HJB equation and the necessary and sufficient condition for optimal control to be [8]

$$0 = Q(e) + W_e^{*T}(e)f(e) - W_e^{*T}(e)gB^{-1}g^T W_e^*(e) / 4 \quad (25)$$

with  $W^*(0) = 0$ . It is also known that the following relation is applicable [11]

$$J_{1e}^T(f(e) + gu_e^*(e)) = -J_{1e}^T \bar{Q}(e) J_{1e} \quad (26)$$

where  $J_{1e}$  is the cost function. Tracking results are possible by modifying (24) to obtain an expression for the overall control input as

$$u_v = u_d + u_e^*(e) \quad (26)$$

with the feedforward control input  $u_d$  as previously given.

#### 2.4.4. Single Online Approximator (SOLA)-Based Optimal Control of

**Helicopter.** Usually, in adaptive critic based techniques, two OLAs [11] are used for optimal control, since one is used to approximate the cost function and the other is used to generate the control action. In this paper, the adaptive critic for optimal control of a helicopter is accomplished using only one OLA [11]. For the SOLA to learn the cost function, the cost function is rewritten using the OLA representation as given below

$$W(e) = \Gamma^T \Phi(e) + \varepsilon \quad (27)$$

with  $\Gamma \in \mathbb{R}$  the constant target OLA vector,  $\Phi(e) : \mathbb{R}^n \rightarrow \mathbb{R}^L$  a linearly independent basis vector such that  $\Phi(e) = 0$ , with  $\varepsilon$  the OLA reconstruction error. The target OLA vector and reconstruction errors are assumed to be upper bounded, with  $\|\Gamma\| \leq \Gamma_M$  and  $\|\varepsilon\| \leq \varepsilon_M$  [12]. The OLA cost function gradient in (27) is

$$\partial W(e) / \partial e = W_e(e) = \nabla_e^T \Phi(e) \Gamma + \nabla_e \varepsilon \quad (28)$$

Using (28), the optimal control input in (24) and the HJB equation in (25) can be expressed as

$$u_e^*(e) = -B^{-1} g^T \nabla_e^T \Phi(e) \Gamma / 2 - B^{-1} g^T \nabla_e \varepsilon / 2 \quad (29)$$

$$H^*(e, \Gamma) = Q(e) + \Gamma^T \nabla_e \Phi(e) f(e) - \Gamma^T \nabla_e \Phi(e) C \nabla_e^T \Phi(e) \Gamma / 4 + \varepsilon_{HJB} = 0 \quad (30)$$

where  $C = gB^{-1}g^T > 0$  is bounded with  $C_{min} \leq \|C(e)\| \leq C_{max}$  for  $C_{min}$  and  $C_{max}$  and

$$\begin{aligned} \varepsilon_{HJB} &= \nabla_e \varepsilon^T (f(e) - \frac{1}{2} gB^{-1}g^T (\nabla_e^T \Phi(e) \Gamma + \nabla_e \varepsilon)) + \frac{1}{4} \nabla_e \varepsilon^T gB^{-1}g^T \nabla_e \varepsilon \\ &= \nabla_e \varepsilon^T (f(e) + gu_e^*) + \frac{1}{4} \nabla_e \varepsilon^T C \nabla_e \varepsilon \end{aligned} \quad (31)$$

is the OLA residual reconstruction error. The OLA estimate of (27) is given by

$$\hat{W}(e) = \hat{\Gamma}^T \Phi(e) \quad (32)$$

with  $\hat{\Gamma}$  the OLA estimate of the target vector  $\Gamma$ . In the same way the estimate for the optimal control input in (29) can be expressed as  $\hat{u}_e^*(e) = -B^{-1}g^T\nabla_e^T\Phi(e)\hat{\Gamma}/2$ . With this input, the overall input to the unmanned helicopter system is modified from (26) to accommodate the NN-based optimal control input and may be written as

$$\hat{u}_v = u_d + \hat{u}_e^*(e) \quad (33)$$

An initial stabilizing control is not required to implement this proposed SOLA-based scheme. The estimate-based Hamiltonian is

$$\hat{H}^*(e, \hat{\Gamma}) = Q(e) + \hat{\Gamma}^T \nabla_e \Phi(e) f(e) - \hat{\Gamma}^T \nabla_e \Phi(e) C \nabla_e^T \Phi(e) \hat{\Gamma} / 4 \quad (34)$$

From the definition of the OLA cost function approximation (32) and the Hamiltonian function (34), it is clear that both become zero when  $\|e\| = 0$ . Recollecting the HJB equation in (23), the OLA estimate  $\hat{\Gamma}$  should be tuned such that  $\hat{H}^*(e, \hat{\Gamma}) = 0$ .

Unfortunately, only tuning  $\hat{\Gamma}$  to minimize  $\hat{H}^*(e, \hat{\Gamma})$  does not guarantee the stability of the nonlinear helicopter system (20) throughout the OLA learning process. Consequently, the OLA tuning algorithm is designed to minimize (34) while maintaining the stability of (20) is given as [11]

$$\begin{aligned} \dot{\hat{\Gamma}} = & -\alpha_1 \frac{\hat{\beta}}{(\hat{\beta}^T \hat{\beta} + 1)^2} (Q(e) + \hat{\Gamma}^T \nabla_e \Phi(e) f(e) - \hat{\Gamma}^T \nabla_e \Phi(e) C \nabla_e^T \Phi(e) \hat{\Gamma} / 4) \\ & + \Sigma(e, \hat{u}_e) \frac{\alpha_2}{2} \nabla_e \Phi(e) g B^{-1} g^T(e) J_{1e}(e) \end{aligned} \quad (35)$$

with  $\hat{\beta} = \nabla_e \Phi(e) f(e) - \nabla_e \Phi(e) C \nabla_e^T \Phi(e) \hat{\Gamma} / 2$ ,  $\alpha_1 > 0$  and  $\alpha_2 > 0$  design constants,

$J_{1e}(e)$  as defined previously, and the operator  $\Sigma(e, \hat{u}_e)$  given by

$$\Sigma(e, \hat{u}_e) = \begin{cases} 0 & \text{if } J_{1e}^T(e) \dot{e} = J_{1e}^T(e) (f(e) - g B^{-1} g^T \nabla_e^T \Phi(e) \hat{\Gamma} / 2) < 0 \\ 1 & \text{otherwise} \end{cases} \quad (36)$$

The first term in (35) minimizes (34) and has been derived using a normalized gradient descent scheme with the auxiliary HJB error defined as  $E_{HJB} = (\hat{H}^*(e, \hat{\Gamma}))^2 / 2$ .

The second term in the OLA tuning law in (35) ensures that the system states remain bounded while the SOLA scheme learns the optimal cost function. The basis function is given by  $\Phi(e) = [\nabla_e e \nabla_e e^2 \nabla_e e^3 \nabla_e \sin(e) \nabla_e \sin(2e) \nabla_e \tanh(e) \nabla_e \tanh(2e)]^T$ . The SOLA-based HJB tracking design for an unmanned helicopter is illustrated in Figure 1.

**2.4.5. Stability Analysis.** The proofs to be introduced shortly are built on the basis of the work of [7] and [11]. It is found that the control input consists of a predetermined virtual control or feedforward term,  $u_d$ , and an optimal feedback term that is a function of the gradient of the optimal cost function. In order to implement the optimal control in (22), the SOLA based control law is used to learn the optimal feedback tracking control after necessary modifications, such that the OLA tuning algorithm is able to minimize the Hamiltonian while maintaining the stability of the helicopter system.

The boundedness of  $\|J_{1e}\|$  and therefore the system state errors, which are necessary for Theorem 1, may be found in [11]. Theorem 1, which is provided next, establishes the optimality of the single network adaptive critic controller feedback term. Lemma 2 is then provided because it provides a stability condition needed for the proof for Theorem 3. Theorem 3 establishes the virtual control term stability and the stability of the entire resulting system.

*Theorem 1 (Optimality and convergence of the single network adaptive critic controller feedback term).* Given the nonlinear helicopter UAV system defined in (3), with target HJB equation (25), let the SOLA tuning law be given by (35). Let the control input be given by (24). Then the velocity tracking error and NN parameter estimation

errors of the cost function term are UUB for all  $t \geq t_0 + T$ , and the tracking error feedback system is controlled in a near optimal manner. That is,  $\|u_e^* - \hat{u}_e\| \leq \varepsilon_u$  for a small positive constant  $\varepsilon_u$ .

The proof is performed in terms of state error  $e$  in order to begin the stability analysis of the optimal controller. But first, the Lyapunov candidate function is given by

$$J_{HJB} = \alpha_4 J_2(e) + \tilde{\Gamma}^T \tilde{\Gamma} / 2 \quad (37)$$

where its first derivative is expressed as

$$\dot{J}_{HJB} = \alpha_4 J_{e2}^T(e) \dot{e} + \tilde{\Gamma}^T \dot{\tilde{\Gamma}} \quad (38)$$

The proof is performed in the same manner as the proof for the first step of Theorem 3, which will be introduced shortly. For the proof of Theorem 3, Lemma 2 is needed.

*Lemma 2 (Stability condition).* If an affine nonlinear system is asymptotically stable and the cost function given in [11] is smooth, then the closed-loop dynamics are asymptotically stable [11].

*Theorem 3 (Overall system stability).* Given the unmanned helicopter system with target HJB equation (25), let the tuning law for the SOLA be given by (35), and let the virtual control input be as in (19). Then there exist constants  $b_{J_e}$  and  $b_\Gamma$  such that the OLA approximation error  $\tilde{\Gamma}$  and  $\|J_{1e}(e)\|$  are UUB for all  $t \geq t_0 + T$  with ultimate bounds given by  $\|J_{1e}(e)\| \leq b_{J_e}$  and  $\|\tilde{\Gamma}\| \leq b_\Gamma$ . Further, OLA reconstruction error  $\|W^* - \hat{W}\| \leq \varepsilon_{r1}$  and  $\|u_v - \hat{u}_v\| \leq \varepsilon_{r2}$  for small positive constants  $\varepsilon_{r1}$  and  $\varepsilon_{r2}$ .

Proof: First, begin with the positive definite Lyapunov function candidate

$$J = \alpha_2 J_1(e) + \tilde{\Gamma}^T \tilde{\Gamma} / 2 + \frac{1}{2} \delta_1^T \delta_1 + \frac{1}{2} \delta_2^T \delta_2 + \frac{1}{2} \delta_3^T \delta_3 + \frac{1}{2} \delta_4^T \delta_4 + \frac{1}{2} \epsilon_3^T \epsilon_3 + \frac{1}{2} \epsilon_4^T \epsilon_4 \quad (39)$$

The proof may then be divided into steps, with the first part of the Lyapunov function candidate considered first.

**Step 1:** Consider the optimal control Lyapunov function candidate

$$J_{HJB} = \alpha_2 J_1(e) + \tilde{\Gamma}^T \tilde{\Gamma} / 2 \quad (40)$$

Differentiating, one obtains

$$\dot{J}_{HJB} = \alpha_2 J_{1e}^T(e) \dot{e} + \tilde{\Gamma}^T \dot{\tilde{\Gamma}} \quad (41)$$

With  $J_1(e)$  and  $J_{1e}(e)$  as previously given. If  $\|e\|=0$ ,  $J_{HJB}(e) = \tilde{\Gamma}^T \tilde{\Gamma} / 2$ ,  $\dot{J}_{HJB}(e) = 0$ , and  $\|\tilde{\Gamma}\|$  remains a bounded constant. For online learning, however, it is the case that  $\|e\| > 0$ . Then, using the affine nonlinear system, the optimal control input, and the tuning law's error dynamics along with the derivative of the Lyapunov candidate function

$J_{HJB}$ , one arrives at

$$\begin{aligned} \dot{J}_{HJB} &= \alpha_2 J_{1e}^T(e) (f_e(e) - \frac{1}{2} g B^{-1} g^T \nabla_e^T \Phi(e) \hat{\Gamma}) - \frac{\alpha_1}{\rho^2} (\tilde{\Gamma}^T \nabla_e \Phi_e (\dot{e}_1^* + \frac{C \nabla_e \mathcal{E}}{2}))^2 \\ &\quad - \frac{\alpha_1}{8\rho^2} (\tilde{\Gamma}^T \nabla_e \Phi_e C \nabla_e^T \Phi(e) \tilde{\Gamma})^2 - \frac{3\alpha_1}{4\rho^2} \tilde{\Gamma}^T \nabla_e \Phi(e) (\dot{e}_1^* + \frac{C \nabla_e \mathcal{E}}{2}) \tilde{\Gamma}^T \nabla_e \Phi(e) C \nabla_e^T \Phi(e) \tilde{\Gamma} \\ &\quad - \frac{\alpha_1}{\rho^2} \tilde{\Gamma}^T \nabla_e \Phi(e) (\dot{e}_1^* + \frac{C \nabla_e \mathcal{E}}{2}) \mathcal{E}_{HJB} - \frac{\alpha_1}{2\rho^2} \tilde{\Gamma}^T \nabla_e \Phi(e) C \nabla_e^T \Phi(e) \tilde{\Gamma} \mathcal{E}_{HJB} \\ &\quad - \Sigma(e, \hat{u}_e) \frac{\alpha_2}{2} \tilde{\Gamma}^T \nabla_e \Phi(e) g B^{-1} g^T J_{1e}^T(e) \end{aligned} \quad (42)$$

Completing the square, simplifying, and using Cauchy-Schwartz yields

$$\begin{aligned} \dot{J}_{HJB} &\leq \alpha_2 J_{1e}^T(e) (f_e(e) - \frac{1}{2} g(e) B^{-1} g^T \nabla_e^T \Phi(e) \hat{\Gamma}) \\ &\quad - \Sigma(e, \hat{u}_e) \frac{\alpha_2}{2} \tilde{\Gamma}^T \nabla_e \Phi(e) g B^{-1} g^T J_{1e}^T(e) - \frac{\alpha_1}{\rho^2} \|\tilde{\Gamma}\|^4 \beta_1 + \frac{\alpha_1}{\rho^2} \eta(\varepsilon) + \frac{\alpha_1}{\rho^2} \beta_2 \delta^4(e) \end{aligned} \quad (43)$$

where  $\beta_1 = \nabla \Phi_{min}^4 C_{min}^2 / 64$ ,  $\beta_2 = 1024 / C_{min}^2 + 1.5$ ,  $\eta(\varepsilon) = 64 / C_{min}^2 + 3(\varepsilon_M^4 + \varepsilon_M^4 C_{max}^2) / 2$ ,



$\varepsilon_M'$  is an upper bound on the OLA reconstruction error, and  $0 < \nabla\Phi_{\min} \leq \|\nabla\Phi(e)\|$ . Now

it is necessary to consider the case  $\Sigma(e, \hat{u}_e) = 0$ :

$$\dot{J}_{HJB} \leq -(\alpha_2 \dot{e}_{\min} - \alpha_1 \beta_2 K^*) \|J_{1e}(e)\| - \frac{\alpha_1 \|\tilde{\Gamma}\|^4 \beta_1}{\rho^2} + \frac{\alpha_1 \eta(\varepsilon)}{\rho^2} \quad (44)$$

This is less than zero if  $\alpha_2/\alpha_1 > \beta_2 K^*/\dot{e}_{\min}$ ,

$$\|J_{1e}(e)\| > \alpha_1 \eta(\varepsilon) / (\alpha_2 \dot{e}_{\min} - \alpha_1 \beta_2 K^*) \equiv b_{Je0} \quad (45)$$

or

$$\|\tilde{\Gamma}\| > \sqrt[4]{\eta(\varepsilon)/\beta_1} \equiv b_{\Gamma0} \quad (46)$$

where  $K^*$  is a constant. Next, to consider the case  $\Sigma(e, \hat{u}_e) = 1$ :

$$\begin{aligned} \dot{J}_{HJB} &\leq \alpha_2 J_{1e}^T(e) (f_e(e) - \frac{1}{2} C (\nabla_e^T \Phi(e) \Gamma + \nabla_e \varepsilon)) + \frac{\alpha_2}{2} J_{1e}^T(e) C \nabla_e \varepsilon - \frac{\alpha_1}{\rho^2} \|\tilde{\Gamma}\|^4 \beta_1 + \frac{\alpha_1 \eta(\varepsilon)}{\rho^2} \\ &+ \frac{\alpha_1}{\rho^2} \beta_2 \delta^4(e) = \alpha_2 J_{1e}^T(e) (f_e(e) + g u^*) + \frac{\alpha_2}{2} J_{1e}^T(e) C \nabla_e \varepsilon - \alpha_1 \frac{\alpha_1 \beta_1}{\rho^2} \|\tilde{\Gamma}\|^4 + \frac{\alpha_1}{\rho^2} \beta_2 K^* \|J_{1e}\| \end{aligned} \quad (47)$$

Lemma 4 yields

$$\dot{J}_{HJB} \leq -\frac{\alpha_2 \bar{Q}_{e,\min} \|J_{1e}(e)\|^2}{2} - \frac{\alpha_1 \|\tilde{\Gamma}\|^4 \beta_1}{\rho^2} + \frac{\alpha_1 \eta(\varepsilon)}{\rho^2} + \frac{\alpha_2 C_{\max}^2 \varepsilon_M'^2}{(4\bar{Q}_{e,\min})} + \frac{\alpha_1^2 \beta_2^2 K^{*2}}{(\alpha_2 \rho^4 \bar{Q}_{e,\min})} \quad (48)$$

with  $0 < \bar{Q}_{e,\min} \leq \|Q_e(e)\|$ , which is a uniformly ultimately bounded (UUB) result. The

second part of the Lyapunov function candidate considered next.

**Step 2:** Consider the virtual control Lyapunov function candidate

$$J_{\text{feedforward}} = S_1 + S_2 + S_3 + S_4 \quad (49)$$

with  $S_1 = 0.5 \delta_1^T \delta_1$ ,  $S_2 = 0.5 \delta_2^T \delta_2$ ,  $S_3 = 0.5 \delta_3^T \delta_3 + 0.5 \epsilon_3^T \epsilon_3$ , and  $S_4 = 0.5 \delta_4^T \delta_4 + 0.5 \epsilon_4^T \epsilon_4$ . It

has been shown that this selection of Lyapunov candidate guarantees stability in [7].

Applying elements integral to (19) gives the derivative of the Lyapunov function

$$\dot{\mathbf{j}}_{feedforward} = \dot{S}_1 + \dot{S}_2 + \dot{S}_3 + \dot{S}_4 = -\frac{1}{m} \delta_1^T \delta_1 - \delta_2^T \delta_2 - \delta_3^T \delta_3 - \delta_4^T \delta_4 - \epsilon_3^T \epsilon_3 - \epsilon_4^T \epsilon_4 \quad (50)$$

So  $\dot{\mathbf{j}}_{feedforward} < 0$ , which is an asymptotically stable (AS) result. To quickly review the elements in this stability analysis,  $\delta_1$  is used for the error in the tracking along with  $\epsilon_3$ ,  $\delta_2$  regulates the translational velocity,  $\delta_3$  and  $\delta_4$  take roll and pitch angles into consideration, and  $\epsilon_3$  and  $\epsilon_4$  are used for the error in the orientation (yaw) and corresponding rotational velocity.

**Step 3:** Consider the stability of the entire system. Combining

$$\begin{aligned} \dot{\mathbf{j}}_{HJB} + \dot{\mathbf{j}}_{feedforward} = & -\frac{\alpha_2 \bar{Q}_{e,min} \|J_{1e}(e)\|^2}{2} - \frac{\alpha_1 \|\tilde{\Gamma}\|^4 \beta_1}{\rho^2} + \frac{\alpha_1 \eta(\varepsilon)}{\rho^2} + \frac{\alpha_2 C_{max}^2 \varepsilon_M'^2}{(4\bar{Q}_{e,min})} \\ & + \frac{\alpha_1^2 \beta_2^2 K^{*2}}{(\alpha_2 \rho^4 \bar{Q}_{e,min})} - \frac{1}{m} \delta_1^T \delta_1 - \delta_2^T \delta_2 - \delta_3^T \delta_3 - \delta_4^T \delta_4 - \epsilon_3^T \epsilon_3 - \epsilon_4^T \epsilon_4 \end{aligned} \quad (51)$$

Lemma 3 then ensures  $\dot{\mathbf{j}}_{HJB} < 0$  given that

$$\|J_{1e}(e)\| > \sqrt{C_{max}^2 \varepsilon_M'^2 / (2\bar{Q}_{e,min}^2)} \equiv b_{J_{1e}}, \quad (52)$$

and

$$\|\tilde{\Gamma}\| > \sqrt[4]{\eta(\varepsilon) / \beta_1 + \alpha_1 \beta_2^2 K^{*2} / (\beta_1 \alpha_2 \bar{Q}_{e,min})} \equiv b_{\tilde{\Gamma}} \quad (53)$$

which allows the conclusion that  $\|W^*(e) - \hat{W}(e)\| \leq \|\tilde{\Gamma}\| \|\Phi(e)\| + \varepsilon_M \leq b_{\tilde{\Gamma}} \Phi_M + \varepsilon_M \equiv \varepsilon_{r1}$

and  $\|u_e^*(e) - \hat{u}_e(e)\| \leq \lambda_{max}(B^{-1}) g_M b_{\tilde{\Gamma}} \Phi_M' / 2 + \lambda_{max}(B^{-1}) g_M \varepsilon_M' / 2 \equiv \varepsilon_{r2}$ . Then

$\dot{\mathbf{j}}_{HJB} + \dot{\mathbf{j}}_{feedforward} < 0$  provided that (52) and (53) hold. Because the feedforward term is

asymptotically stable, the resulting bound on the error for the overall control input is

$\|u_v^* - \hat{u}_v\| \leq \lambda_{max}(B^{-1}) g_M b_{\tilde{\Gamma}} \Phi_M' / 2 + \lambda_{max}(B^{-1}) g_M \varepsilon_M' / 2 \equiv \varepsilon_{r2}$ , which is the same as the

bound for the SOLA-based control. In other words, the overall system is UUB with the bounds from (108) and (109), completing the proof.  $\square$

The dynamics presented at the beginning of the paper provide

$$\bar{S}(\omega) = \begin{bmatrix} 0^{3 \times 1} & -\omega \times J \omega \end{bmatrix}^T. \text{ Actually, however, this is a simplification of the real}$$

dynamics, which include an additional coupling term such that

$$\bar{S}(\omega) = [R(\Theta)Kw_d \quad -\omega \times J \omega]^T, \text{ with}$$

$$K = \frac{1}{l_M} \begin{bmatrix} 0 & 1 & 0 \\ -1 & 0 & 1/l_t \\ 0 & 0 & 0 \end{bmatrix} \quad (54)$$

This coupling term is relatively small, but the robustness against neglecting the term has been demonstrated using a nonlinear controller and is available for the interested reader in [7].

## 2.5. SIMULATION RESULTS

Simulation results for the unmanned helicopter are presented in this section. All simulations are performed in Simulink and demonstrate the performance of the proposed control scheme. The simulations take into account the aerodynamic features previously presented as part of the helicopter model. Note that the following gains and constants were used:  $m = 9.6\text{kg}$ ,  $\bar{g} = 9.8\text{m/s}^2$ ,  $\mathcal{J} = \text{diag}([0.40 \ 0.56 \ 0.29]^T)\text{kg} \cdot \text{m}^2$ ,

$$p = \text{diag}([1.11.11.1]^T), [p_{11} \ p_{22} \ p_{33}] = [1.1 \ 1.1 \ 1.1], l_t = 1.2\text{m}, l_m = 0.27\text{m},$$

$$Q_M = 0.002, Q_T = 0.0002, \text{ and } B = \text{diag}([0.1 \ 0.1 \ 0.1 \ 0.001]^T). \text{ The optimal}$$

controller employs seven hidden layer neurons, with gains set to  $\alpha_1 = 100$  and  $\alpha_2 = 1$ .

The helicopter's initial position and orientation are set to zero. Figure 2 displays the capabilities of the helicopter when taking off and transitioning to hover. Figure 3 shows the helicopter transitioning from hover to landing. Figures 4 and 5 highlight the helicopter's tracking capability. Figures 6-11 show the error convergence, main rotor input convergence, velocity convergence, acceleration convergence, and U-vector magnitude when taking off and hovering. Figures 12 and 13 provide plots of the cost function  $J_{1e}(e) = 0.5e^2$  for the Take-off case in Figure 2, and Figures 14-16 show three-dimensional tracking capabilities. It is important to note that the main rotor thrust and tail rotor thrust should approach constant values rather than zero in order to keep the helicopter in hover, while the main rotor blade roll and pitch angles should approach zero.

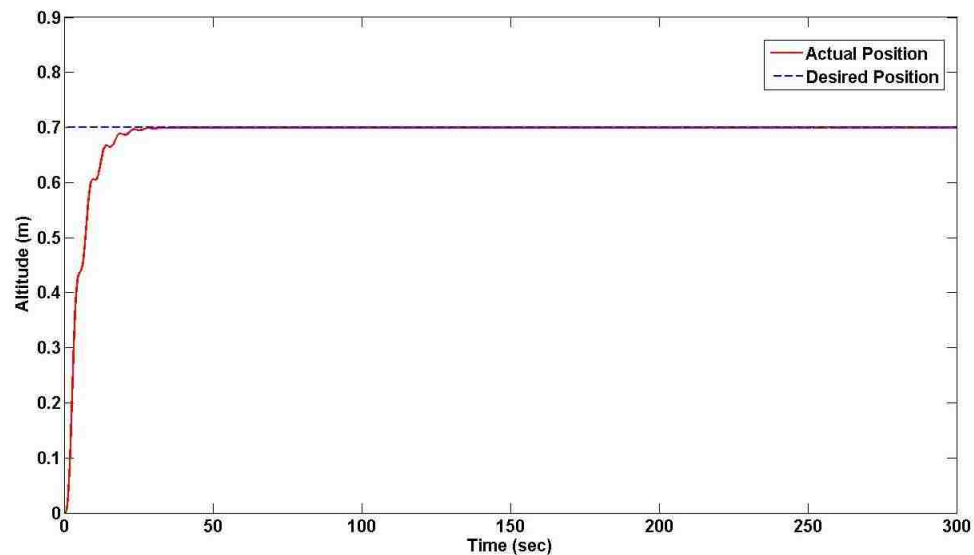


Figure 2.2. Helicopter Altitude during Take-off

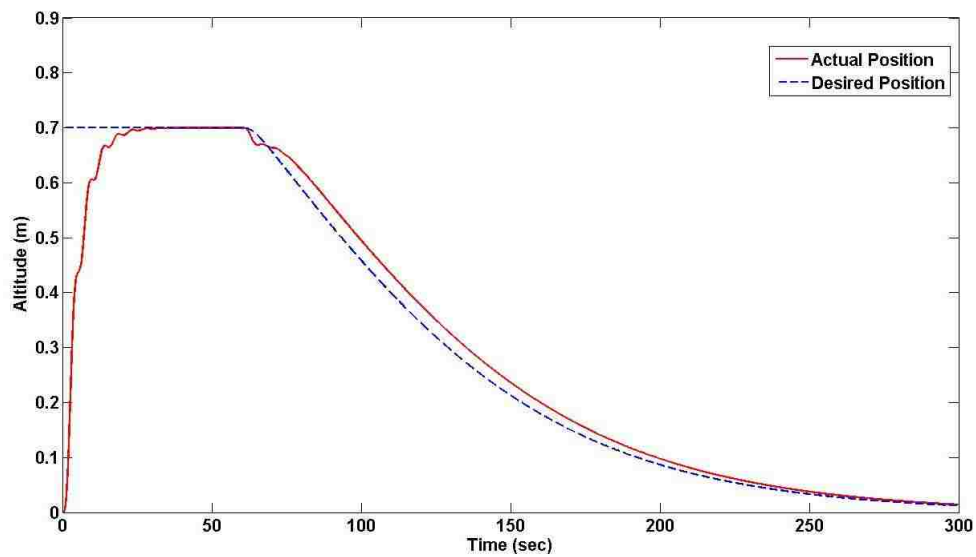


Figure 2.3. Helicopter Altitude during Landing

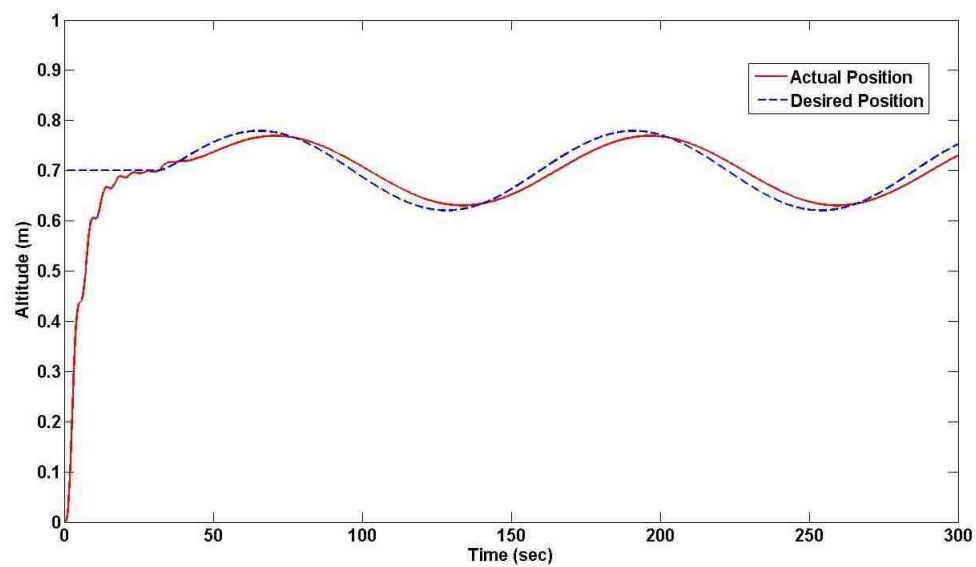


Figure 2.4. 2D Helicopter Trajectory Tracking

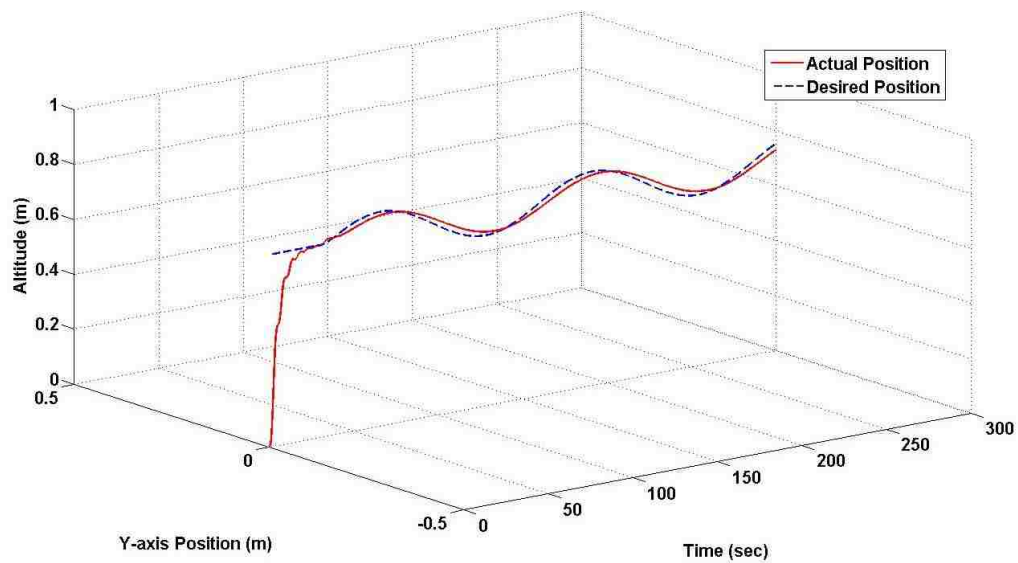


Figure 2.5. 3D Perspective of Helicopter Trajectory Tracking

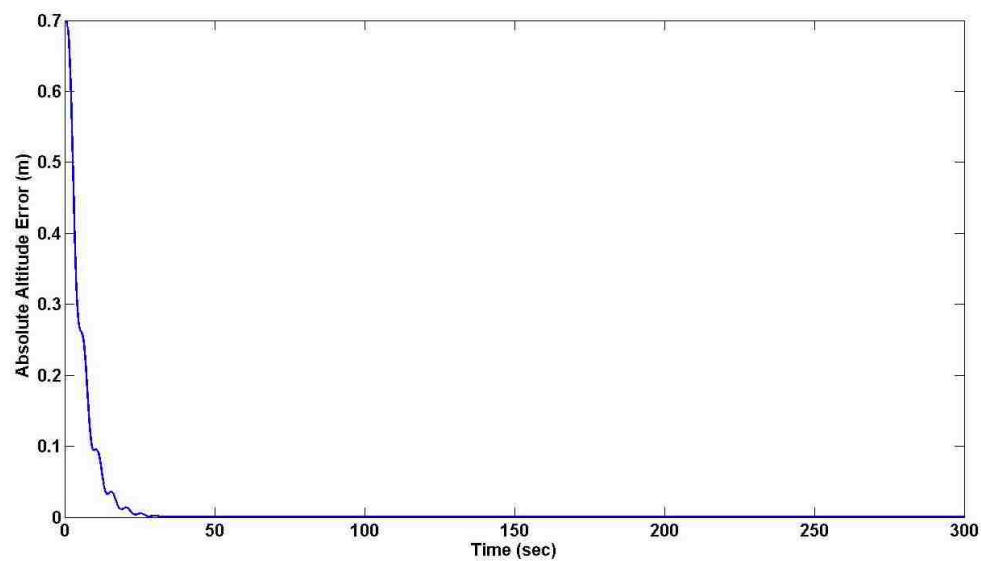


Figure 2.6. Absolute Error in Altitude during Take-off

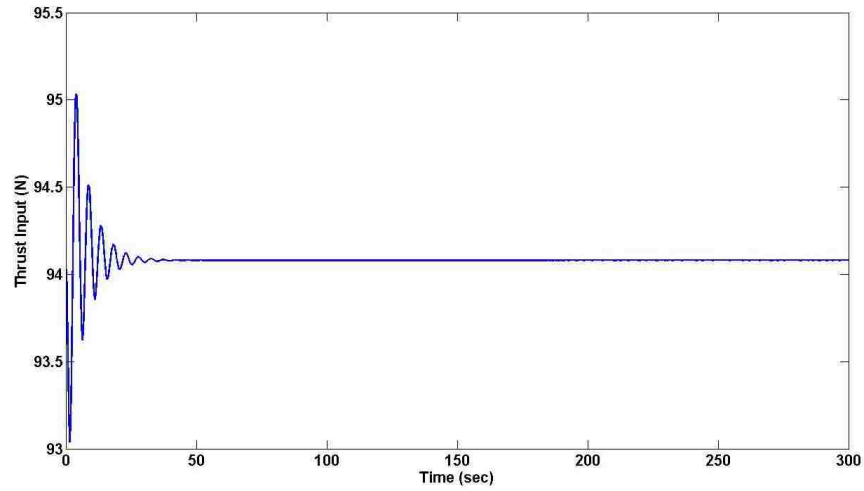


Figure 2.7. Main Rotor Control Input during Take-off

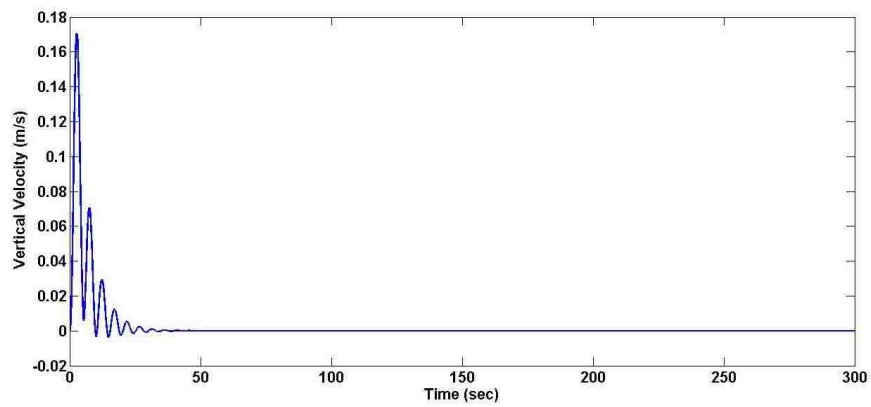


Figure 2.8. Vertical Velocity during Take-off

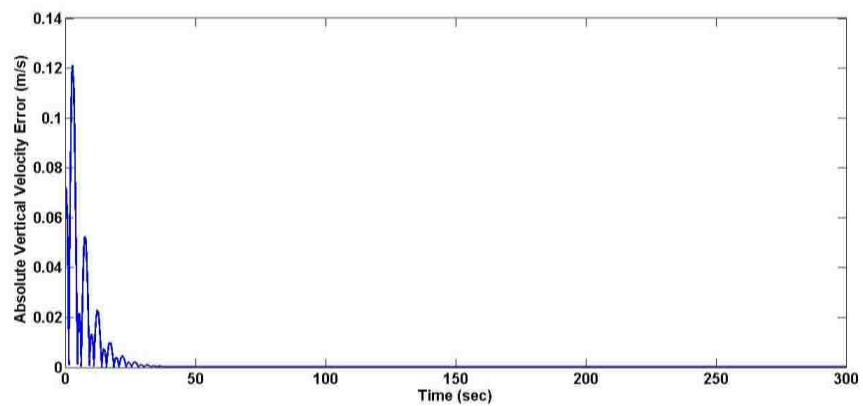


Figure 2.9. Absolute Error in Vertical Velocity during Take-off

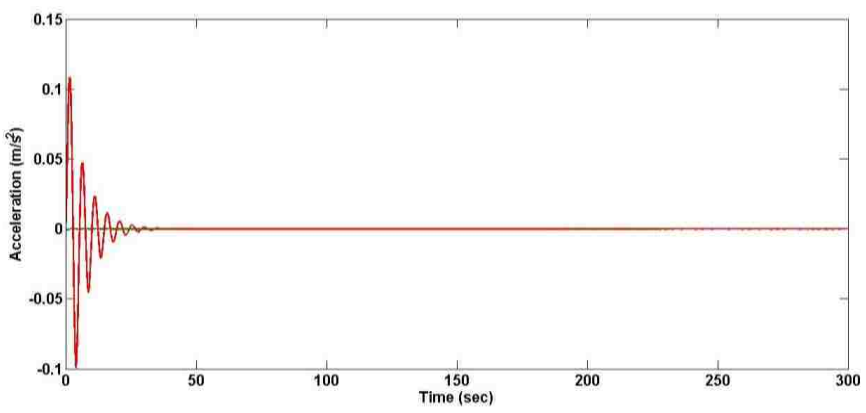


Figure 2.10. Acceleration during Take-off

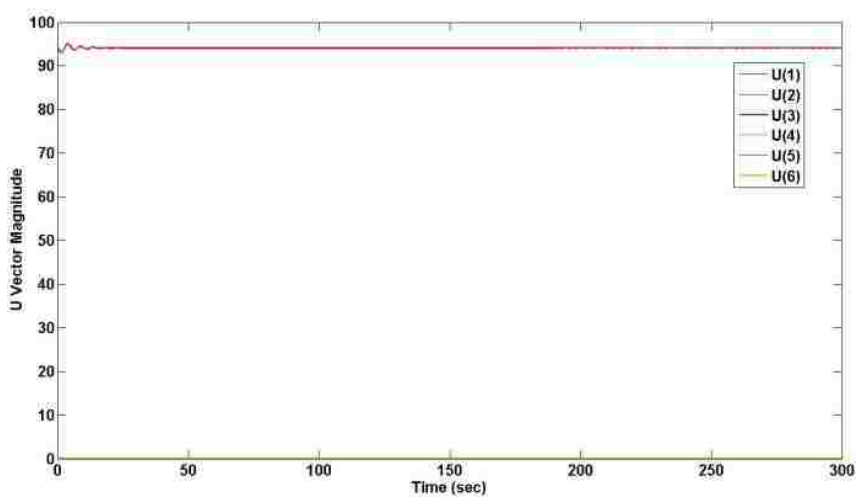


Figure 2.11. Magnitude of U-vector

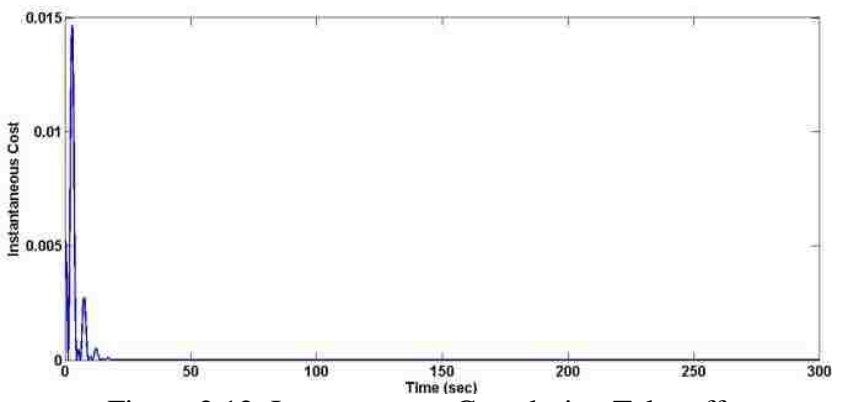


Figure 2.12. Instantaneous Cost during Take-off



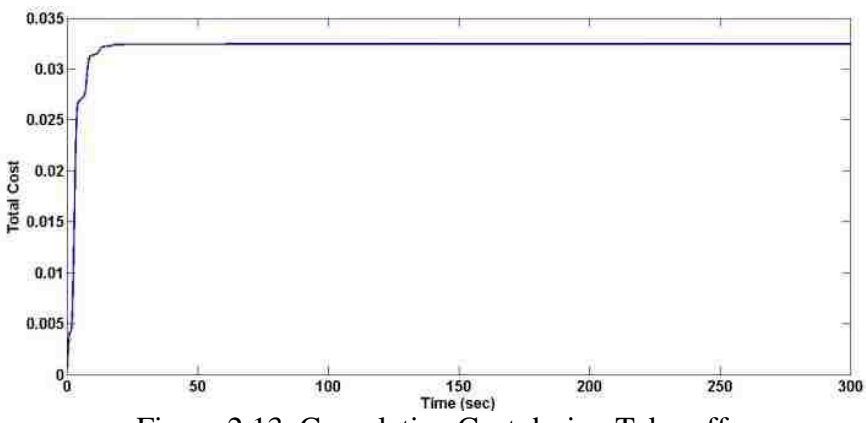


Figure 2.13. Cumulative Cost during Take-off

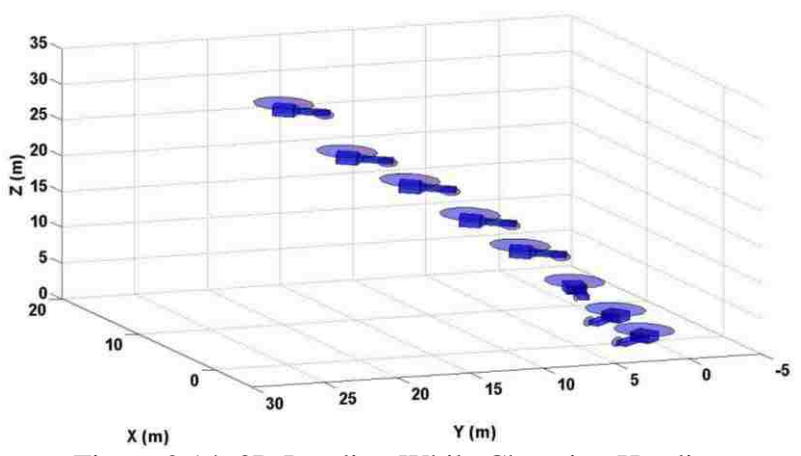


Figure 2.14. 3D Landing While Changing Heading

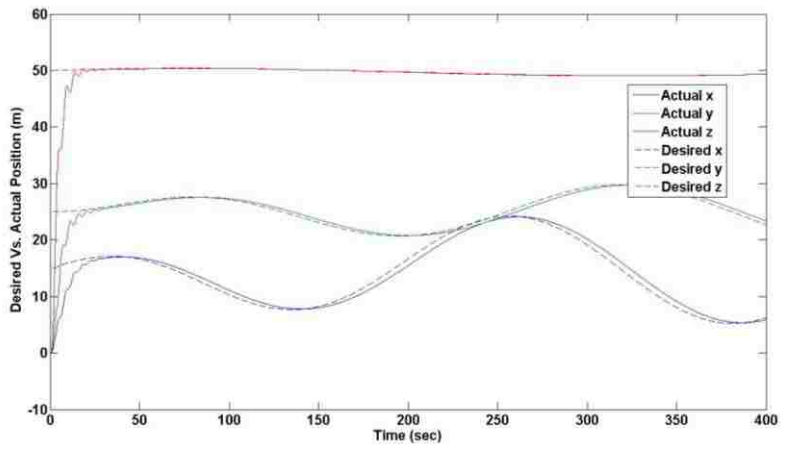


Figure 2.15. 3D Trajectory Tracking

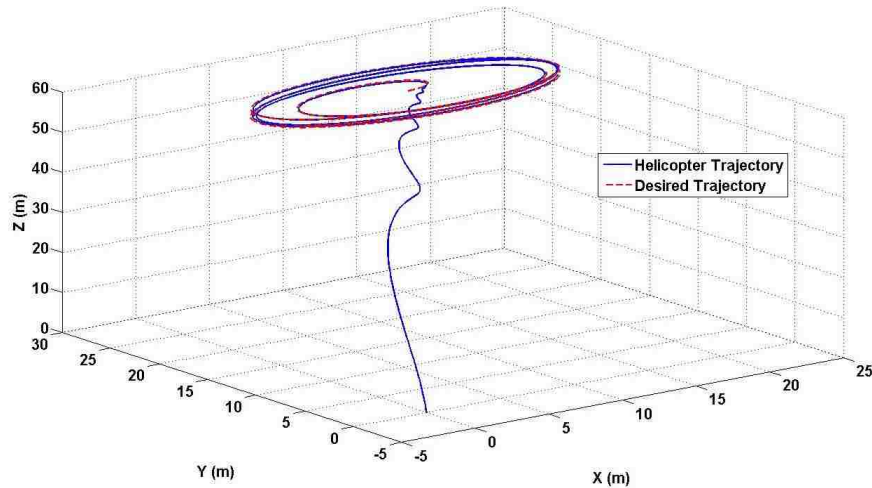


Figure 2.16. Take-off and Circular Hovering

## 2.6. HARDWARE RESULTS

The hardware is divided into two parts – the first part consisting of the helicopter UAV and its onboard systems, and the second part consisting of the ground control station. The helicopter UAV is equipped with a processor board as well as a sensor board, with the processor board functioning as the onboard control system. The sensor board has an array of sensors and connections to external sensors including GPS, an ultrasonic range finder, a three-axis gyro, a three-axis accelerometer, a barometric pressure sensor, and a temperature sensor. Some testing was performed with an infrared range finder as well. The outputs of the processor board are pulse-width-modulated (PWM) signals which drive the motor for the main rotor as well as for four servo motors. Three of the servo motors control the swashplate which adjusts the main rotor roll and pitch as well as the rotors' angle of attack. The fourth servo controls the thrust generated by the tail rotor.

The ground control station is linked to the helicopter UAV by Xbee communications modules, which function as wireless transmitter/receivers. A laptop is at

the heart of the ground control station. A Matlab program on the ground control station reads the incoming data from an external Xbee module via USB port, which it treats as a virtual serial communications port. The incoming data is read one byte at a time and assembled into complete telemetry messages. The telemetry messages follow the international MAVLink communications protocol for small-scale UAVs. After the messages have been assembled, they are checked for errors by making use of the checksum built into the messages. At this point, the ground control station is also able to report the packet loss rate, thereby monitoring the quality of communications. Any corrupt messages are discarded.

The messages are then sorted by message type, and the data is collected from each message. The MAVlink messages used for this system primarily contain sensor data. The sensor data is then processed and sent to the control system. The control system uses the sensor data for the states or the outputs and generates control outputs accordingly. These outputs are then packaged into MAVlink messages which are transmitted by Xbee back to the helicopter, which reads the actuator commands and controls the motors as instructed.

An Align Trex 500 was selected for the helicopter airframe. This selection was made based on the quality of the Align Trex series of helicopters, availability of spare parts, and size. The 500 series is small enough to keep costs down and is relatively easy to work with, has a reputation for being considerably more stable than the next smallest size, the 450 series, and has stability on the order of the larger 600 series helicopters, but without the costs associated with larger helicopters. The Align Trex 500 performed very well during testing, and is well-crafted with precision-machined metal and carbon-fiber

composite components. The processor board and the sensor board were both designed by DIY Drones, which is a leader in small-scale autopilots for fixed-wing aircraft. The boards have the advantage of being relatively robust, with open-source code, a large online support base, and numerous advantages over similar products from other companies. At the time of publication, hardware development is continuing.

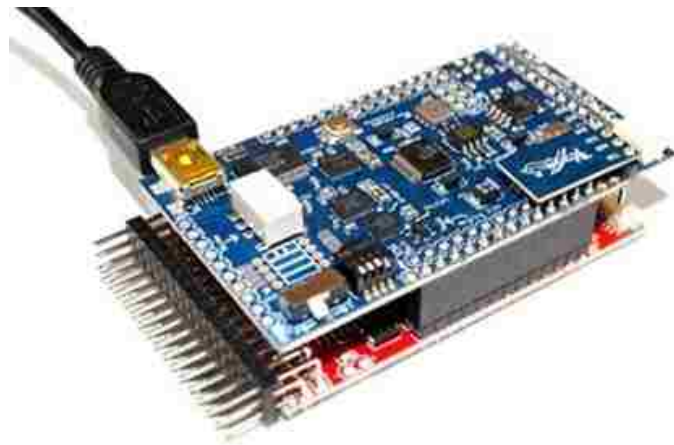


Figure 2.17. Processor & Sensor Boards

## 2.7. CONCLUSION

A NN based optimal control law has been proposed for an unmanned helicopter with dynamics written in strict-feedback form. This controller uses a single online approximator for optimal tracking. The SOLA-based adaptive approach is designed to learn the infinite horizon continuous-time HJB equation, and the corresponding optimal control input that minimizes the HJB equation is calculated forward-in-time. Further, optimality of the controller has been demonstrated. A virtual control structure was used to compensate for a mathematical requirement of the optimal controller. Simulation results

confirm that an unmanned helicopter with this control system is capable of tracking. This confirms the potential for practical application for a large and expanding set of both military and civilian roles.

## 2.8. REFERENCES

- [1] Naskrent, D., et al., "NATO Air and Space Power in Counter-IED Operations: a Primer," Joint Air Power Competence Center, 2010.
- [2] Unnamed Author. (2011, September 7). Defense Industry Daily [Online]. Available: <http://www.defenseindustrydaily.com/USMC-Looks-for-an-Unmanned-Cargo-Helicopter-06672/>
- [3] T. J. Koo and S. Sastry, "Output Tracking Control Design of a Helicopter Model Based on Approximate Linearization," in *Proceedings 37th IEEE Conference on Decision and Control*, Tampa, FL, 1998, pp. 3635-3640.
- [4] N. Hovakimyan, N. Kim, A. J. Calise, and J. V. R. Prasad, "Adaptive Output Feedback for High-bandwidth Control of an Unmanned Helicopter," in *Proceedings of AIAA Guidance, Navigation, and Control Conference*, Montreal, Canada, 2001, pp. 1-11.
- [5] E. N. Johnson and S. K. Kannan, "Adaptive Trajectory Control for Autonomous Helicopters," *Journal of Guidance, Control and Dynamics*, Vol. 28, pp. 524-538, 2005.
- [6] Palunko, I., Fierro, R., and Sultan, C., "Nonlinear Modeling and Output Feedback Control Design for a Small-scale Helicopter," in *Proceedings Of 17<sup>th</sup> Mediterranean Conference. on Control and Automation*, Thessaloniki, Greece, pp. 1251-1256, 2009.
- [7] B. Ahmed, H. R. Pota and M. Garratt, "Flight Control of a Rotary Wing UAV Using Backstepping," *International Journal of Robust and Nonlinear Control*, Vol. 20, pp. 639-658, 2010.
- [8] R. Enns and J. Si, "Helicopter Trimming and Tracking Control Using Direct Neural Dynamic Programming," *IEEE Transactions on Neural Networks*, Vol. 14, pp. 929-939, 2003.
- [9] T. Dierks and S. Jagannathan, "Output Feedback Control of a Quadrotor UAV Using Neural Networks," *IEEE Transactions on Neural Networks*, Vol. 21, pp. 50-66, 2010.

- [10] Isidori, A., "Nonlinear Control Systems," Berlin, Springer, 1995.
- [11] T. Dierks and S. Jagannathan, "Optimal Control of Affine Nonlinear Continuous-time Systems," in *Proceedings of American Control Conference*, Baltimore, Maryland, pp. 1568-1573, 2010.
- [12] F. L. Lewis, S. Jagannathan, and A. Yesilderek, "Neural Network Control of Robot Manipulators and Nonlinear Systems," London, Taylor & Francis, 1999.
- [13] F. L. Lewis and V. L. Syrmos, "Optimal Control," 2nd ed. Hoboken, NJ, Wiley, 1995.
- [14] R. Mahoney and T. Hamel, "Robust Trajectory Tracking for a Scale Model Autonomous Helicopter," *International Journal of Robust and Nonlinear Control*, Vol. 14, pp. 1035-1059, 2004.

## 2. CONCLUSIONS AND FUTURE WORK

### 2.1 CONCLUSIONS

This thesis presents optimal control schemes for both state and output feedback control of unmanned, underactuated helicopters, forward-in-time, with the helicopter dynamics expressed in a form appropriate for backstepping control. The control schemes are applied to both hovering and trajectory tracking, and the controller tuning is completed independently of the trajectories to be flown. The control scheme is fully online in real-time, and stability is demonstrated using Lyapunov analysis. Simulations are provided for initial verification of the work and hardware implementation yields opportunity for further verification.

The first paper addresses output feedback control with a neural-network observer that has not previously been applied to helicopter UAVs. A method is provided for compensating for the requirement that  $f(0) = 0$  by introducing a virtual controller to work jointly with the optimal controller. The mathematical stability proofs show convergence of the observer's state estimates to the actual states and the convergence of the actual states to the desired states, which is driven by the dynamic controller. Simulation results provide visual confirmation of the helicopter hovering and trajectory tracking, with plots included to show both the overall system performance as well as the performance of the observer individually for this application.

The second paper approaches the same problem but employs state feedback, and therefore does not require an observer. Simulation results and stability analysis are provided similarly to the first paper, but the second paper is augmented by a section on

the hardware implementation. This section includes the hardware used and specific technologies and algorithms employed for the hardware.

## **2.2 FUTURE WORK**

There are many challenges associated with nonlinear control of helicopter UAVs. Although many of these challenges are addressed in this work and other challenges have been addressed in past works, additional challenges still remain. One area for possible future improvement is the development of a superior feedforward controller. Although the feedforward controller in this work performs well, better trajectory tracking results are theoretically possible. In addition, there is potential for greater robustness to sensor noise, as the current approach requires significant filtering of sensor data.

Another area with potential for future improvements pertains to the hardware implementation. Specifically, sensor fusion algorithms for UAVs could still be improved. The direction-cosine matrix algorithm used in this thesis outperforms the unscented Kalman filter, but the performance remains imperfect and further refinements such as replacing the linear feedback loop are possible. An additional area for future contributions would be in the development of more sophisticated swash plate mapping algorithms.

The current work maps the control outputs to the actuators in a linear fashion. Although some other works devote more attention to actuator dynamics, the author has not seen any work that fully addresses this challenge in a satisfactory manner. All of these areas present opportunities for future work.



**VITA**

David John Nodland was born in 1984. He earned his Bachelor of Science in Electrical Engineering in 2008 and his Master of Science in Electrical Engineering in December, 2011.

